UNIVERSITY OF CALIFORNIA,
IRVINE

# Study of Packaging and Assembly Materials for Thermal Performance Enhancement of Optoelectronic Devices with Small Form Factor

DISSERTATION

submitted in partial satisfaction of the requirements
for the degree of

DOCTOR OF PHILOSOPHY

in Engineering

by

Linjuan Huang

Dissertation Committee:
Professor Frank G. Shi, Chair
Professor James C. Earthman
Professor Chin C. Lee

2017

# TABLE OF CONTENTS

# LIST OF FIGURES

# LIST OF TABLES

# ACKNOWLEDGMENTS

I would like to express the deepest appreciation to my committee chair, Professor Frank G. Shi, who has supported me over the past four years both financially and spiritually. He persistently provided novel ideas and helpful criticism when I prepared for the manuscripts that lay a solid foundation for this dissertation. He guided me in the right direction while giving me the freedom to expand my research filed.

I would like to thank my committee members, Professor James C. Earthman and Professor Chin C. Lee, who have served as my dissertation committee members, and provided pertinent suggestions.

In addition, a thank you to my colleagues, Dr. Bohan Yan, Dr. Yuchou Shih, Dr. Yue Shao, and Dr. Gunwoo Kim. They are both my co-workers and "teachers". I've learned a lot from them, not only experimental or simulation technical skills, but also the inclination to support each other as a team.

Finally, allow me to express my most sincere gratitude to my family, my mother, father, sister, brother-in-law, and niece. Especially my mother, it's such a wonderful journey to pursue my PhD degree with your selfless love.

# CURRICULUM VITAE

**Linjuan Huang**

2005-2009 B.S. in Optical Information Science and Technology, Sichuan University, China

2010-2013 M. S. in Optical Engineering, Zhejiang University, China

2013-2017 Ph. D. in Engineering, University of California, Irvine

## FIELD OF STUDY

Thermal management of electronic packaging and devices

## PUBLICATIONS

Linjuan Huang, Yuchou Shih, Frank Shi, "Effect of Thinning Encapsulant Layer on Junction and Phosphor Temperature of White Light Emitting Diodes", IEEE Trans. on Compon., Packaging & Manufact. Tech., pp. 1628 – 1634, 2015.

# ABSTRACT OF THE DISSERTATION

Study of Packaging and Assembly Materials for Thermal Performance Enhancement of Optoelectronic Devices with Small Form Factor

By

Linjuan Huang

Doctor of Philosophy in Engineering

University of California, Irvine, 2017

Professor Frank G. Shi, Chair

Recently, there is an evident trend of ever-thinner and intricate opto-electronic package and devices, which brings about severer thermal issues as well as unprecedented challenges for the thermal design. Not only thickness of opto-electronic package itself will raise the peak temperature and pose a potential risk to electronic devices, but also the limited-space and interacted opto-electro-thermo-mechanical properties restrict the use of traditional active thermal management means and precise estimation of cooling performance. This dissertation aims to numerically and experimentally analyze thermal behaviors of various LED package configurations while thinning it as well as apply novel radiation coating and packaging materials to cooling electronic devices with limited-space. What's more, an opto-thermal coupled numerical method in the application of LED was discussed. Last but not the least, much faster Machine Learning (ML) algorithms were adopted to predict patterns for cooling performance of our thermal radiation coating in Li-ion battery system and acceleration stage before the onset of thermal runaway, which is the key to cut-off the battery before explosion.

It’s found that: (1) LED packages have different thermal behaviors for various configurations while thinning it. There can be a 5-10 ℃ of temperature change for single-chip LED. (2) For white LEDs and light bars in direct view LED backlight units (DLED-BLUs), our thermal conductive Die Attach Adhesive (DAA) and thicker encapsulant are able to increase the power level by up to 1.5 times. (3) Our thermal radiation can effectively decrease the peak temperature by 14.5 ºC for linear LED modules as well as boost the uniformity of temperature distribution. (4) The thermal performance of LED package is different with and without considering optical effect. So optical effect should not be neglected while conducting thermal simulation for opto-electronic devices. (5) Machine learning algorithms can shorten prediction time of thermal performance of passive radiation material from 1 day to less than 0.5 min, compared with finite element method. A practical system design to effectively prevent explosion of Li-ion battery system is provided, too.

# CHAPTER 1:

# INTRODUCTION

An important industrial trend in electronic devices is the continuing reduction in module thickness and raise in complexity to meet the customer demands. For instance, the slimmest smartphone is only 4.75mm and the slim TV set can be less than 2 coins thick, as shown in Fig. 1.1. However, thinner electronic packages and devices, including LED package, also present new challenges for the thermal design. On one hand, CPUs with higher performance or LED screens with larger brightness and light output generate more and more heat to dissipate. On the other hand, thinner electronic devices mean limit-space for applying space consuming thermal management strategies such as active cooling methods and higher power density.


Fig. 1.1. Schematic of slim smartphone and TV set.

There are diverse configurations of LED packages: Surface-Mount Device (SMD), Chip-on-Board (COB), Flip-Chip, Chip-Scale Package (CSP) and so on. For phosphor-converted (pc) white LED, there are also different types: in-cup, chip coating and remote. However, how the peak temperature of different LED emitters change with thickness is unknown. Thermal resistance network is able to roughly analyze it. Thermal resistance is defined as length

of material divided by its thermal conductivity and area. Thermal resistance networks are analogy to electrical resistance networks and commonly employed to analyze steady state heat transfer. Three-dimensional thermal resistance circuit model of white LED package is displayed in Fig. 1.2. It can be seen that the total thermal resistance includes thermal resistance in both vertical and horizontal direction as well as thermal convection resistance between packaging materials and the air. And thermal resistance above LED chip, which represents upper heat dissipation of LED package, should not be neglected when studying thermal effect of thickness of encapsulant layer.

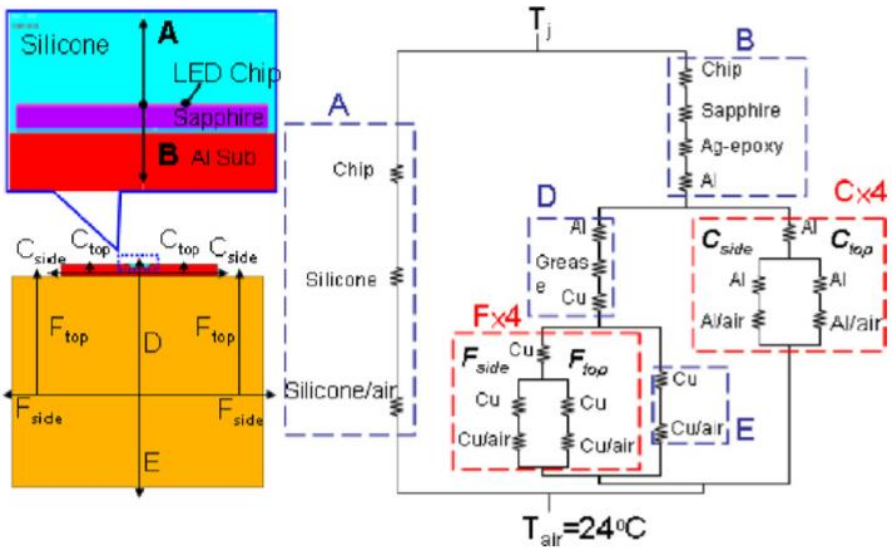


Fig. 1.2. Three-dimensional thermal resistance circuit model of white LED package [1].

Thermal behavior of LED package with less thickness can also be investigated by experiments. For example, Forward Voltage Method (FVM) can be conducted to measure junction temperature of LEDs [2]. The behind schema in Fig. 1.3 is that, there is a linear relationship region between voltage and junction temperature. After measuring two more voltage-temperature value pairs and obtaining the linear relationship, we are able to estimate junction temperature according to voltage.

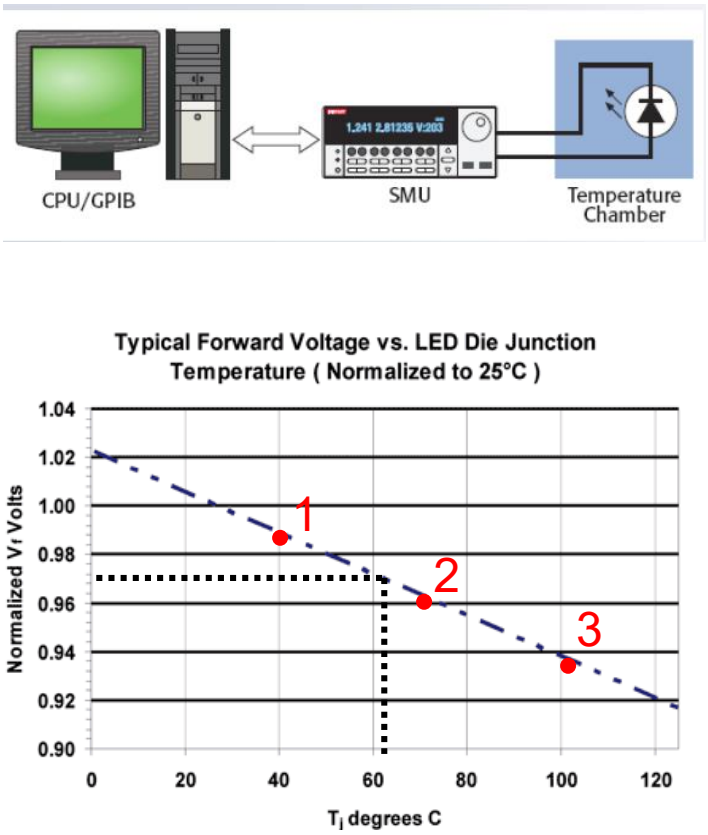


Fig. 1.3. Experimental setup and schema of Forward Voltage Method (FVM).

In this dissertation, Finite Element Method (FEM) software ANSYS is the main tool to do numerical simulation. The advantages of FEM are to provide a fast prediction of the assumed models while maintaining acceptable accuracy and deal with electro-thermo-mechanical coupled problems. The simulation results are compared and validated with experimental and analytical results. FEM model of a flip-chip LED package mounted on Printed Circuit Board (PCB) and its temperature distribution can be found in Fig. 1.4.

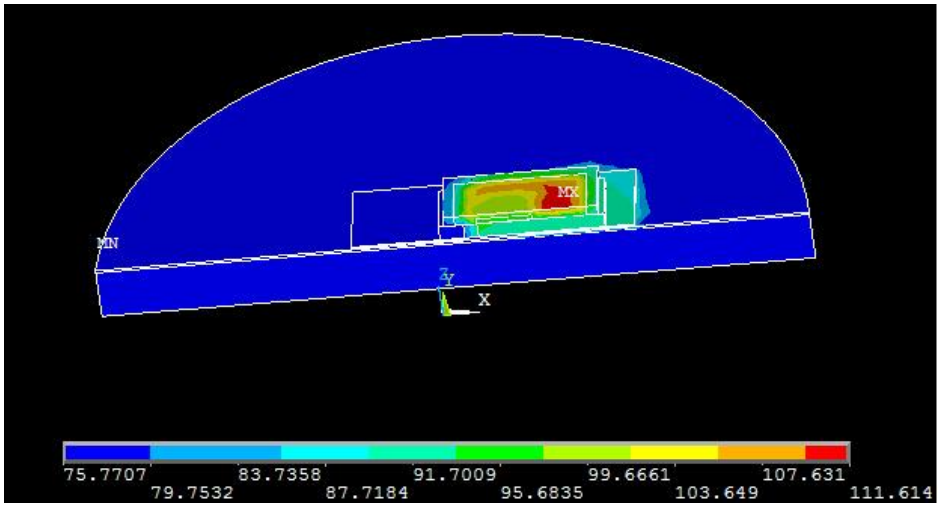


Fig. 1.4. Temperature distribution of a flip-chip LED package model calculated by ANSYS.

Due to the limit-space of thinner electronic devices, passive cooling methods are more promising than active ones. Novel packaging materials with higher thermal conductivity and less thickness such as our developed thermal conductive Die Attach Adhesives (DAAs) [3] and thinner encapsulant layer are good choices. For silicone based DAA materials, clear DAA has the lowest thermal conductivity but the least thickness, and white DAA is more thermal conductive but thicker. There is a trade-off between the thermal conductivity and thickness, in order to find DAA material with the lowest thermal resistance. Packaging materials with low thermal resistance can effectively cool down junction and improve light output efficiency without increasing production cost too much. Thus the cost-performance ratio is lowered.

Another novel passive cooling strategy is our polymer-filler composites coated on the board of LED modules. There are different types and weight percentages of fillers: ZnO, $TiO_2$, BN, with weight percentage from 5% to 12.5%. It's only 50 μm thick, with a good dielectric properties and high emissivity. It can be applied in electronic devices with a small form factor to eliminate hotspots. To eliminate hotspots means, controlling the maximum temperature of hotspots under specified threshold as well as enhancing uniformity of the overall temperature distribution.

Thus, the polymer-filler composites can not only transfer heat into the environment but also redistribute temperature map of the whole device to make it more uniform. Additionally, the effect of radiation coating will be enhanced for the case with small thermal convection. According to Stefan–Boltzmann law, the black-body radiant emittance is proportional to the fourth power of its thermodynamic temperature [Equ. 1-1]. It can be understandable that small thermal convection brings about higher surface temperature, hence more obvious effect of thermal radiation. Besides, the thermal effect of thermal radiation coating also depends on its area, thickness, interfacial thermal resistance, which will be discussed in Chapter 6.

$$j = \sigma T^4 \tag{1-1}$$

In which, $\sigma$ is the Stefan–Boltzmann constant.

The issues of Li-ion battery explosion (Fig. 1.5) have pose potential threaten to public safety and given rise to widespread attentions [4-5]. Based on the above analysis, thermal radiation coating can be adopted to stimulate thermal duration of Li-ion battery system. FEM can be conducted to calculate the peak temperature. Then, using the FEM model parameters and temperature values as the input, machine learning algorithms can be developed to dramatically speed up the prediction.

Fig. 1.5. Li-ion battery explosion for smartphone and electrical car.

As shown in Fig. 1.6, three thermal regimes are observed for Li-ion battery: normal joule heating that can be dissipated in battery pack with external cooling strategy; acceleration stage when solid electrolyte interphase (SEI) begins to be decomposed and self-heating between electrolyte and anode generates gas and more heat; thermal runaway when cathode and anode react rapidly. In the first stage, there is no obvious change on voltage of battery or other detectable parameters. Once the third stage is triggered, the thermo-chemical reaction will happen instantly and uncontrollably. So, if the pattern of second stage is able to be predicted, Li-ion battery explosion can be prevented in time. Machine learning algorithms are used for fast prediction before the onset of thermal runaway. Microprocessor Unit (MPU) and CPU can monitor battery parameters real-timely and input into machine learning models to learn more precisely. Machine learning code will output the likelihood of Li-ion battery explosion, above the threshold of which the battery will be controlled or cut off.

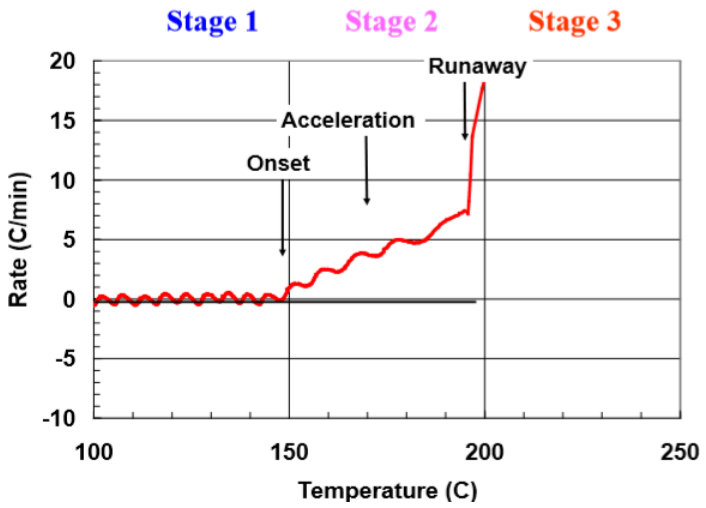


Fig. 1.6. Three thermal stages during forced thermal ramp test of Li-ion Gen 2 [6].

## Reference

[1] M. Y. Tsai, C. H. Chen, and C. S. Kang, “Thermal measurements and analyses of low-cost high-power LED packages and their modules”, Microelectro. Reliability, 52, (5), pp. 845–854, May 2012.

[2] Y. Xi and E. F. Schubert, “Junction–temperature measurement in GaN ultraviolet light-emitting diodes using diode forward voltage method”, Appl. Phys. Lett., 85, (12), pp. 2163-2165, 2004.

[3] Y. C. Chou, G. Kim, L. J. Huang, J. P. You, and F. G. Shi, “Role of Transparent Die Attach Adhesives for Enhancing Lumen Output of Mid-Power LED Emitters with Standard MESA Structure”, IEEE Trans. on Compo. Packag. Manuf. Tech., 2015, 5, (6), pp. 731-736.

[4] J. G. Quintiere, S. B. Crowley, R. N. Walters, R. E. Lyon, and D. Blake. (2016, Febr.). Fire Hazards of Lithium Batteries. National Technical Information Services (NTIS). Virginia. [Online]. Available: https://www.fire.tc.faa.gov/pdf/TC-TN15-17.pdf

[5] D. Doughty and E. P. Roth, “A General Discussion of Li Ion Battery Safety”, The Electrochem. Socie. Interf., 2012.

[6] D. H. Doughty, “Li-ion Battery Abuse Tolerance Testing—An Overview.” *Proc. AABC*, Honolulu, HI, June 2005.

# CHAPTER 2:

# EFFECT OF THINNING ENCAPSULANT LAYER ON JUNCTION AND PHOSPHOR TEMPERATURE OF WHITE LIGHT EMITTING DIODES

## 2.1. Abstract

Thinning of encapsulant layer for light emitting diodes (LEDs) is a current major technological trend. The influence of encapsulant thickness on the junction temperature as well as the maximum phosphor temperature for blue and white LEDs is studied systematically for the first time. By using finite element method (FEM) and forward voltage method (FVM), it is demonstrated that, in contrast to common belief, a thinned encapsulant layer for relatively low power LED emitters with an input electrical power of 0.5W will lead to an increase in the junction temperature for white LEDs fabricated using different methods including phosphor volume distributed in-cup method and chip coating method, as well as for monochromatic blue LEDs. It is also demonstrated that, different from the effect of encapsulant thickness on the junction temperature, a reduction in encapsulant thickness results in a decrease in the maximum phosphor temperature for in-cup white LEDs, and an increase in the phosphor temperature for the chip phosphor-coating white LEDs. For example, the largest phosphor temperature drop of in-cup white LED can be as high as 5°C. The effect of thermal conductivity of leadframe and phsophor concentration under different encapsulant thickness is also indicated.

## 2.2 Introduction

An important industrial trend in white LED emitters is the continuing reduction in package

thickness to meet the need for both backlighting and lighting applications [1-4]. For example, the latest packaged LED emitter as thin as of 0.5 mm has now been in production [5-6]. It is commonly believed that as an encapsulant layer thickness being reduced, its thermal resistance will be reduced[7-9], and thus the contribution of upward thermal conduction is expected to play an increasing role in the overall thermal dissipation of a packaged LED emitter. Therefore, the junction temperature is also expected to decrease with decreasing thickness of encapsulant layer, or the thickness of package. By the same consideration, it is believed that as the thickness of white LED emitter being reduced, its phosphor temperature will also be reduced. However, there is no report on the improved thermal performance of packaged LED emitters as a result of reduced encapsulant thickness or overall package thickness.

Thus, the objective of the present work is to investigate the LED junction temperature as well as the maximum phosphor temperature as a function of encapsulant thickness, for white LED emitters based on the two most often used phosphor application methods, i.e., phosphors are evenly distributed inside encapsulant (in-cup method) or phosphors are evenly coated on the surface of LED chip, i.e., chip coating method [10].

It is found that, a thinned encapsulant will increase the junction temperature of both monochromatic and white LED emitters, in contrast to common belief. A decrease in encapsulant thickness is found to decrease the maximum phosphor temperature by 3-6℃ for in-cup white LED emitters with an input electrical power of 0.5W, while the phosphor temperature for the chip-coating white LED emitters is increased as the encapsulant thickness is reduced. The implications of the results presented are also discussed.

## 2.3 Experimental and Numerical Methods

### 2.3.1 Simulation

3-D Finite Element Method (FEM) is employed to investigate the effect of encapsulant thickness on thermal performance of packaged LED emitters, as schematically shown in Figure 2.1 (a). The blue LED chip is attached to the center of the reflector cup of the leadframe by using a die attaching adhesive. Then silicone encapsulant is dispensed into the cavity of the reflective cup to encapsulate the LED chip. Finally, the packed LED is soldered to an Al-based PCB. By symmetrical consideration, only of a LED emitter is taken into consideration, as indicated in Figure 2.1 (b). The package adopted is a typical 5050 leadframe (5.0x5.0x1.3mm) based package.

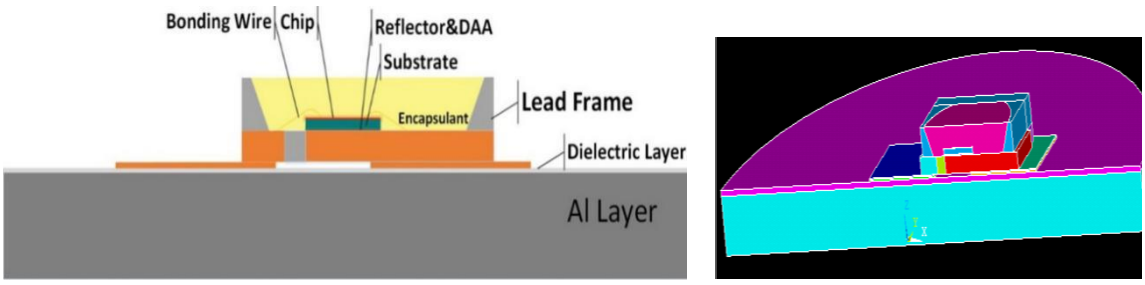


(a) (b)

Fig. 2.1. (a) Cross sectional and (b) 3D schematics of packaged LED emitter used in the work.

The volumetric heat source is taken as uniformly distributed in the chip layer, since the ratio of chip size and PCB size is relatively small. An input electrical power to the LED emitter is taken to be 0.5W and the plug-in efficiency is set as 30%. LED emitter is suspended in the middle of the oven. Therefore, only forced thermal convection ($h=34\ W/m^2K$) boundary condition is applied to surface of the whole model. The encapsulant thickness will be changed from 0.2 to 0.9

mm. Thermal conductivity and geometry information of each component in the LED package model is summed in Table 2.1.

TABLE 2.1. THERMAL CONDCUTIVITY AND GEOMETRY INFORMATION OF EACH LED COMPONENT

| Component | Material | Thickness(mm) | Thermal conductivity |
|---|---|---|---|
| Chip | GaN/AlGaN | 0.887*0.887*0.00365(Width*Length*Thickness) | 130 |
| Substrate | Sapphire | 0.1 | 20 |
| DAA | Silicone | 0.02 | 0.2 |
| Lead | Copper alloy | 0.3 | 259.6 |
| Leadframe | PPA-EMC | 5.0*5.0*1.2(Width*Length*Thickness) | 0.35-0.9 |
| Encapsulant | Silicone | 0.2-0.9 | 0.18-1.0 |
| Reflector | Al | 0.0015 | 237 |
| Dielectric | Epoxy | 0.1 | 0.25 |
| PCB core | Al | 1 (Radius=6.5) | 237 |

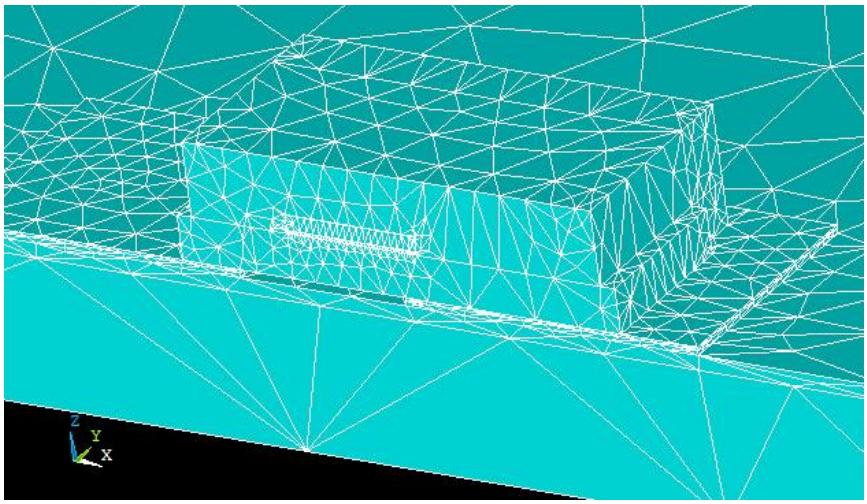


Fig. 2.2. Mesh of the simulation model when the number of element is 19252.

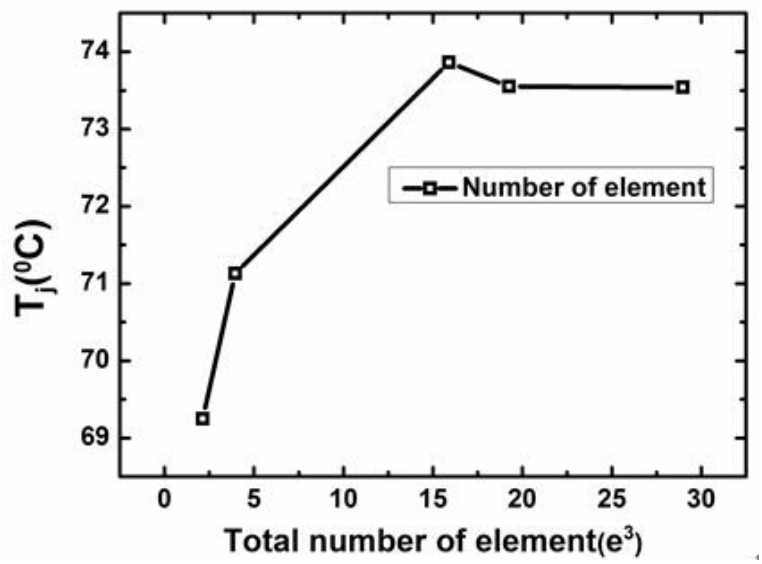


Fig. 2.3. Mesh sensitivity of the simulated junction temperature.

Mesh sensitivity has been an inherent methodological issue for FEM calculation. Figure 2.2 gives the mesh pattern used for the temperature calculation. As can be seen, the mesh density is moderate and doesn't add much burden to the CPU and memory. With the same condition and model, number of element of the whole model is varied from 2124 to 28975 to detect the effect of mesh sensitivity. The first two mesh patterns are obtained by decreasing element number manually while the other three are by setting up auto mesh size level from 10 (coarsest) to 1 (finest). The results presented in Figure 2.3 show that junction temperature can change largely with number of element less than 15K. As the mesh is finer, however, the results tend to be stable. Our typical number of element is around 20K, which is within sensitivity-free range.

### 2.3.2 Experiment

The packaging process is as follows: (1) the 5050 leadframe used in this experiment is cleaned by isopropyl alcohol and baked at 80 ℃ prior to use; (2) the blue LED chip is attached to

the leadframe; (3) the samples are then cured with its proper curing conditions; (4) Wire-bonding is performed to electronically connect the LED chip onto the leadframe; (5) The silicone encapsulant used is Dow Corning 6630; (6) the samples then are cured at 150℃ for 2 hours; (7) LED package is soldered to PCB. Encapsulant of LED is grinded and thinned by 0.2mm each time, from 0.9 mm to 0.2 mm. We did not dispense encapsulant with different thickness because encapsulant is arc-shaped, thickness of which is hard to define and volume of encapsulant added cannot be precisely controlled.

Forward Voltage Method (FVM) is conducted to measure junction temperature of LEDs [11-12]. It is easily operated and has a high precision, the standard error of the junction temperature Tj measurement is less than 0.5℃. First, LEDs with different thickness are positioned at the center of oven, with its electrodes connected to voltage meter. Then, voltage-temperature curves for reference are given by measuring output voltage at temperature of 40℃, 70℃, 100℃, respectively. The input signal is pulsed current, which won't introduce self-heating effect into LED chip. After the LED emitter is cooled down, a steady current of 150mA is added on it for 10 min to get the ultimate output voltage. By fitting voltage-temperature curves for reference, the relationship between voltage and temperature is derived. Finally, the junction temperature of LED with different encapsulant thickness can be obtained [13].

The capability of PCB material to resist higher temperature has been concerned by LED engineers and manufacturers. Hence, the infrared thermal gun is used to measure temperature of PCB under different encapsulant thicknesses.

### 2.4 Results

2.4.1 The Packaged Blue LED Emitters

Figure 2.4 shows the change of junction temperature with encapsulant thickness. As demonstrated, the experimental and simulation results are fully in agreement. For the packaged white LED emitter with an encapsulant thickness of 0.5mm, the measured junction temperature is 74.0℃, while the simulation result is 74.5℃, which is again fully in agreement with each other. Uncertainty analysis is made by testing three times for each sample and drawing the error bar for experimental results. Standard deviation of the average of measured junction temperature is within 0.29℃, which is comparatively small for the junction temperature itself.

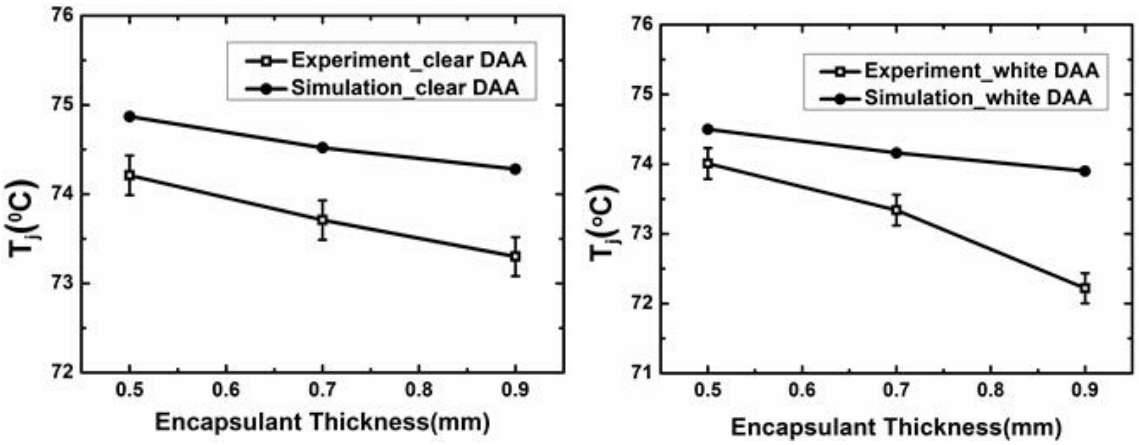


(a) (b)

Fig. 2.4. Junction temperature as function of encapsulant thickness for the packaged LED emitters with (a) clear DAA and (b) white DAA.

A thicker encapsulant leads to a higher thermal resistance, which will result in a higher junction temperature. However, it can be found from Figure 2.4 that the junction temperature for both packaged blue and white LEDs decreases with increasing encapsulant thickness. The apparent

contradictory is due to the effect of thermal spreading resistance. Thermal spreading resistance is defined as the thermal resistance on the heat surface, which can be demonstrated in Eq. (1-1) [14]:

$$R_{spreading} = (T(a,b,c) - \bar{T}(Z=t))/\mathrm{Q} \quad (1\text{-}1)$$

Where $T(a,b,c)$ is the temperature at the center of the surface contact with the heat source, $\bar{T}(Z=t)$ is the average temperature within that surface, and Q is heat power produced by the heat source.

Researchers such as M. M. Yovanovich and Seri Lee have worked on calculation of thermal spreading resistance under different conditions, including isotropic and compound heat flux channel, isothermal and uniform heat flux on heat source [15-16]. In ref. [14], the calculated model with uniform heat flux and constant convective heat transfer coefficient can be applied to analyze our LED model. According to Equation 20 and Figure 6, the dimensionless thermal spreading resistance will increase with thinner plate (in our model, Biot number is 0.238 and dimensionless plate thickness is from 0.36 to 0.64). Figure 2.5 [17] illustrates this thermal spreading resistance effect in LED model. A decreased plate thickness will increase the effect of thermal spreading resistance, which can lead to an increase in the total thermal resistance, and thus an enhanced chip temperature.

In order to further clarify this effect, we calculated $R_{spreading}$ by applying Eq. (1-1) and FEM simulation mentioned in Section II. As can be seen from Table 2.2, spreading thermal resistance will increase with thinner encapsulant layer, as predicted in Figure 2.5.

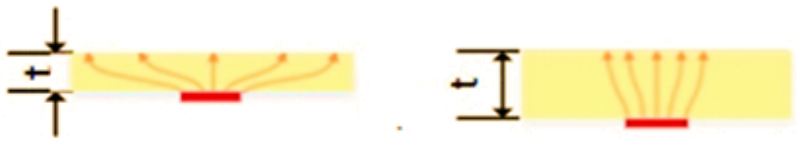

(a) (b)

Fig. 2.5. Schematic drawing of thermal spreading resistance changing from (a) thin to (b) thick encapsulant.

TABLE 2.2. CALCULATED SPREADING THERMAL RESISTANCE WITH DIFFERENT ENCAPSULANT THICKNESSES

| Encapsulant thickness(mm) | | | | |
|---|---|---|---|---|
| 0.3 | 73.48 | 69.66 | 0.35 | 10.91 |
| 0.5 | 73.1 | 69.56 | 0.35 | 10.11 |
| 0.9 | 72.48 | 69.32 | 0.35 | 9.03 |

In addition, a thinner encapsulant leads to a reduced available surface area for thermal convection, which can contribute to the increase of the total thermal resistance and thus the junction temperature.

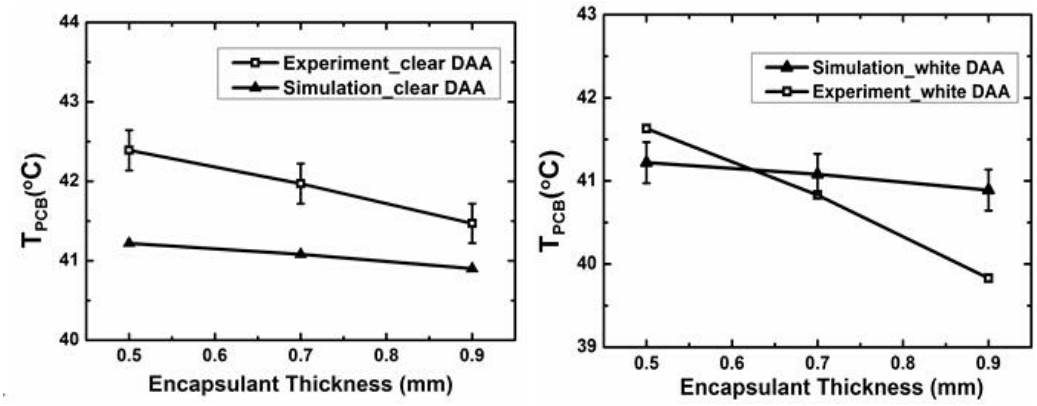


(a) (b)

Fig. 2.6. Change of PCB surface temperature with different encapsulant thickness for (a) clear DAA and (b) white DAA.

Measurement of PCB temperature was also conducted to verify the simulation results. Figure 2.6 shows the effect of encapsulant thickness on temperature of PCB surface. The simulation results are in good agreement with experimental results. PCB temperature is lower with thicker encapsulant because the corresponding junction is cooler. The change is slight, which means thickness of encapsulant will not affect the thermal reliability of PCB.

In summary, a thinning of encapsulant for blue LED will lead to an increase in the LED junction temperature. Such an increase is relatively small for low input electrical power of 0.5W, and there is a potential for further reduction in packaged LED emitter thickness for low input electrical power (0.5W). In addition, the agreement between the experimental and the simulation results for the present relatively non-complicated case, i.e., the junction temperature of blue LED emitters, serve as the verification of the simulation methods used.

### 2.4.2 Packaged White LED Emitters

For white LED emitters, heat generation of phosphor layer has been studied thoroughly

[18-21]. Figure 2.7 illustrates the simulation model and temperature distribution of apackaged white LED emitter with consideration of phosphor heat generation. In-cup and chip-coating phosphor configurations are generally used in low- and mid-power white LED application and are analyzed herein. For both phosphor coating and in-cup phosphor case, the thermal conductivity of phosphor-silicone composite is taken to be 0.2262 W/mK with phosphor weight percentage of 37% and thickness of phosphor layer is 0.1mm [17]. 70% of total power of 1W is set to be transferred into heat within the chip. The heat power of chip is 0.5W*70%=0.35W. Phosphor emission efficiency is set to 50%. So the heat power of phosphor layer is 0.5W*30%*50%=0.075W. It is assumed that phosphor particles are uniformly dispensed into the encapsulant layer and the heat generation rate (heat power per volume of phosphor layer) is constant within phosphor layer. Then the heat generation rate of chip and phosphor can be calculated by dividing heat power with the corresponding volume, the information of which has been given in Section IIA. The boundary condition applied is same as mentioned in the previous simulation part.

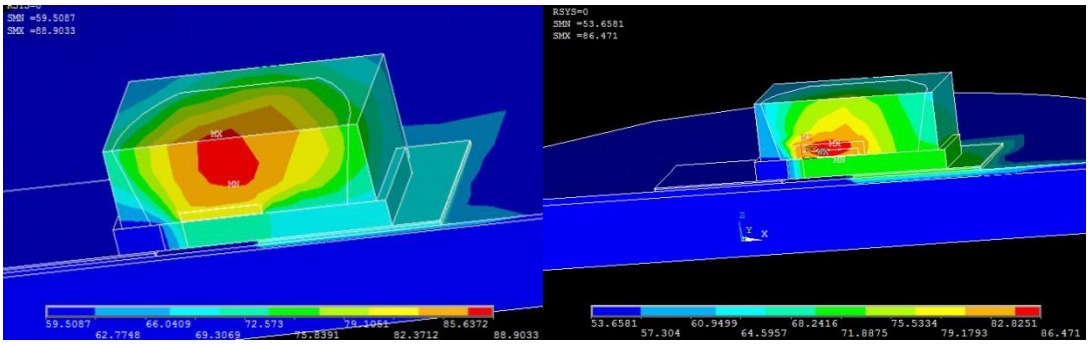


(a) (b)

Fig. 2.7. Temperature distribution for (a) in-cup and (b) phosphor chip coating white LED emitters.

A hotspot shift phenomenon can be observed, especially for the in-cup case. Figure 2.8 shows the simulated temperature distribution for both in-cup and chip-coating cases with different encapsulant thicknesses. It is evident that for the in-cup case, hotspot will shift from the junction to the upper surface of encapsulant when the encapsulant thickness is increased. However, for the chip coating case, the hotspot only shifts slightly and the maximum temperature decreases with larger encapsulant thickness.

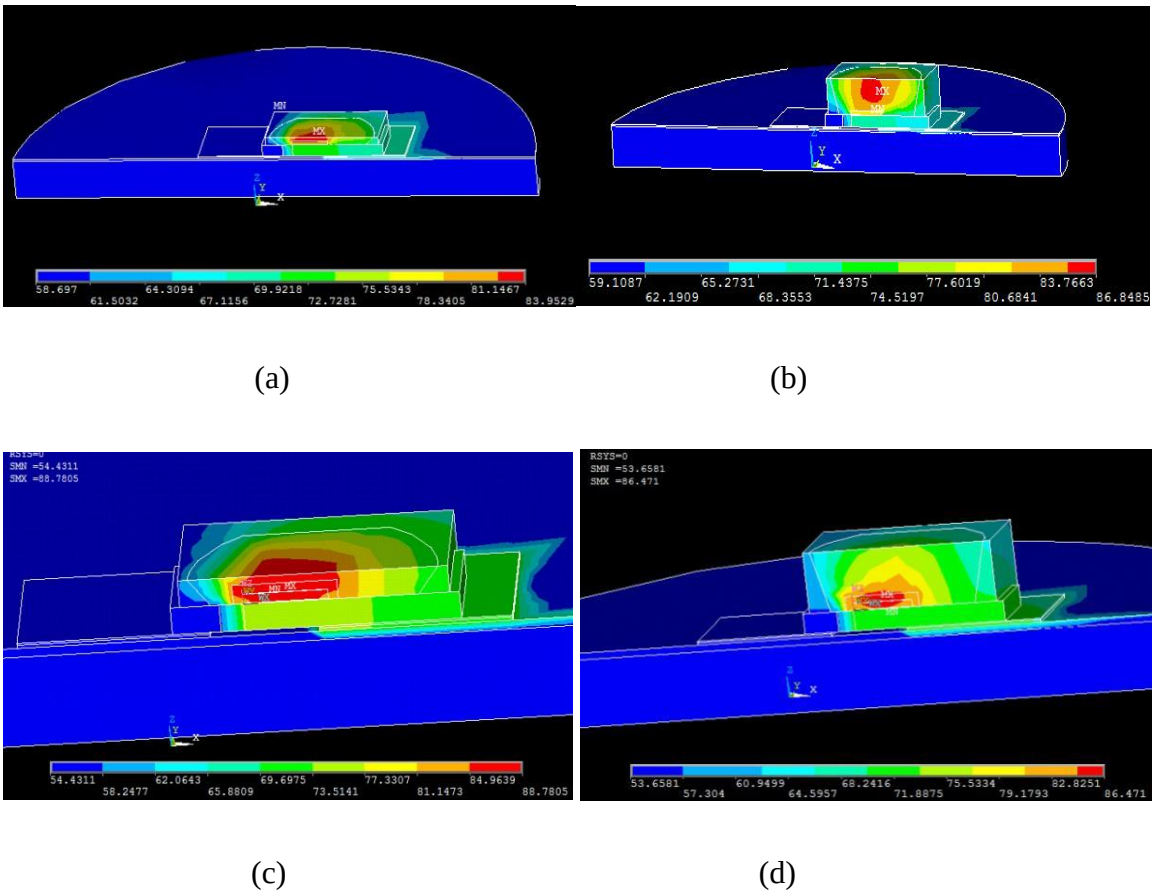


(a) (b)

(c) (d)

Fig. 2.8. Hotspot shift phenomenon of white LED with encapsulant thicknesses from (a) 0.2mm to (b) 0.9mm for in-cup case and from (c) 0.3mm to (d) 0.9mm for phosphor chip-coating case.

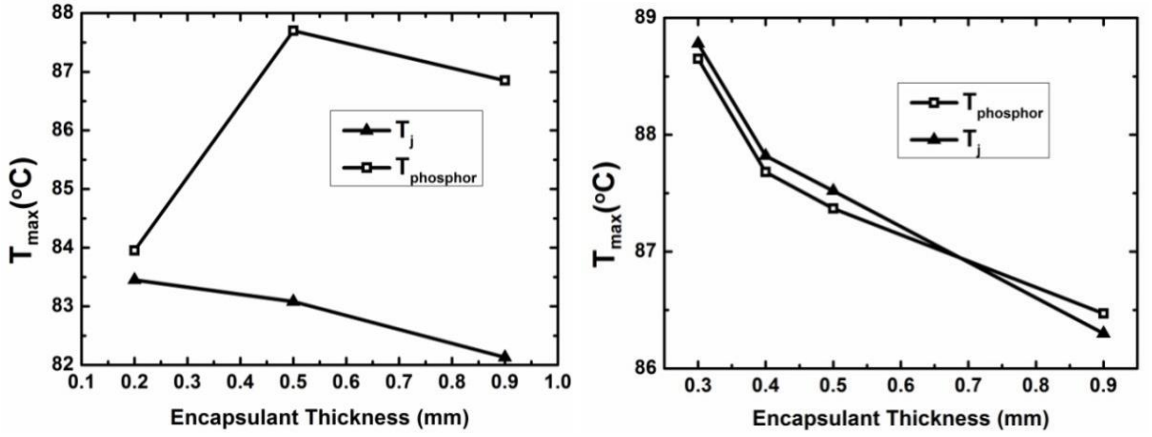


(a) (b)

Fig. 2.9. Maximum temperature of phosphor layer and junction changes with different encapsulant thicknesses for (a) in-cup and (b) chip-coating cases.

Figure 2.9 gives maximum temperature of both phosphor layer and junction under different encapsulant thickness. As seen in Figure 2.9 (a), for in-cup case, maximum phosphor temperature increases with larger encapsulant thickness, contrast to that of blue LEDs. For chip-coating cases, with encapsulant thickness being reduced, both junction and phosphor temperatures are higher. For in-cup cases with different phosphor concentration, thickening encapsulant can raise $T_{phos}$ by 3-6℃. Hence, phosphor breakdown issue with different encapsulant thicknesses should be paid attention.

Chip-coating white LEDs are similar to blue LEDs with a more complex heat source formed by both chip and phosphor layer. For in-cup case, when encapsulant is thicker, the effective heat source of phosphor-silicone composite (at the center of encapsulant layer) is farther from another heat source-the chip. And since thermal conductivity of encapsulant is as low as 0.2W/m-K, heat dissipated from phosphor is restricted within encapsulant and accumulates. But when the

encapsulant is still thicker, thermal power density within phosphor-silicone composite is further reduced, and thus maximum phosphor temperature will be also decreased.

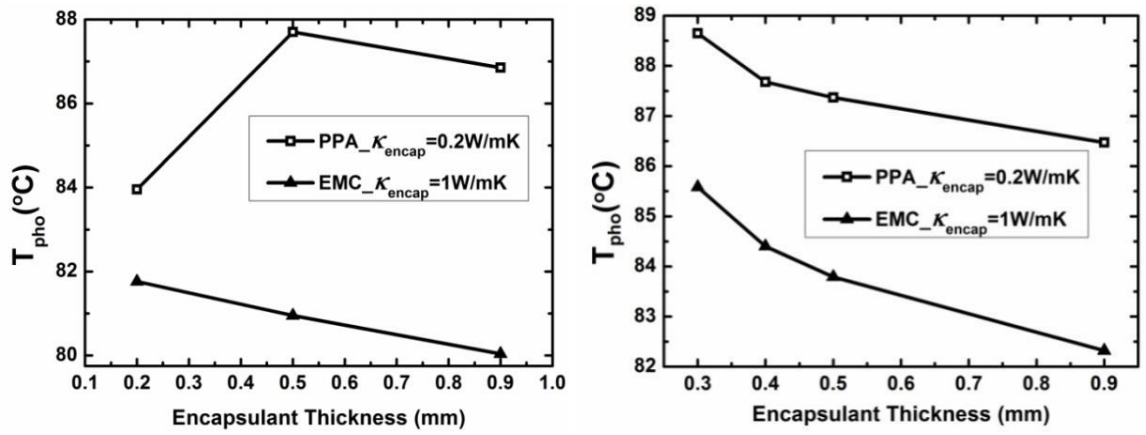


(a) (b)

Fig. 2.10. $T_{phos}$ vs. $H_{encap}$ with different encapsulant and leadframe for (a) in-cup phosphor and (b) phosphor coating case.

Figure 2.10 is the maximum temperature of phosphor layer changing with encapsulant thickness under different encapsulant and leadframe materials. It suggests that increasing thermal conductivity of encapsulant and leadframe can decrease the higher phosphor temperature brought by thinner encapsulant. For chip-coating case, phosphor temperature is more stable and can be pulled down by 3-4℃. For in-cup case, phosphor temperature is reduced by 7℃. The temperature reduction is because, with thermal conductive encapsulant, upward thermal dissipation is strengthened. By using epoxy molding compound (EMC) which has a higher thermal conductivity, thermal resistance of leadframe is reduced and more heat can be blew away by thermal convection. This result may stimulate the market demand of thermal conductive encapsulant and EMC.

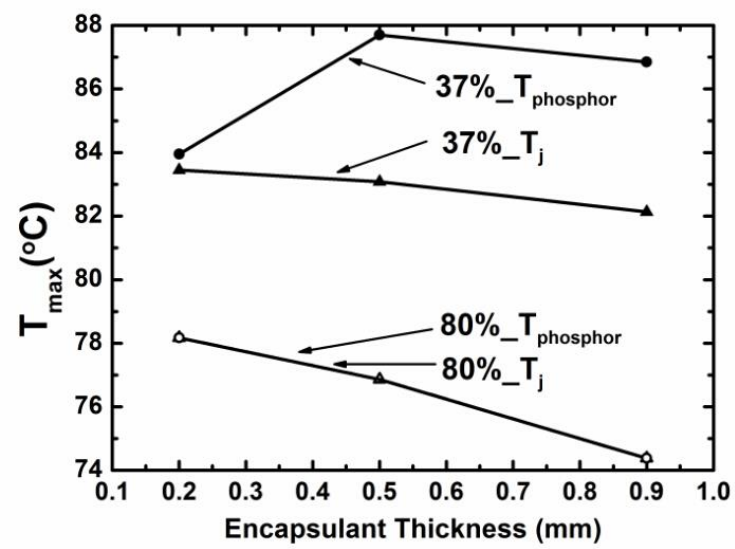


Fig. 2.11. Maximum phosphor and junction temperature as function of phosphor weight percentage and encapsulant thickness.

The effect of phosphor concentration on thermal performance of in-cup phosphor white LED is demonstrated in Figure 2.11. Higher concentration of phosphor can increase thermal conductivity of phosphor-encapsulant composite, which enhances thermal dissipation within chip-coating LEDs. Another observation is that when phosphor weight percentage is higher than 50%, maximum temperature of phosphor and junction tends to be identical with each other.

## 2.5. Conclusions

Thermal performance of mid-power LED with different encapsulant thicknesses is studied in this paper. Both FEM simulation and FVM experimental method are employed. We thinned the LED by grinding the ecapsulant layer and obtained the junction temperature by detecting the forward voltage of LED. Contrary to common understanding, junction temperature can be increased when thinning LED emitters. Furthermore, mesh sensitivity analysis of the LED

finite element model is also provided to reduce result uncertainty. For chip coating white LED, maximum phosphor temperature tends to decrease with encapsulant thickness; while phosphor temperature of in-cup phosphor LED has the opposite behavior at first. Some suggestions can be provided for LED thickness design: (1) for monochromatic LED, thickness of encapsulant has slight impact on junction and PCB temperature, thus it is safe to change the encapsulant thickness; (2) there is a peak phosphor temperature when encapsulant thickness is changed for in-cup phosphor LED, which should be treated carefully; (3) thermal conductive encapsulant and EMC leadframe can compensate temperature increase within LED; (4) phosphor concentration can also change thermal behavior of phosphor layer with different encapsulant thicknesses. Further work may include the influence of encapsulant thickness on COB (chip on board) LED and smaller package strategy, such as CSP (chip scale package).

**Reference**

[1] F. T. Kim, C. R. Lee, D. Kim, and B. F. Baek, "Parametric study of efficient thermal dissipation in a LED back light unit", *Microeletro. Int.*, 2011, 28, (3), pp. 12-18.

[2] Led package with encapsulant having planar surfaces, by T. Lowes, E. Tarsa, S. Heikman,B. Keller, J. Reiherzer, H. Benjamin. (2015, March 18). US Patent 20150194580 A1.

[3] G. H. Liu, Z. Z. Zhou, Y. Shi, Q. Liu, J. Q. Wan, Y. B. Pan, ″Ce: YAG transparent ceramics for applications of high power LEDs: Thickness effects and high temperature performance″, Material Let., 2015, 28, (3), pp. 12-18.

[4] G. A. Luiten, “Thermal challenges in LED-driven display technologies: state-of-the-art,” in *Thermal management for LED applications*, New York: Springer, 2013, pp. 477.

[5] R. Rao, B. Mos, T. Overes, E. H.A. Langendijk, “Masking LED hotspots in a thin direct lit back light unit using semitransparent and perforated masks”, *Optics Commun.*, 2013.

[6] S. K. Kim, “Analysis on thermal management schemes of LED backlight units for liquid crystal displays”, *IEEE Trans. on Compo. Packag. Manuf. Tech.*, 2012, **2**, (11), pp. 1838-1846.

[7] E. Juntunen, O. Tapaninen, A. Sitomaniemi, V. Heikkinen, “Effect of phosphor encapsulant on the thermal resistance of a high-power COB LED module”, *IEEE Trans. on Compo. Packag. Manuf. Tech.*, 2013, **3**, (7), pp. 1148-1154.

[8] F. S. Hwu, H. C. Cheng, Y. H. Hu, G. J. Sheu, “The influence of the thermal resistance of LED packaging with different submount and surrounding conditions”, *Trans. Canadian Society for Mech. Engineering*, 2013, **37**, (3), pp. 765.

[9] L. Kim, W. J. Hwang, M. W. Shin, “Thermal Resistance Analysis of High Power LEDs with Multi-chip Package”, in *IEEE Electr. Compo. Tech. Conf.*, June 2006, pp. 1076-1081.

[10] H. Luo, J. K. Kim, E. F. Schubert, J. Cho, C. Sone, and Y. Park, “Analysis of high-power packages for phosphor-based white-light-emitting diodes”, *Applied Phy. Lett.*, 2005, **86**, pp. 243505-1-243505-4.

[11] J. P. You, N. T. Tran, and F. G. Shi, “Light extraction enhanced white light-emitting diodes with multi-layered phosphor configuration”, *Opt. Exp.*, 2010, **18**, (5), pp. 5055-5060.

[12] J. P. You, N. T. Tran, Y. C. Lin, Y. He, and F. G. Shi, “Phosphor-Concentration-Dependent characteristics of white LEDs in different current regulation modes”, *J. Electro. Material*, 2010, **38**, (6), pp. 761-766.

[13] Y. Xi, and E. F. Schubert, "Junction-temperature measurement in GaN ultraviolet light-emitting diodes using diode forward voltage method", *Applied Phy. Lett.*, 2004, **85**, (12), pp. 2163-2165.

[14] Y. S. Chen, K. H. Chien, Y. S. Tseng, Y. K. Chan, "Determination of optimized rectangular spreader thickness for lower thermal spreading resistance", *J. Electron. Packag.* 2009, **131**, 011004.

[15] S. Lee, S. Song, V. Au, K. P. Moran, "Constriction/spreading resistance model for electronics packaging", *ASME/JSME Thermal Engineering Conf.*, 1995, **4**, pp. 199-206.

[16] Y. S. Muzychka, J. R. Culham, M. M. Yovanovich, "Thermal spreading resistance of eccentric heat sources on rectangular flux channels", *Trans. of the ASME*, 2003, **178**, (125), 2013.

[17] K. S. Yang, C. H. Chuang, C, W. Tu, *et al.*, "Thermal spreading resistance characteristics of a high power light emitting diode module", *Applied Thermal Engin.*, 2014, **70**, pp. 361-368.

[18] B. Yan, N. T. Tran, J. P. You and F. G. Shi, "Can junction temperature alone characterize thermal performance of white LED emitters?", *IEEE Photonics Tech. Lett.*, 2011, **23**, (9), pp. 555-557.

[19] X. B. Luo, and R. Hu, "Calculation of phosphor heat generation in phosphor-converted light-emitting diodes", *Int. J. Heat and Mass Transfer*, 2014, **75**, pp. 213-217.

[20] X. B. Luo, X. Fu, F. Chen, and H. Zheng, "Phosphor self-heating in phosphor converted light emitting diode packaging", *Int. J. Heat and Mass Transfer*, 2013, **58**, pp. 276-281.

[21] R. Hu, X. Luo, and H. Zheng, "Hotspot location shift in the high-power phosphor-converted white light-emitting diode packages", *Jpn. J. Appl. Phys.*, 2012, **51**, 09MK05.

# CHAPTER 3:

# ENCAPSULANT THICKNESS OPTIONS AS A FACTOR TO IMPACT THERMAL PERFORMANCE OF CHIP-ON-BOARD (COB) LIGHT EMITTING DIODES

## 3.1 Abstract

There is an important trend in light emitting diodes (LED) industry to produce continuously thinner package. Chip-on-Board (COB) packaged LED, as a promising thermal efficient package structure, has rarely been investigated for its thermal performance under smaller package thickness. In this work, encapsulant or overall package thickness as a factor to influence the junction temperature as well as the maximum phosphor temperature for COB LEDs is presented. Finite element method (FEM) is employed and validated by forward voltage method (FVM). As shown in the results, for single-chip COB LEDs with standard MESA structure and volume distributed phosphor, there is a lowest point in the maximum temperature while thinning encapsulant layer. But for multi-chip COB LEDs, the junction and phosphor temperature will be reduced with thinner encapsulant. In both cases, the largest deviation of the maximum temperature with different encapsulant thickness can be more than 10℃. Parametric studies of other critical factors such as different Die Attach Adhesive (DAA) materials and radius of encapsulant while thinning encapsulant thickness are also provided. There are two ways to enlarge the input power of COB LED: one is to raise the input power into each chip; the other is to increase the number of chips. It's interesting to find the different thermal behaviors for the two cases. Larger input power will cause a more stable maximum temperature for COB LEDs. While more chips lead to higher variation of the maximum temperature with respect to encapsulant thickness.

## 3.2 Introduction

Recently, research on ultra-thin LED package is further stimulated by the enormous market demand for backlighting and mobile electronics [1-3]. As indicated in [4], the thinnest surface-mount device (SMD) LED package is only 0.25mm. It is figured out by Huang [5] that, while thinning encapsulant layer, there is a peak value of the maximum temperature, instead of decreased maximum temperature as is commonly considered. COB LED package, which mounts LED chips directly on board, can considerably decrease junction-to-case thermal resistance Rj-c and dissipate heat in an effective way. Therefore, thermal performance of single-chip or multichip COB LED packages has been broadly investigated [6-8]. However, no paper as known by the author has been published about thermal analysis of COB packaged LED with reduced encapsulant thickness or overall package thickness.

Thus, this work aims to study thermal performance of COB packaged LED changed with encapsulant layer thickness. Both junction temperature and the maximum phosphor temperature are calculated. COB LEDs with standard MESA structure and phosphor volume distributed encapsulant is adopted here.

The results shows that a thinned encapsulant will cause a lowest maximum temperature for single-chip COB LED. But for multichip COB LED, a decrease in encapsulant thickness is found to decrease the maximum phosphor temperature as well as junction temperature. Parametric studies for different DAAs and radius of encapsulant under different encapsulant thickness are also discussed.

## 3.3 Numerical Methods

In order to study the factor of encapsulant thickness in thermal analysis of COB packaged LED emitters, 3-D Finite Element model employed in this paper is schematically shown in Fig 3.1 (a). Half of the model is considered because of its symmetry. Firstly, both clear and white DAAs are utilized to directly mount blue LED chips onto Printed Circuit Board (PCB) within the emitting area. Secondly, encapsulant made of silicone-phosphor composite is uniformly dispensed into the circular cavity. Thirdly, the packed PCB is attached to straight fin heat sink with Thermal Interface Material (TIM). The COB LED package referred is Citizen CLU025 series. Single-chip COB LED model was first developed for simplicity and then extended to multichip case.

Forward Voltage Method (FVM) has been attempted to experimentally verify a similar SMD LED package FEM model. The detailed procedures can be reached in [5]. The only difference between the models in [5] and this work is lead layer, whose thermal resistance occupies little portion of junction-to-case thermal resistance $R_{j\text{-}c}$. Thus the simulation model mentioned above can be considered feasible.

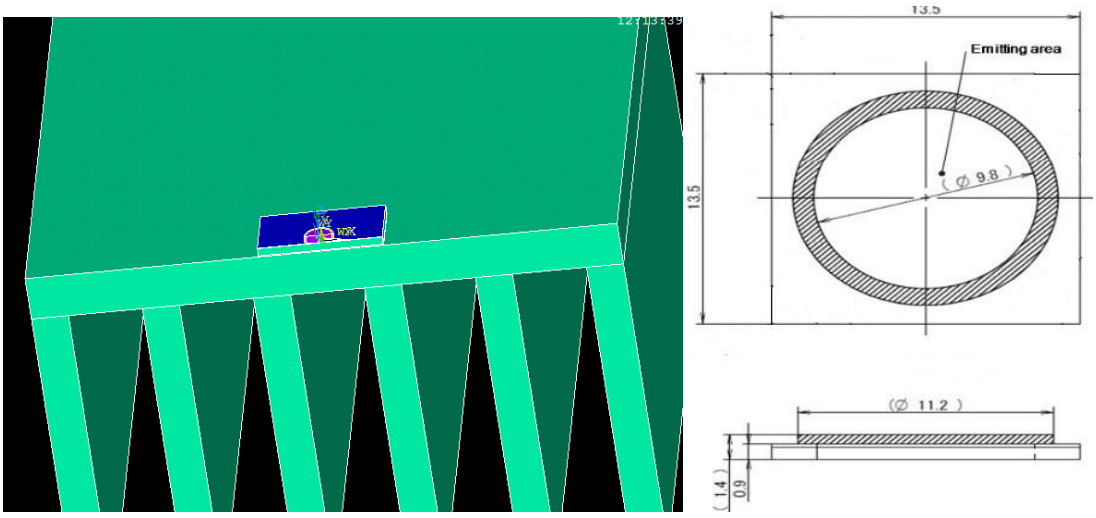


(a) (b)

Fig. 3.1. (a) 3D schematics of COB LED (for both single-chip and multi-chip cases) with

heat sink. (b) Detailed dimensional information of COB packaged LED.

Because each LED chip is small compared with PCB layer, the temperature distribution non-uniformity can be ignored and the chip layer is considered as heat source with constant heat generation rate. The electric power input onto each chip is set as 0.5W if not specified otherwise. And plug-in efficiency is assumed to be 30%, which means 70% of total electric power is transferred into thermal power. Thus the heat generation rate is the thermal power divided by volume of LED chip. Further, Surface of the whole model is applied with forced thermal convection (h=34 $W/m^2K$). The range of encapsulant thickness is within 0.3-0.9 mm. Thermal and size information of COB LED package materials is summarized in Table 3.1.

TABLE 3.1. THERMAL CONDUCTIVITY AND GEOMETRY INFORMATION OF EACH LED COMPONENT

| Component | Material | Thickness (mm) | Thermal conductivity (W/m-K) |
|---|---|---|---|
| Chip | GaN/AlGaN | 0.887*0.887*0.00365(Width*Length*Thickness) | 130 |
| Substrate | Sapphire | 0.1 | 20 |
| DAA | Silicone | 0.02 | 0.2 |
| Lead | Copper alloy | 0.3 | 259.6 |
| Leadframe | PPA-EMC | 5.0*5.0*1.2 (Width*Length*Thickness) | 0.35-0.9 |
| Encapsulant | Silicone | 0.2-0.9 | 0.18-1.0 |
| Reflector | Al | 0.0015 | 237 |
| Dielectric layer | Epoxy | 0.1 | 0.25 |
| PCB&heat | Al | 1 (Radius=6.5) | 237 |

### 3.4 Results

3.4.1 Single-chip COB LED

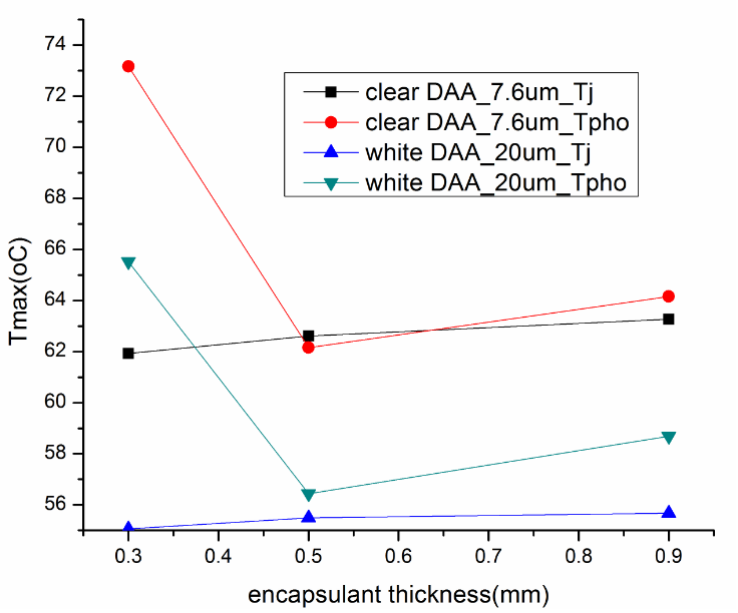


Fig. 3.2. The effect of encapsulant thickness on maximum temperature of COB LED under two typical DAAs.

According to Fig. 3.2, with increased encapsulant thickness, there is a lowest maximum temperature of COB LED investigated. At first, the maximum temperature drops dramatically to a lowest point. One reason is with thicker encapsulant layer, the outer surface of LED package for thermal convection is larger and more heat can be dissipated into air by thermal convection. The other reason is the spread thermal resistance within encapsulant layer will be decreased with larger encapsulant thickness. Thus the overall thermal resistance is smaller, which enhances heat transportation. When encapsulant thickness exceeds 0.5mm, however, the maximum phosphor temperature rises slowly. This is because with certain amount of phosphor (to keep constant correlated color temperature (CCT)), thicker encapsulant layer means larger volume of encapsulant, which has a poor thermal conduction. As encapsulant layer is even thicker, more and

more heat generated by phosphor particle is accumulated within encapsulant layer. So the maximum phosphor temperature is increased instead. It also shows that junction temperature keeps stable as encapsulant thickness changes.

Although clear DAA has a smaller thickness (typically 7.6 μm), it still introduces a higher maximum temperature to LED. Comparatively, LED with thicker white DAA, can cool down phosphor temperature in a large extent. This indicates that white DAA is a better choice than clear DAA in the view of thermal management. According to research in our lab, LED with white DAA has similar optical properties that that with clear DAA. In this sense, we should wisely chose white DAA to better LED performance.

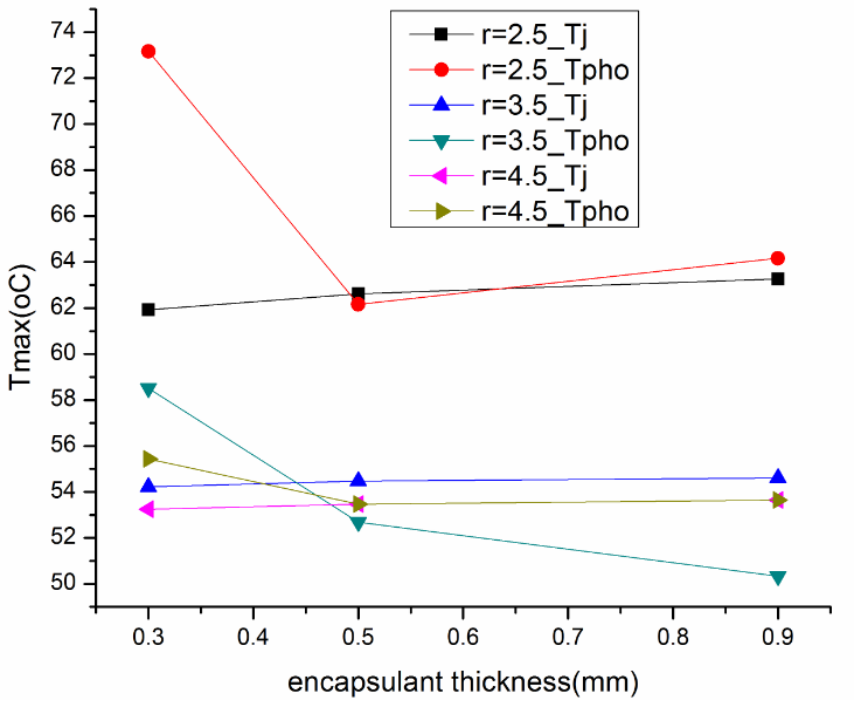


Fig. 3.3. Radius of encapsulant layer as a factor for encapsulant thickness-maximum temperature relationship.

With different radius of encapsulant layer, thermal behavior of phosphor layer as well as junction changes. On one hand, the difference between phosphor and junction temperature is smaller with larger radius of encapsulant. On the other hand, the point of lowest maximum temperature shifts with the encapsulant radius. When the encapsulant radius is as large as 4.5mm, phosphor and junction temperature is already close to each other and encapsulant thickness won't affect the maximum temperature much.

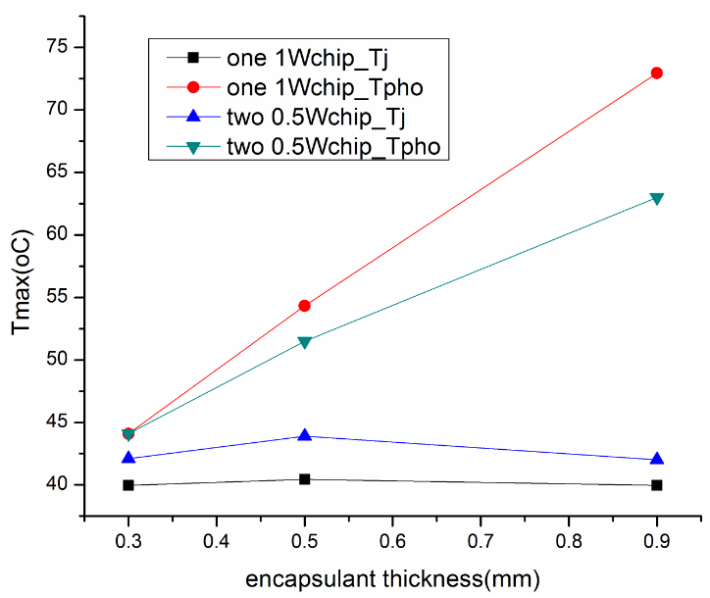


Fig. 3.4. Comparison between the case of one 1W chip and that of two 0.5W chips.

As we can see, power consumption (1W) is the same, but the thermal behavior is different. The maximum temperature, which is phosphor temperature here, of LED with one 1W chip is higher than that with two 0.5W chips. And the temperature difference is increased with thicker encapsulant. This is a proof from thermal perspective that, LED with multiple small-power chips has a better thermal performance than that with single high-power chip. CCT is 3000K here.

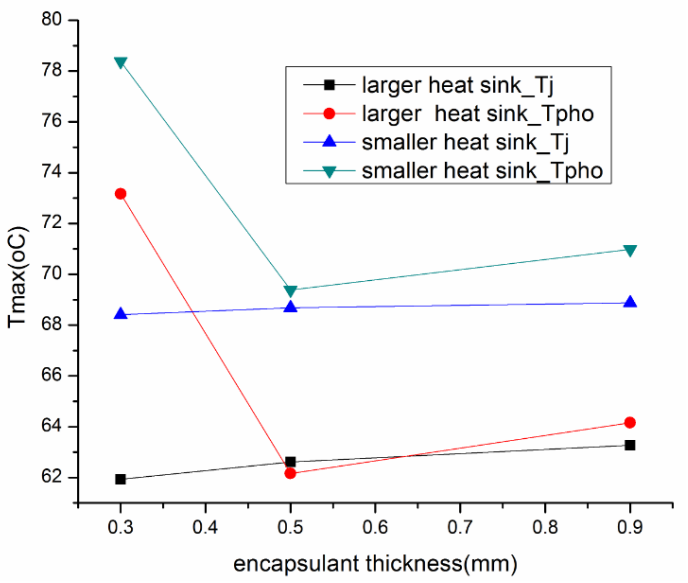


Fig. 3.5. Encapusulant thickness vs. the maximum temperature, with different sizes of heat sink.

For COB LED with a few chips or single chip, the heat sink can't be too big for the cost and package reason. However, with smaller heat sink, the thermal issue of LED will arise. One way to handle this is painting a thermal radiative coating to it. The coating is cost effective and can cool down the LED further according to our previous simulation results.

### 3.4.2 Multichip COB LED

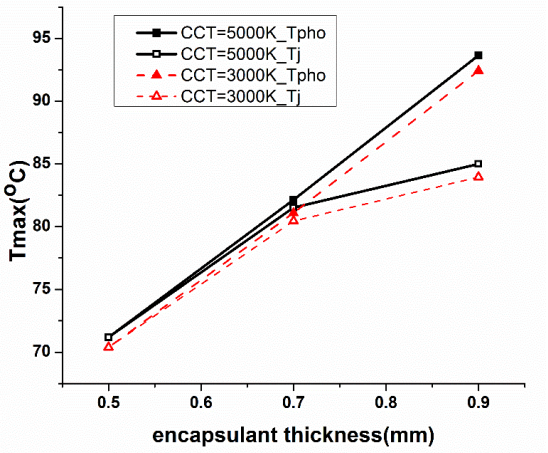

Fig. 3.6. Max. phosphor and junction temperature vs. encapsulant thickness for multichip COB LED (with different CCT).

Single chip COB LED module is extended to multichip COB case (12 chips in series and 2 chips in parallel). The gap between neighboring chips is 0.19mm. As can been seen in Fig. 3.6, instead of a lowest temperature while changing encapsulant thickness, both junction and phosphor temperature will increased with encapsulant thickness. For multichip COB LED, the effect of phosphor heating is more dominate than that of thermal convection mention in Section 3.4.1. With lower CCT, maximum temperature drops. When encapsulant thickness is larger than 0.7mm, the thicker encapsulant layer is, the higher difference between junction and the maximum phosphor temperature.

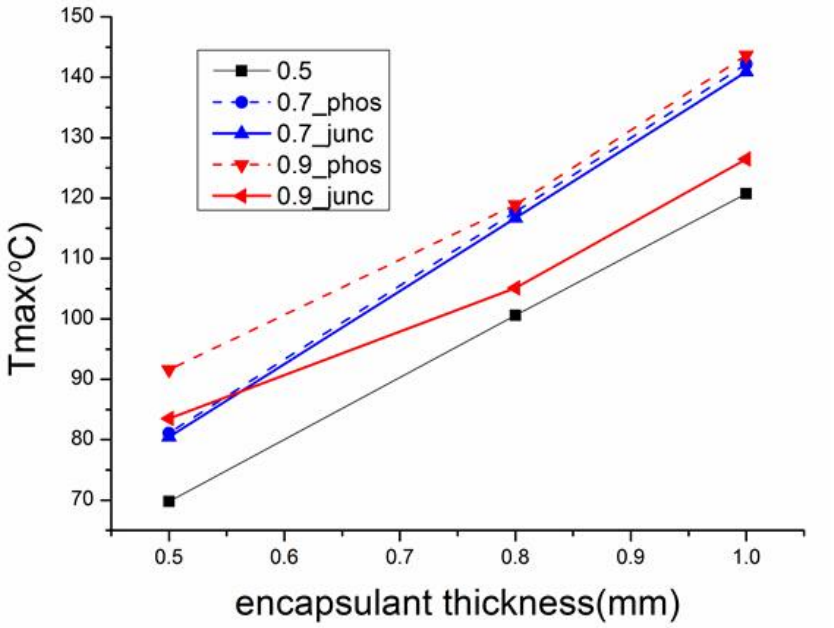


Fig. 3.7. Maximum temperature vs. encapsulant thickness with input power for each chip.

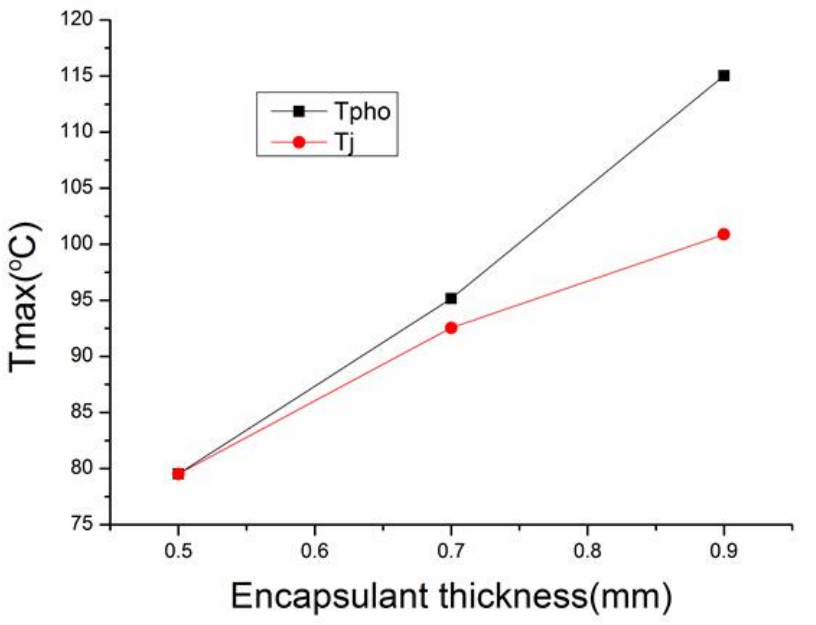


Fig. 3.8. Maximum temperature vs. encapsulant thickness with 36 number of chips.

To change total electrical power consumed, there are two strategies: change input power on each chip from 0.5W to 0.75W; change the number of chips from 24 to 36. According to fig. 3.8, increasing the number of chips won't change the thermal behavior of COB LED with different encapusulant thickness much. While raising input power for each chip in Fig. 3.7, the maximum temperature tends to be stable for encapuslant thicker than 0.7mm.

### 3.5 Conclusions

In this paper, it is indicated that encapsulant thickness is an import factor to affect thermal behavior of both single-chip and multichip COB packaged LED. 3-D FEM model is established to study the effect of encapsulant thickness and verified by the experimental work in [5]. According to the numerical results, there is a lowest value of the maximum temperature while increasing

encapsulant thickness from 0.2-0.9mm for single-chip COB LED. For the multichip case, however, the maximum temperature will keep rising with larger encapsulant thicknes. Other critical parameters such as different DAAs, radius of encapsulant layer, CCT are also investigated to help systematically understand the effect of encapsulnat thickness. To increase the overall input power, more chips and larger input power for each chip can result in different variation of the maximum temperature with encapsulant thickness.

**Reference**


[1] Y. J. Tsai, R. C. Lin, H. L. Hu, et al., "Novel electrode design for integrated thin-film GaN LED package with efficiency improvement", *IEEE Photonics Tech. Lett.*, 2013, 25, (6), pp. 609-611.

[2] E. J. Seo, "Slim LED package," U.S. Patent 8963196, Feb. 24th, 2015.

[3] R. Rao, B. Mos, T. Overes, E. H.A. Langendijk, "Masking LED hotspots in a thin direct lit back light unit using semitransparent and perforated masks", *Optics Commun*., 2013.

[4] Kingbright's 0.25mm Ultra-Thin 0603 SMD LEDs. Kingbright Comp., CA. [Online]. Available: https://www.digikey.com/us/en/ph/Kingbright/SMDLEDs.htl?WT.z_Tab_Cat=Featured%20Products

[5] L. J. Huang, Y. C. Shih, and F. G. Shi, "Effect of Thinning Encapsulant Layer on Junction and Phosphor Temperature of White Light-Emitting Diodes", *IEEE Trans. on Compo. Packag. Manuf. Tech.*, 2015, 5, (11), pp. 1628-1634.

[6] S. P. Ying and W. B. Shen, "Thermal analysis of high-power multichip COB light-emitting

diodes with different chip sizes", IEEE Trans. Electr. Device, 2015, 62, (3), pp. 896-901.

[7] S. Labau, N. Picard, A. Gasse, et al., "Chip on board packaging of light emitting diodes and thermal characterizations", Electro. Compo. Tech. Conf., 2009, pp. 848-853.

[8] M. Ha and S. Graham, "Development of a thermal resistance model for chip-on-board packaging of high power LED arrays", Microelec. Reliability, 2012, 12, pp. 836-844.

# CHAPTER 4:

# IMPACT OF LED PACKAGING MATERIALS ON THERMAL PERFORMANCE OF EMC BASED WHITE LEDS AND LIGHT BARS IN DIRECT VIEW LED BACKLIGHT UNITS (DLED-BLUS) FOR LARGE SIZE LCD DISPLAYS

## 4.1 Abstract

Thermal control coating materials with high cooling effect are critical in many applications Epoxy Mounding Compound (EMC) based white light-emitting diodes (WLEDs) have gained its popularity for direct view LED backlight units (DLED-BLUs) because of their high heat and yellowing resistance. Therefore, impact of packaging materials on input power levels of EMC based WLEDs for DLED-BLU light bars in large size liquid crystal display (LCD) is systematically investigated in this work. Raising the input power to each light bar means, less light bars are needed to meet the total power and brightness requirement. The results show that, by adopting thermal conductive die attach adhesive (DAA) and thicker encapsulant layer, power level of each light bar can be increased by up to 1.5 times. This means, for every 3 light bars, cost of 1 light bar can be saved for the LED BLU in LCD. The effect of EMC on WLED failure is also discussed.

## 4.2 Introduction

Backlighting for large size LCD displays is now rapidly moving to the DLED type because of its advantages in cost and quality [1-4]. In fact, more than 60% of LCD TVs produced in 2015

are estimated to be DLED-BLU based. The mainstream white LEDs used for DLED BLUs are mainly 2538 and 3030 package based. There is a need to increase the power level for each WLED emitter and thus its lumen output, so that the number of LEDs as well as the number of light bars used in DLED-BLUs might be reduced. Besides, over the last two to three years, there is a great shift in moving polyphthalamide (PPA) based packages to polycyclohexylene-dimethylene terephthalates (PCT) based packages and to EMC packages [5]. This is because the thermal-radiation resistance of leadframe reflector increases in the order of PPA, PCT and EMC and thus the latest WLED emitters used in DLED-BLUs are now mainly EMC based. The objective of the present work is to conduct a systematic investigation of EMC based WLEDs, to determine the impact of package materials including leadframe reflector, die attach adhesive, encapsulant and Printed Circuit Board (PCB) on possible input power to the emitters as well as the light bars.

It is found that the hotspot is located in the center of encapsulant layer and the junction will reach the critical temperature before EMC does. The cause of yellowing on EMC should be due to the combination of radiation and thermal degradation [6]. Besides, by using the thermal conductive DAA developed by our lab [7], the input power to the light bar can be increased by 1.4 times. This means that, for every seven light bars, 2 of them can be saved to meet the total power or brightness requirement. Furthermore, by adopting both thermal conductive DAA and thicker encapsulant, an input power raise of 50% can be even achieved.

### 4.3 Numerical Methods

3-D Finite Element Method (FEM) is employed to scrutinize the effect of different packaging materials on thermal performance of LED light bars, as schematically shown in Fig. 4.1 [8]. Six blue LED emitters are directly attached to the PCB layer by using DAAs. Flat

encapsulation is formed by dispensing the composite of silicone and phosphor onto the chip. Finally, the packed PCB is soldered to the aluminum heat sink.

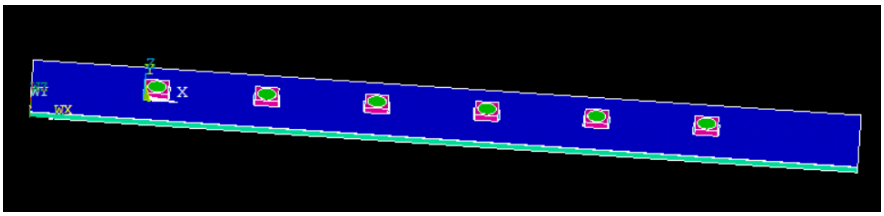

Fig. 4.1. 3-D schematics of light bar.

The volumetric heat source is taken as uniformly distributed in the chip layer, since the ratio of chip volume and PCB volume is relatively small. The input electrical power to each LED emitter is taken to be 1-3 W and the plug-in efficiency is set as 30%. The phosphor layer is treated as the second heat source because of Stoke's loss [9]. The light conversion efficiency of silicone/phosphor composites is set as 50%, which is a typical value for LED packages of light bar. The metal core PCB (MCPCB) is assembled in the backlight chamber with heat sink at the bottom. Therefore, a small thermal convection (h = 0-5 $W/m^2K$) boundary condition is applied to upper and side surface of the LED bar. The temperature of bottom surface is set as constant (70°C) assuming the heat sink has a perfect cooling performance. Thermal conductivity and geometry information of each component in the LED package model is summarized in Table 4.1. Figure 4.2 displays the simulated (a) whole and (b) detailed temperature distribution for the light bar model.

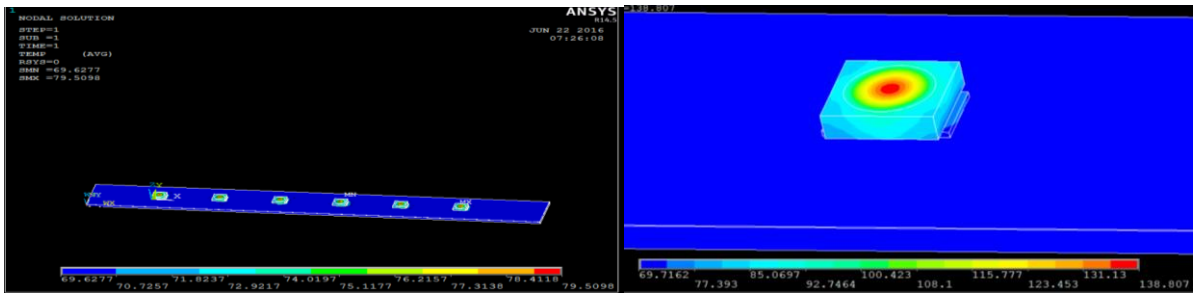

(a) (b)

Fig. 4.2. (a) The whole and (b) detailed temperature distribution of a light bar.

TABLE 4.1. THERMAL CONDUCTIVITY AND GEOMETRY INFORMATION OF EACH LED PACKAGING COMPONENT

| Component | Material | Thickness (mm) | Thermal conductivity (W/m-K) |
|---|---|---|---|
| **Chip** | GaN/AlGaN | 0.61*0.61*0.003 | 130 |
| **Substrate** | Sapphire | 0.1 | 20 |
| **DAA** | Silicone | 0.004-0.009 | 0.2-1.0 |
| **Lead** | Copper alloy | 0.2 | 259.6 |
| **Leadframe** | Epoxy Molding | 3.0*3.0*0.32 | 0.9 |
| **Encapsulant** | Silicone | 0-0.9 | 0.18 |
| **Dielectric** | Epoxy | 0.036 | 1.1 |
| **PCB metal** | Al | 0.9 | 237 |

## 4.4 Results

### 4.4.1 The Effect of EMC

According to temperature distribution of the light bar showed in Fig. 4.2 (b), the hotspot of the whole model locates in the center of encapsulant layer. First, it is assumed that encapsulant

is a 0.3mm-thick layer with thermal conductivity of 0.206 W/K-m and the thermal conductivity of DAA is 0.2 W/K-m. The junction temperature reaches the critical value (150℃) when the input power is 1.5 W, while the maximum temperature of EMC is only 126℃. This EMC temperature is below its maximum service temperature (178℃). However, it's observed that EMC will turn yellow or black with input power higher than 1.5 W. This is because the yellowing or discoloration of EMC is resulted from both optical radiation and thermal degradation. Moreover, epoxy will be degraded when junction temperature reaches 150 ℃ [10]. Thus, SMD LED with EMC can at most withstand an input power of 1.5 W.

### 4.4.2 The Effect of DAA

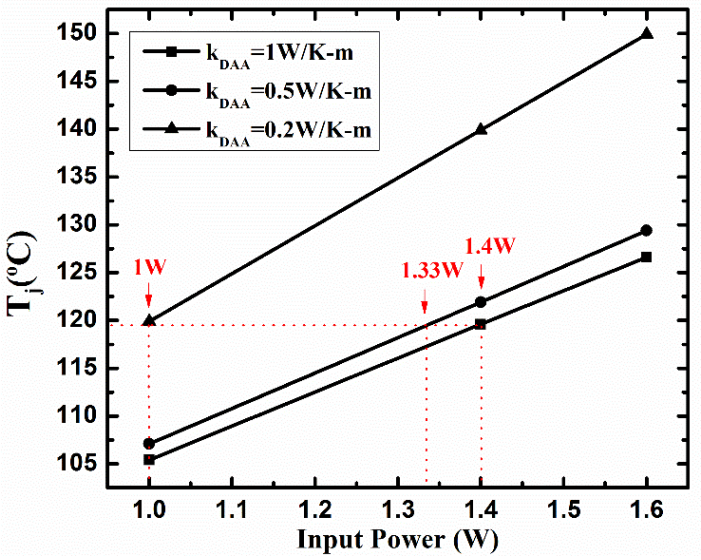


Fig. 4.3. The critical input power when junction temperature reaches the maximum value.

Figure 4.3 presents the critical input power when junction temperature reaches the maximum value under different DAAs. When thermal conductivity of the DAA has a low value of 0.2 W/K-m (DAA1), the maximum input power employed can be 1 W. However, when thermal conductivity of DAA is increased to 0.52 W/K-m (DAA2) [11] and 1 W/K-m (DAA3), the input power applied to each LED emitter can be 1.33 W and 1.4 W, respectively. That means, for the case of LED backlight unit in a TV display, less number of light bars are needed to maintain the same total power output or brightness if DAAs with higher thermal conductivities are adopted. Assume that originally the number of light bars with 1W WLEDs is seven, after changing to a DAA material with thermal conductivity of 1 W/K-m, the number of light bars needed can be reduced to five. The materials and processing cost of two light bars can be saved since cost of different DAA materials only occupy a negligible portion of the total cost of backlight unit. Similarly, for every four light bars with 1W WLEDs, the cost of 1 light bar can be saved by utilizing DAA with thermal conductivity of 0.52 W/K-m.

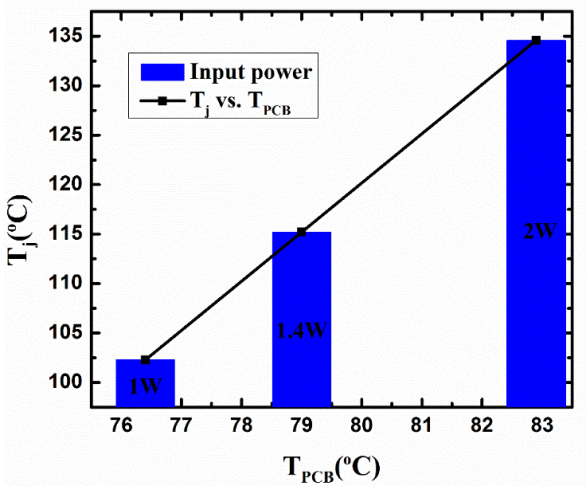


Fig. 4.4. The relationship between PCB and junction temperature with different input power.

Researches carried out recently compare the junction and PCB temperature under different PCBs and pitch distances [12-13]. According to our results in Fig. 4.4, temperature of PCB changes linearly with junction temperature. Given the input power, PCB temperature can be used to predict junction temperature because it′s facile to measure. Here, the maximum PCB temperature is 85℃ for commercial LED products.

### 4.4.3 The Effect of Encapsulant

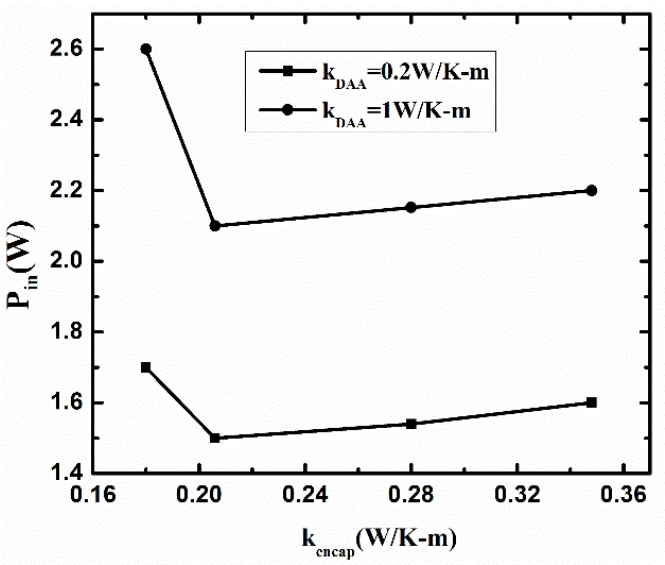


Fig. 4.5. The critical input power when junction temperature reaches the maximum value changes with thermal conductivity of encapsulant.

Figure 4.5 shows the maximum input power allowed changes with thermal conductivity of encapsulant. Here, the thickness of enccapsulant layer is set to 0.3 mm with in-cup phosphor configuration. There is a minimum value of input power with different encapsulant composite materials and phosphor concentration. The reason is, when thermal conductivity of encapsulant is

decrease from 0.348 to 0.206, more heat will accumulate within encapsulant layer, less power LED can withstand; when thermal conductivity further drops, density of phosphor layer is less, thus the heat generated by phosphor, then it's safe to apply larger input power. By using a DAA material with thermal conductivity of 1 W/K-m, the maximum input power can be as high as 2.6 W, while the commonly used DAA ($\kappa$ = 0.2 W/K-m) can only withstand input power of 1.7 W.

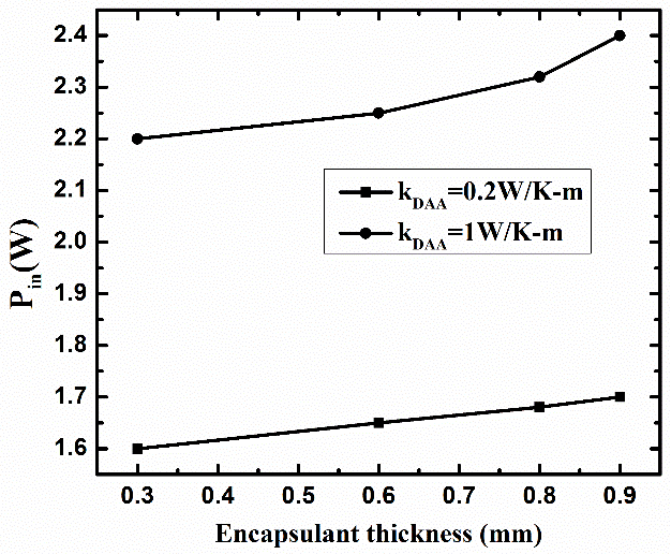


Fig. 4.6. The critical input power when junction temperature reaches the maximum value as a function of encapsulant thickness.

Figure 4.6 shows the critical input power when junction temperature reaches the maximum value, as a function of encapsulant thickness. As demonstrated in Fig. 4.6, under larger encapsulant thickness, the input power can be increased for 0.2 W with the DAA of higher thermal conductivity. However, there is a tradeoff because increasing encapsulant thickness can also make the overall light bar thicker, which may not meet the demand of continuously slimmer displays nowadays. For DAA with thermal conductivity of 1 W/K-m, the input power of light bar with 0.9 mm thick encapsulant can be 1.5 times higher than that with 0.3 mm thick encapsulant and DAA1.

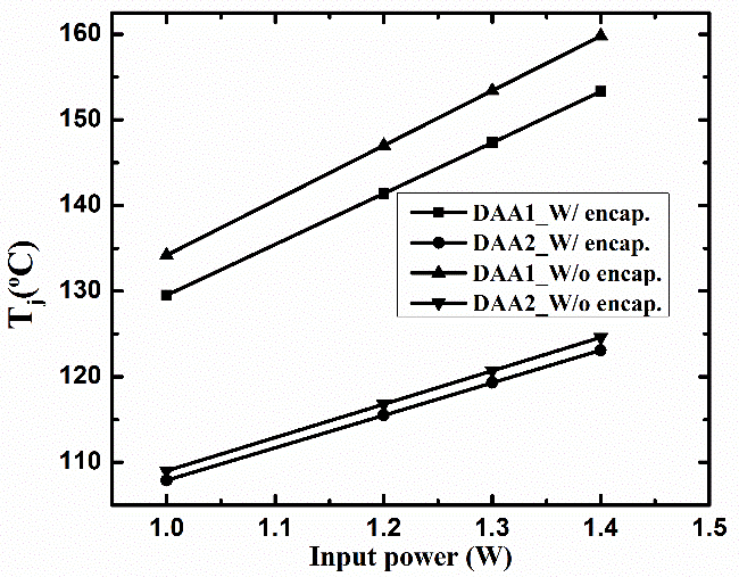


Fig. 4.7. Junction temperature changes with input power with and without encapsulant.

Figure 4.7 compares junction temperature of LED with and without encapulant, and it is shown that the removal of encapsulation layer will increase junction temperature Tj for the case of DLED-BLU. With DAAs of higher thermal conductivity, encapsulant layer has a less effect on Tj because larger portion of heat power is transferred downward into PCB layer.

### 4.5 Conclusions

In this work, thermal modeling for light bars was developed to study the effect of important packaging materials on power consumption of EMC based LED backlights. The results showed that by employing DAA or encapsulant materials with higher thermal conductivities, the input power to each emitter can be increased and less light bars are needed in the LED backlight unit application. As shown in the result, the maximum input power is 1.5 W for an EMC-based SMD LED with the common DAA ($\kappa$ = 0.2 W/K-m). With the thermally conductive DAA ($\kappa$ = 1 W/K-m), at most 2 out of 7 light bars can be saved while maintaining the requirement of the same brightness. Further enhancement in thermal management could be achieved by changing DAA and

encapsulant materials simultaneously. This work presents a practical means to improve the cost-performance ratio and power efficiency of backlight units.

**References**


[1] X. H. Lee, C. C. Lin, Y. Y. Chang, H. X. Chen and C. C. Sun, "Power management of direct view LED backlight for liquid crystal display", *Opt. & Laser Tech.*, vol. 46, pp. 142-144, 2013.

[2] H. J. Kim and S. W. Kim, "Enhancement of physical and optical performances of polycarbonate-based diffusers for direct-lit LED backlight unit by incorporation of nanoclay platelets", *J. Appl. Polymer Sci*., vol. 133, no. 6, Feb. 2016.

[3] C. C. Sun, I. Moreno, S. H. Chung, W. T. Chien, C. T. Hsieh and T. H. Yang, "Brightness management in a direct LED backlight for LCD TVs", *J. SID*, vol. 16, no.4, pp. 519-526, 2008.

[4] S. K. Kim, "Analysis on Thermal Management Schemes of LED backlight units for liquid crystal displays", *IEEE Trans. Comp. Packag. Manuf. Tech.*, vol. 2, no. 11, Nov, 2012.

[5] Judy Lin. (2013, July). Trend of LED package manufacturers entering EMC lead frame technology to target mid/high power LED. LEDinside, a Business Division of TrendForce Corp., Taiwan. [Online]. Available: http://www.ledinside.com/intelligence/2013/7/asia_manufacturers_emc_lead_frame_strategy

[6] Y. C. Lin, Y. Zhou, N. T. Tran, and Fran G. Shi, "Materials for Advanced Packaging", *Springer Science & Business Media*, 2008, pp. 629-680.

[7] G. Kim, Y. Shih, J. P. You, and Fran G. Shi, "Optical role of die attach adhesive for white LED emitters: light output enhancement without chip-level reflectors", *J. Solid State Lighting*, vol. 2, pp. 1-8, 2015.

[8] C. Y. Tang, J. J. Huang, Y. L. Peng, M. Y. Tsai, and P. Liang, "The role of thermal properties of PCB substrates in heat dissipation of LED back light bars", *14th intl. Conf. EMAP,* 13-16 Dec. 2012.

[9] L. Li, C. Yuan, R. Hu, H. Zheng and X. Luo, "Study on the effect of the phosphor distribution on the phosphor layer temperature in light emitting diodes by lattice Boltzmann method", *15th intl. Conf. Elec. Pack. Tech.*, pp. 671-675, 2014.

[10] F. M. Steranka, J. Bhat, *et. al*., "High Power LEDs – Technology Status and Market Applications," *Phys. Status, Solidi (a),* vol. 194, no. 2, pp. 380-388, 2002.

[11] K. Zhang, J. Li, *et. al.*, "Highly Thermal Conductive Transparent Die Attach Material for LEDs," *17th Elect. Packag. Tech. Conf.,* 2015, pp. 1-4.

[12] S. K. Kim, J. Kang and S. Y. Kim, "Thermal characteristics of LED light source in flat panel display backlight system," *Proc. IPACK*, July 2007, pp. 1-4.

[13] B. R. Park and H. Y. Cha, "Thermal consideration in LED array design for LCD backlight unit applications," *IEICE Elect. Express,* vol. 7, no. 1, pp. 40-46, Jan. 2010.

# CHAPTER 5:

## ALL-NUMERICAL OPTO-THERMAL COUPLED ANALYSIS OF MONOCHROMATIC LED PACKAGE UNDER DIFFERENT DIE ATTACH ADHESIVE (DAA) MATERIALS

### 5.1. Abstract

Low thermal dissipation efficiency of LED package has act an obstacle to further increase its luminous output and life time. Meanwhile, the overall light radiation power can directly determine thermal power of LED package. Therefore, thermal and optical field within LED is coupled with each other and should be considered simultaneously. This paper aims to take opto-thermal coupled analysis of monochromatic LED all-numerically and verify it with more accurate light output and temperature measurement. ANSYS and Lighttools are conducted to implement the all-numerical approach and forward voltage method is employed in the junction temperature testing. Here, all-numerical opto-thermal coupled method means setting input thermal power of LED as electrical power minus calculated optical power, then iterate to get final temperature distribution. Further, Al filled DAA and white DAA with different filler concentration, which has a great impact of thermal resistance of the whole LED package, is prepared and compared on this opto-thermal coupled method. It is found that, instead of decreasing with filler-concentration of DAA without considering opto-thermal coupling, junction temperature will have a peak value while filler-concentration of DAA is increased and opto-thermal coupling is counted. This is an evidence that we should not neglect optical effect while conducting thermal simulation for LED package. The cases with commercial AlN DAA and self-developed white DAA are compared and discussed.

## 5.2 Introduction

Light Emitting Diode (LED) is a promising solid-state lighting solution because of its long lifetime and small form factor [1]. However, research on LED is challenged because the optical, thermal, electrical, mechanical fields within it are coupled with each other [2-4]. For example, poor thermal dissipation in LED package can reduce the luminous efficiency, while heat generation rate can be determined by calculated optical losses [3]. Most of papers study only optical or thermal properties of LED packages for simplicity and convenience. Recently, researchers are looking for numerical and experimental means to solve opto-thermal coupling problems of monochromatic or white LED package. Dassanayake in [5] introduced a heat sink thermally coupled with LED light source, which is from the perspective of mechanical design. Wenzl in [6] proposed a combined optical and thermal simulation method, which can lower temperature increase in phosphor-silicone composite. This paper only focus on heat generation within phosphor layer, instead of the whole LED package. Zeng in [7] provides a systematic investigation of electro-opto-thermal coupling method for white LED. It utilized simulation and experimental methods together to give an accurate and feasible prediction of optical and thermal features of different package types: filling, molding and remote. But it still needs to do experiments to determine parameters for coupling simulation. Therefore, an all-numerical opto-thermal coupled method without additional experiments needs to be developed.

What's more, DAA material in LED package can be formulated with different type and weight percentage of fillers. Some typical fillers are BN, SiO2, ZnO and AlN [8-9]. With larger weight percentage of fillers, more light will be trapped within DAA layer and less light will be emitted out of LED package, while thermal conductivity of DAA layer can be increased and

luminous efficiency is higher. Thus, the optical or thermal behavior of LED package will be changed with increasing weight percentage of fillers.

As discussed above, this paper aims to develop an all-numerical opto-thermal coupling method to predict thermal behavior of LED package with different weight percentage of fillers in DAA.

In this work, firstly, LED package model for both Finite Element method (FEM) software ANSYS and illumination design software Lighttools is established. Then combining both software, coupled opto-thermal results with different filler concentration are obtained and analyzed. Finally, FVM experiments are conducted to verify the simulation results.

### 5.3 Numerical Methods

Leadframe of surface-mounted device (SMD) 3020 is utilized in our simulation. Dimensional information can be seen in Fig. 5.1(a). A conventional lateral LED chip (length=23mil, width=10mil) is soldered onto leadframe with different DAAs. Then the chip is encapsulanted with pure silicone. The whole LED package is mounted on Al based Printed Circuit Board (PCB) with radius of 6mm. The model established by ANSYS in Fig. 5.1(b) is the same as that by Lighttools in Fig. 5.1(c) to keep the consistence between optical and thermal models. For Lighttools, an input power of 1W is added onto the blue LED chip. After setting up material properties listed in Table 1 and running the model, the overall luminous output and light extraction efficiency is obtained. Since the light extraction efficiency is constant for our model, optical simulation only needs to be run once. Thus, thermal load onto FEM model can be calculated as follows:

$$P_{th} = P_{in} - P_{opt} \tag{1}$$

In which, $P_{th}$ is the thermal power, $P_{in}$ is the input electrical power and $P_{opt}$ is the optical power.

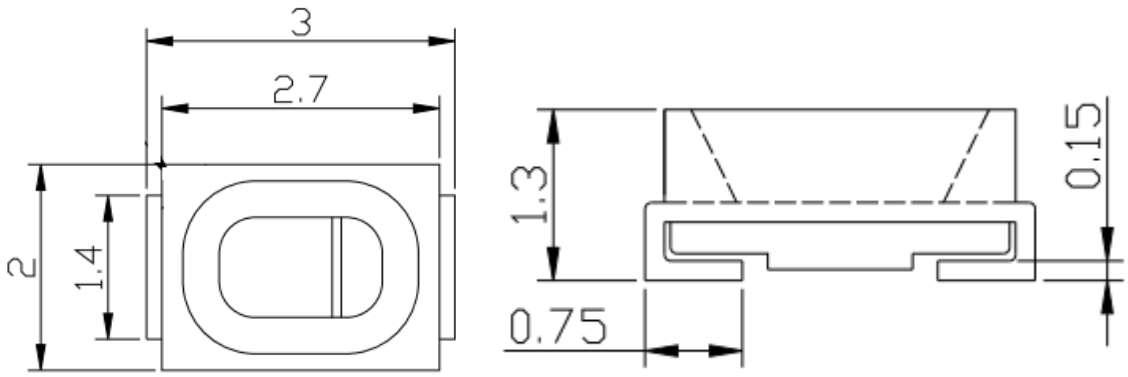


(a)

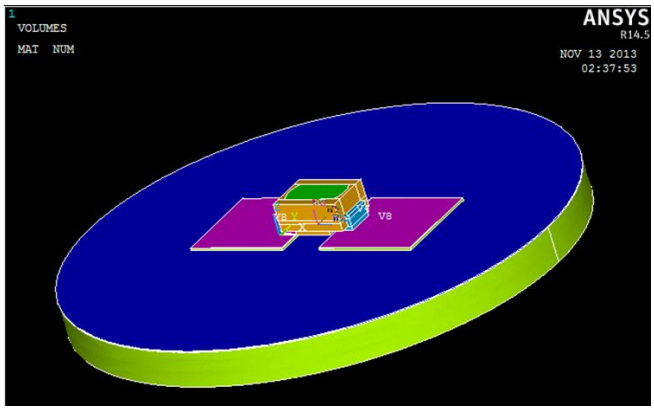


(b)

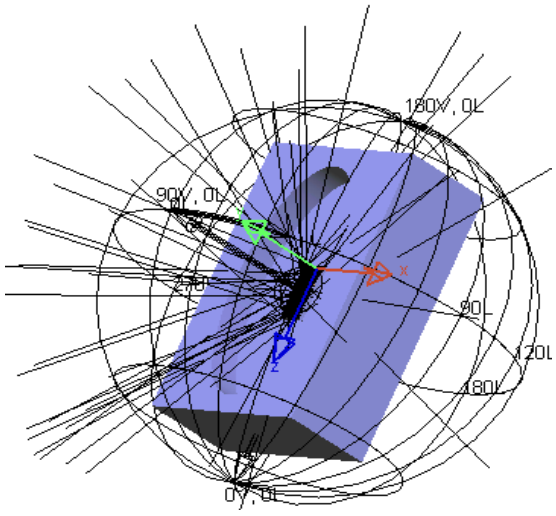


(c)

Fig. 5.1. (a) Dimensional information of leadframe. (b) FEM and (c) Optical model for SMD LED package investigated.

Because each LED chip is small compared with PCB layer, the temperature distribution nonuniformity can be ignored and the chip layer is considered as heat source with constant heat generation rate. The electric power input onto each chip is set as 0.5W if not specified otherwise. And plug-in efficiency is assumed to be 30%, which means 70% of total electric power is transferred into thermal power. Thus the heat generation rate is the thermal power divided by volume of LED chip. Further, Surface of the whole model is applied with forced thermal convection (h=34 W/m2K). The range of encapsulant thickness is within 0.3-0.9 mm. Thermal and size information of COB LED package materials is summarized in Table 5.1.

TABLE. 5.1. THERMAL AND OPTICAL PROPERTIES OF MATERIALS.

| component | material | thermal cond-uctivity (W/m-K) | refractive index | transmittance |
|---|---|---|---|---|
| junction | GaN | 130 | 2.5 | 0.98/μm |
| die substrate | sapphire | 34 | 1.77 | 1 |
| die attach | Transparent silicone | 0.2 | 1.40 | 0.85/mm |
| leadframe substrate | copper | 380 | N/A | N/A |
| reflector | PPA | 0.35 | N/A | N/A |
| encapsulant | silicone | 0.18 | 1.52 | 0.997/mm |
| solder | PbSn | 50 | N/A | N/A |
| dielectric | White paint | 2.2 | N/A | N/A |
| PCB core | Al | 237 | N/A | N/A |

The flowchart of our all-numerical opto-thermal coupled method is shown in Fig. 5.2. As can be seen, after deriving the total thermal power from the FEM model, new optical input power equals to input power minus this thermal power. Then new thermal power will be input power minus extraction efficiency multiplied by new optical power. Iterate by updating thermal power into FEM model until thermal power reaches a stable value. Finally, output the junction temperature to analyze thermal behavior of LED package under different DAA filler types and

concentration. Two thermal conductive fillers are chosen in this work: AlN and TiO2. And the concentration is also changed while thickness of DAA is kept constant for simplicity.

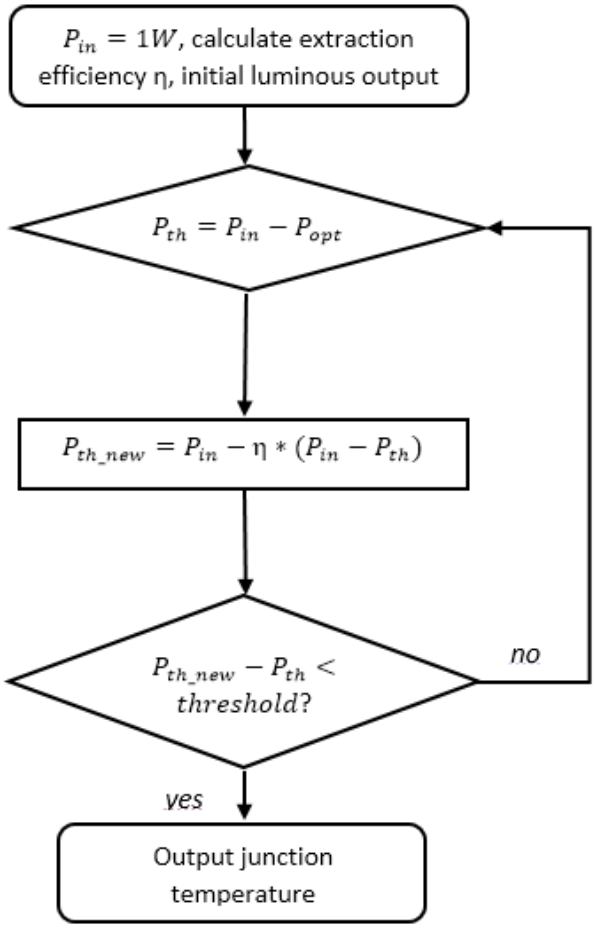


Fig. 5.2. Flowchart of our all-numerical opto-thermal coupled method.

## 5.4 Results

AlN is a potential filler for thermal conductive DAA because of its high thermal conductivity. Luminous output power of LED package calculated by Lighttools is displayed in

Fig. 5.3. With increased weight percentage of AlN filler as well as thickness of DAA, light output will be reduced because of more light trapped among fillers or within DAA.

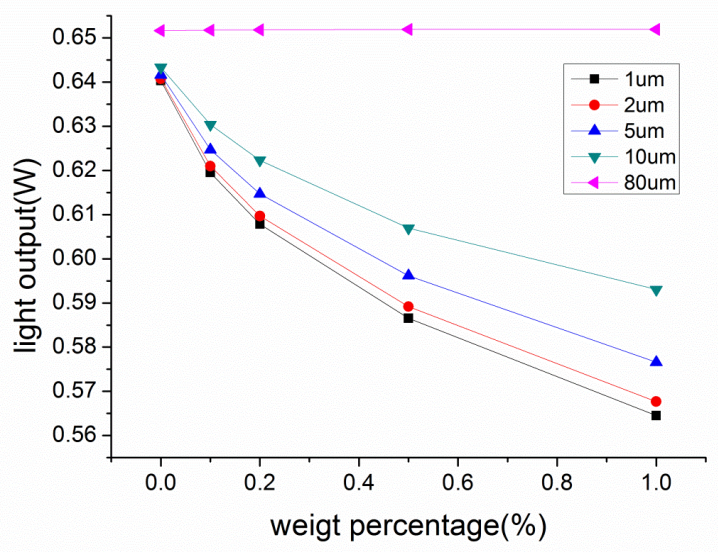


Fig. 5.3. Light output with different thickness of DAA and AlN weight percentage using Lighttools.

Table 5.2 provides junction temperature of LED package under different thickness of DAA and AlN weight percentage. The results are obtained with ANSYS. Thermal conductivity of AlN filler is 1W/m-K. A thermal convection coefficient of 28 W/m2-K is applied onto the whole outer surface of LED package and PCB. Heat flux is thermal power per area of LED chip: 1.8e4 $W/m^2$. Higher weight percentage of filler means larger effective thermal conductivity, which enables DAA to dissipate heat more efficiently. This will increase light output, instead of reducing it in Fig. 5.3. Meanwhile, thicker DAA has a higher thermal resistance and LED junction temperature will rise accordingly. So, light output will drop, contrast to results in Fig. 5.3. The actual junction temperature or light output will unlikely change monotonously with weight percentage of filler.

TABLE 5.2. JUNCTION TEMPERATURE VS. THICKNESS OF DAA AND WEIGHT PERCENTAGE.

| Wt% | V% | $K_{eff}$ (W/m-K) | d=1 μm | d=1.5 μm | d=2 μm |
|---|---|---|---|---|---|
| **10%** | 4.24% | 0.22 | 351.45 K | 425.185 K | 496.656 K |
| **20%** | 9.07% | 0.243 | 337.92 K | 404.96 K | 470.324 K |
| **30%** | 14.6% | 0.273 | 323.384 K | 383.409 K | 442.278 K |
| **40%** | 21% | 0.312 | 308.517 K | 361.504 K | 413.461 K |

Table 5.3 is the comparison of junction temperature before ($T_{j1}$) and after ($T_j$) considering opto-thermal power coupling. As can be seen from the modified junction temperature, when the weight percentage (Wt) is 30%, junction temperature even raised, although the thermal conductivity of DAA is increased. That's because, light output is decreased with weight percentage of AlN filler, which means thermal load added is larger. This indicates that conducting thermal simulation without considering optical calculation can make inaccurate prediction of thermal performance of LED package. Similar thermal behavior of LED with DAA filled by $TiO_2$ can be observed in Table 5.4.

TABLE 5.3. JUNCTION TEMPERATURE OF LED BEFORE AND AFTER CONSIDERING OPTICAL POWER (THE THICKNESS OF DAA IS 1MM).

| Wt% | Heat power ($P_{th}= P_{total} - P_{opt}$) | $K_{eff}$ (W/m-K) | $T_{j1}$ (K) | $T_j$ (K) |
|---|---|---|---|---|
| **10%** | 1.732 e4 | 0.22 | 351.115 | 338.332 |

| | | | | |
|---|---|---|---|---|
| **20%** | 1.765 e4 | 0.243 | 337.92 | 331.349 |
| **30%** | 1.857 e4 | 0.273 | 323.384 | **333.624** |
| **40%** | 1.903 e4 | 0.312 | 308.517 | 326.172 |

TABLE 5.4. JUNCTION TEMPERATURE OF LED BEFORE AND AFTER CONSIDERING OPTICAL POWER (THE THICKNESS OF DAA IS 1MM).

| **Wt%** | **Heat power** ($P_{th}= P_{total} - P_{opt}$) | $K_{eff}$ **(W/m-K)** | $T_{j1}$ **(K)** | $T_j$ **(K)** |
|---|---|---|---|---|
| **10%** | 1.834e4 | 0.88 | 331.836 | 326.87 |
| **20%** | 1.869 e4 | 0.924 | 322.945 | 317.477 |
| **30%** | 1.954 e4 | 0.989 | 312.53 | **320.275** |
| **40%** | 1.995 e4 | 1.104 | 301.237 | 316.9 |

## 5.5 Conclusions

In this paper, an all-numerical opto-thermal coupled method is achieved to make both thermal and optical simulation of monochromatic LED package more efficient as well as accuracy. It's found that, considering optical results in thermal simulation, can reduce the chance of mis-predicting thermal behavior of LED package. This all-numerical means also save the long experiment time, while maintaining satisfied accuracy. So, it's more efficient than other simulation-experimental combined opto-thermal coupling method. The results indicates that junction temperature of LED package will be non-monotonously changed with different filler

concentration. Either Optical or thermal calculation cannot predict the right trend that junction temperature changes. In the future, an all-numerical opto-thermal coupled method for white LED package can be worked on.

**References**

[1] D. A. Steigerwald, J. C. Bhat, D. Collins, R. M. Fletcher, M. O. Holcomb, M. J. Ludowise, P. S. Martin, and S. L. Rudaz, "Illumination with solid state lighting technology," IEEE J. Sel. Top. Quantum Electron. 2002, 8(2), 310– 320.

[2] P. Baureis, "Compact Modeling of Electrical, Thermal and optical LED behavior," IEEE Proc. ESSDERC, 2005, pp. 145-148.

[3] S. Watzke, P. A. Weimar, "Degradation of silicone in white LEDs during device operation a finite element approach to product reliability prediction," Microelec. Reliability, 2015, 55, pp. 733-737.

[4] A. Poppe, G. Farkas, and G. Horvath, "Electrical, thermal and optical characterization of power LED assemblies," THERMINIC, 2006.

[5] M. Dassanayake, S. D. Mel, J. Samarabandu, "Opto-thermal solution for multi-utility solid state lighting device using conic section geometries," U.S. Patent 8 186 852, May 29, 2012.

[6] F. P. Wenzl, C. Sommer, P. Hartmann, P. Pachler, H. Hoschopf, G. Langer, P. Fulmek, J. Nicolics, White light quality of phosphor converted LEDs from a phosphor materials perspective of view: an evaluation based on combined thermal and optical simulations, Proc. of SPIE 2012, 8484, pp. 848403 1-7.

[7] J. W. Zeng, "The research on white LED by the optical and thermal coupling method," M.S. thesis, Dept. Mech. Eng., National Centr. Univ., Jhongli, Taiwan, 2013.

[8] Y. S. Xu and D. D. L. Chung, “Increasing the thermal conductivity of boron nitride and aluminum nitride particle epoxy-matrix composites by particle surface treatments,” Composite Interfaces, 2000, 7(4), pp. 243-256.

[9] J. P. Hong, S. W. Yoon, et al., “High thermal conductivity epoxy composites with bimodal distribution of aluminum nitride and boron nitride fillers,” Thermochimica Acta, 2012, 537, pp. 70-75.

[10] L. J. Huang, Y. C. Shih, and F. G. Shi, “Effect of Thinning Encapsulant Layer on Junction and Phosphor Temperature of White Light-Emitting Diodes”, IEEE Trans. on Compo. Packag. Manuf. Tech., 2015, 5, (11), pp. 1628-1634.

# CHAPTER 6:

# EFFECTIVENESS OF POLYMER COMPOSITE INDUCED PASSIVE RADIATION COOLING IN THERMAL MANAGEMENT OF LED EMITTERS AND MODULES: IMPACT ON HOT SPOT ELIMINATION

## 6.1. Abstract

Effectiveness of polymer composite induced passive radiation cooling in thermal management of LED emitters and modules is elucidated by numerical simulations coupled with key experimental observations. Specifically, various polymer-filler composites coated on the board of LED emitters and modules are investigated for their effectiveness in reducing the board as well as junction temperature. It is demonstrated that, a maximum temperature drop of 11 $^{o}$C can be achieved for the single Chip on Board (COB) LED emitter with 10W input power. Moreover, for the linear LED module, a reduction of 14.53 $^{o}$C is observed in the peak junction temperature of LED emitters with 1W input power in the light bar. The polymer composite coating is also demonstrated to significantly boost the uniformity of temperature distribution and to reduce the risk of hotspot. Some of the key simulation results are further examined to be consistent with analytical modeling. Significant implications of the present polymer composite induced passive radiation cooling results to the challenging thermal design of electronic devices with limited space are also discussed.

## 6.2 Introduction

Passive cooling strategy in the thermal management of electrical devices has its advantage of light weight, small form factor and cost effectiveness. These advantages are more prominent for

the applications of mobile device, laptop, sealed battery system, and other devices and modules with limited space. Passive radiation cooling can no longer be neglected for cooling surface larger than 1 $dm^2$ in mobile and embedded systems [1].

Recently, there is an evident trend of ever-thinner and intricate electronic devices, which brought about the highly thermal non-uniformity or hot spot issue. Special polymer-filler composite coatings [2-11], as a passive radiation cooling method, might offer as a potential hotspot elimination solution. To eliminate hotspots means, controlling the maximum temperature of hotspots under specified threshold as well as enhancing uniformity of the overall temperature distribution. Researchers have devoted efforts to lower down the peak hotspot temperature by optimizing properties of composite coating itself [2-6] and applying it to real product applications [7-11]. Coating thickness, filler size and filler type are among the investigated properties to better radiative cooling of composite coatings. For instance, Hsin, *et al.*[5] focused on different carbon particle composites as thermal radiation coating, which have both excellent emissivity and thermal conductivity. Moreover, after employing composite coating onto the real applications, such as LED packaging, the peak temperature can be significantly reduced. Chung, *et al.*[8] reported the densely-coated composite layer enabled to decrease the total thermal resistance of LED module up to 15%, hence the junction temperature. However, only few papers involve the discussion of composite coating acting to boost temperature uniformity [11]. Further, it's found that the time-efficient and effective simulation tools (such as FEM) are rarely adopted in thermal radiation analysis [9]. The importance of FEM lies in, radiative cooling can be studied separately from conduction and convection cooling with simulation. Hence, the percentage of radiation cooling in the overall cooling effect can be predicted. Then, it can detect the hotspots quickly and shorten the production cycle. Third, for thermal measurement methods such as IR thermometer, it's

complicated to tune the parameters such as emissivity to accurately obtain the temperature distribution, especially for sophisticated devices. FEM software was nevertheless able to calculate complicated models with various emissivity.

Based on our knowledge, none piece of research was able to numerically and systematically elucidate the effectiveness of various thermal radiation coatings in the real applications, and provide guidance of the scenarios that thermal radiation should not be ignored.

The objective of the present work is to investigate, for the first time, the effectiveness of polymer composite induced passive radiation cooling in thermal management of LED emitters and modules by numerical simulations coupled with key experimental observations. First, numerical results for Al board with thermal radiation coating were compared and validated with experimental data. Then, junction temperature of single LED emitter and light bar with and without composite coatings were measured and calculated to indicate their effectiveness of radiation cooling. The uniformity of overall temperature distribution is also displayed by FEM software. The significant impact factors for the effectiveness of radiation coatings, such as board area and thermal convection coefficient were discussed and agreed with analytical modeling. Practical guidance on when and how to consider thermal radiation coatings in the real applications are also provided.

## 6.3 Numerical and Experimental Methods

### 6.3.1 Simulation

According to experimental set-up, a Finite Element Method (FEM) model is employed to investigate the cooling effect of different thermal radiation coating materials, as schematically shown in Fig 6.1. According to Fig. 6.1, the side and bottom surfaces of copper platform are considered adiabatic because of good thermal insulation of cotton and asbestos bricks (shown in

Fig. 6.4). The upper and side surfaces of coating layer are assumed to emit thermal radiation power into the environment and be applied with a free thermal convection coefficient of 25 W/m$^2$-K. The input power onto cartridge heater from DC power supply is 9 W and 25 W. The cartridge heater has a maximum power of 150 W at 110 V. Its radius and length is 4 mm and 50 mm, respectively. The cartridge heater is treated as the heat source with uniformly distributed heat generation, whose power density can be calculated as input power divided by its volume. The thickness of Al board is 0.8 mm and that of coating layer is 0.22 mm. Emissivity of different coating materials have been measured with IR thermometer by researchers in our lab [12].

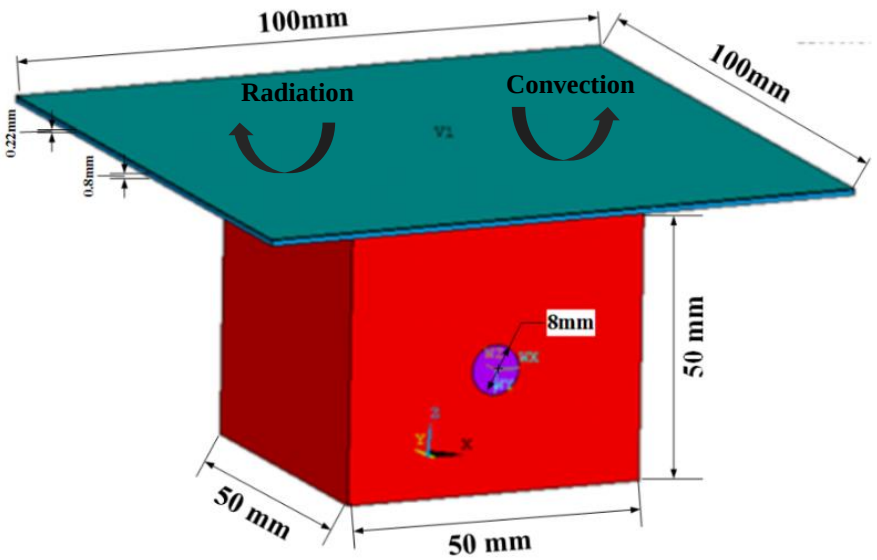


Fig. 6.1. Simulation model of the heating system with coated Al board. Dimension information and boundary conditions are included.

TABLE 6.1. MEASURED EMISSIVITY OF DIFFERENT COATING MATERIALS [12]

| Specimen | Baseline | Silicone | 10% ZnO | 10% $TiO_2$ |
|---|---|---|---|---|
| **Measured** | 0.22 ±0.02 | 0.78 ±0.02 | 0.92 ±0.03 | 0.9 ±0.02 |
| **Reference** | 0.1-0.3 | 0.65-0..8 | 0.85-0.93 | 0.85-0.9 |

Fig. 6.2. Simulation model of thermal radiation coating on PCB of light bar.

A natural thermal convection (h = 5-20 W/$m^2$K) boundary condition is applied to upper and side surface of the LED bar. The thermal convection coefficient of bottom surface is set as 30 W/$m^2$K. The thickness of coating ranges from 36 μm to 64 μm. Other geometry information as well as thermal conductivity of package materials are referred in Table 6.2.

TABLE 6.2. THERMAL CONDUCTIVITY AND GEOMETRY INFORMATION OF EACH LIGHT BAR

| Component | Material | Thickness(mm) | Thermal conductivity (W/m-K) |
|---|---|---|---|
| **Chip** | GaN/AlGaN | 1.1*1.1*0.00365(Width*Length*Thickness) | 130 |
| **Substrate** | Sapphire | 0.1 | 27 |
| **DAA** | Silicone | 0.004 | 0.2 |
| **Lead** | Copper | 0.2 | 259.6 |
| **Leadframe** | EMC | 3.0*3.0*0.3(Width*Length*Thickness) | 0.94 |
| **Encapsulant** | Silicone | 0.3 | 0.2 |
| **Insulation** | RF-4 | 0.036-0.064 | 1.1 |
| **PCB core** | Al | 11.5*113*0.9(Width*Length*Thickness) | 237 |

6.3.2 Experiment

First, various polymer filler composite coatings are prepared. With a Shinky high shear mixer at 2500 r/min for 5 minutes, silicone resin is mixed with various fillers to form the composite coating. The fillers of BN, $Al_2O_3$, ZnO with concentration from 2.5% to 30% are adopted. For example, SEM image of $Al_2O_3$ fillers with the size of 1 micron is shown in Fig. 6.3. Then, the composite was degassed under a vacuum of $10^{-2}$ Pa for 30 minutes to get rid of the trapped air bubbles. Finally, the mixture was coated onto polished Al plates and cured at 150℃ for 2 hours.

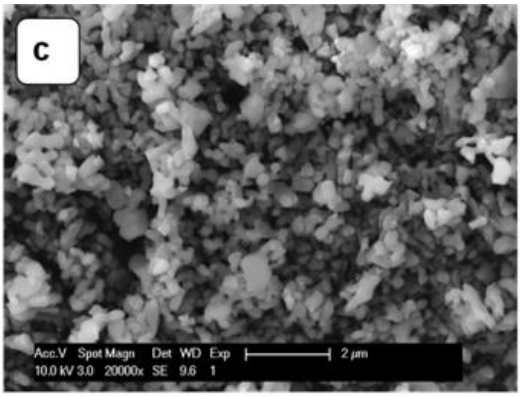


Fig. 6.3. SEM image of $Al_2O_3$ fillers with the size of 1 micron [13].

After specimen preparation, two experimental setups were used to evaluate cooling effect of thermal radiation coating.

*1) Thermal radiation coating on Al board*

The heating platform as shown in Fig. 6.4 consists of a 50 mm × 50 mm × 50 mm copper platform which is thermally insulated in an asbestos brick. Thermally insulated cotton is filled within the small gap between the copper platform and asbestos brick. A cartridge heater as the unique heat source is mounted in a blind hole of the copper block. To reduce interface thermal resistance between the central part of the bottom surface of the specimen and the copper block, a thin layer of heat conductive grease is applied and the screws are tightened. The thermal insulation

of the asbestos brick produces heat flows from the copper platform to the specimen, through the coating into the air. The surface temperature of the board and the coating was detected by two K-type thermocouples. It takes over 120 minutes for both thermocouples to reach a temperature growth rate of 0.1 ℃/5 min. Thus, the data can be read under a steady state. The entire heating system is placed in inside a glass shield without forced air flow. The ambient temperature is kept at 20 ℃.

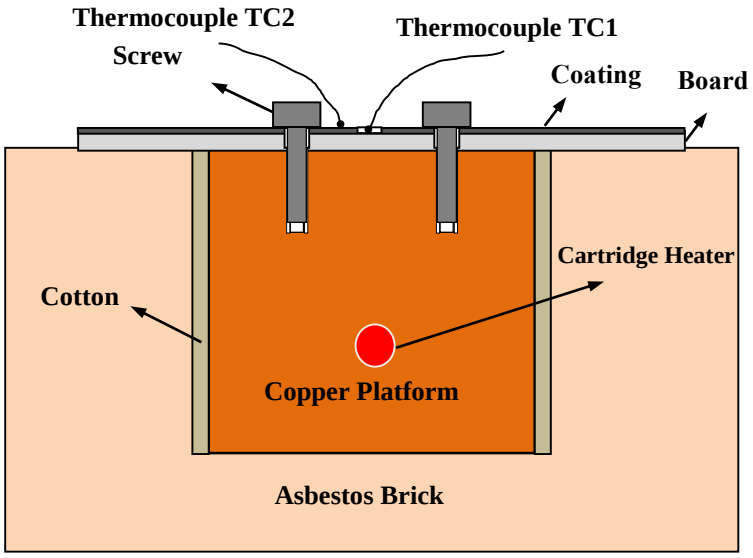


Fig. 6.4. Experimental schematic of the heating system with coated Al board [12].

*2) Thermal radiation coating on PCB with LED emitter*

Different thermal radiation coatings with a thickness of 50 μm were formed on PCB by using a film applier. A surface-mounted LED emitter with input power at 10 W was used as the heat source and a good thermal contact was formed between the LED emitter and the PCB by soldering. The sample was heated by turning on the LED light for 30 minutes. The whole heating system is set up inside a glass shield without forced air flow. The ambient temperature is kept at 23 ºC. The surface temperature of the LED emitter is directly measured by thermometer (Omega,

model CL3515R). Figure 6.5 illustrates the structure of the fabricated emitters and the PCB used in this work.

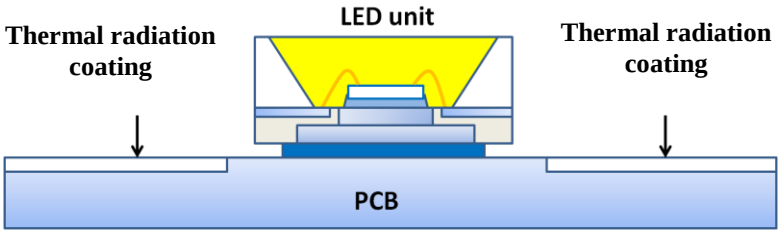


Fig. 6.5. Experimental schematic of thermal radiation coating on PCB with single LED emitter.

## 6.4 Results

### 6.4.1 Thermal radiation coating on Al board

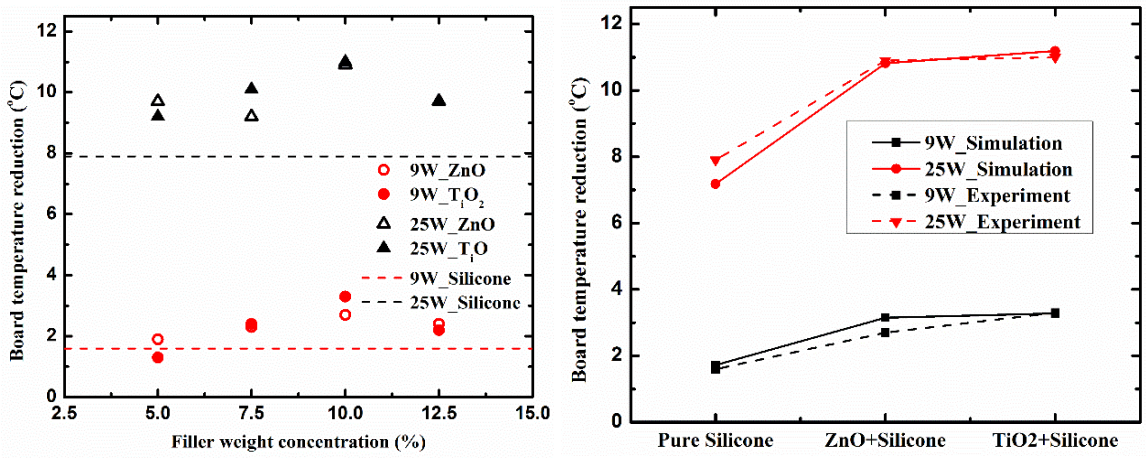


(a) (b)

Fig. 6.6. Measured [12] (a) and Simulated (b) Al board temperature reduction with ZnO filled, $TiO_2$ filled and pure silicone coatings (with respect to baseline). Results under different filler concentrations and input power levels are compared.

Fig. 6.6 (a) demonstrated Al board temperature reduction changing with filler weight concentration from 5% to 12.5%. The baseline refers to the Al board temperature without thermal radiation coating. Different coating materials such as ZnO filled, $TiO_2$ filled and pure silicone are considered and the input power of 9W and 25W are added to the cartridge heater. Al board temperature will increase than decreased with higher filler weight concentration, as shown in Fig. 6.6 (a). This is combined effect of thermal conduction and radiation. Both ZnO and $TiO_2$ as the fillers have higher emissivity than silicone according to Table 6.1. Thereafter, higher filler concentration will introduce larger emissivity and thermal conductivity of the coated composites, thereby causing the board temperature to drop more. Meanwhile, when filler weight concentration is higher than the critical value (10% in this experiment), viscosity of both ZnO filled and $TiO_2$ filled silicone can be further increased and the coating can't be well adhered to Al board. This means that the interfacial thermal resistance will be increased and the board temperature will be higher.

To validate our simulation results, the same numerical model was established to compare the simulation with experiments, as illustrated in Fig. 6.6 (b). The simulation results agree quite well with the experimental results. The error of variation comes from the screws and uncoated region mounted with thermocouple probe, which are ignored in the simulation model for simplicity. Another source of error could be introduced by the thin thermal grease, which is not considered in the simulation, either.

### 6.4.2 Thermal radiation coating on PCB with LED emitter

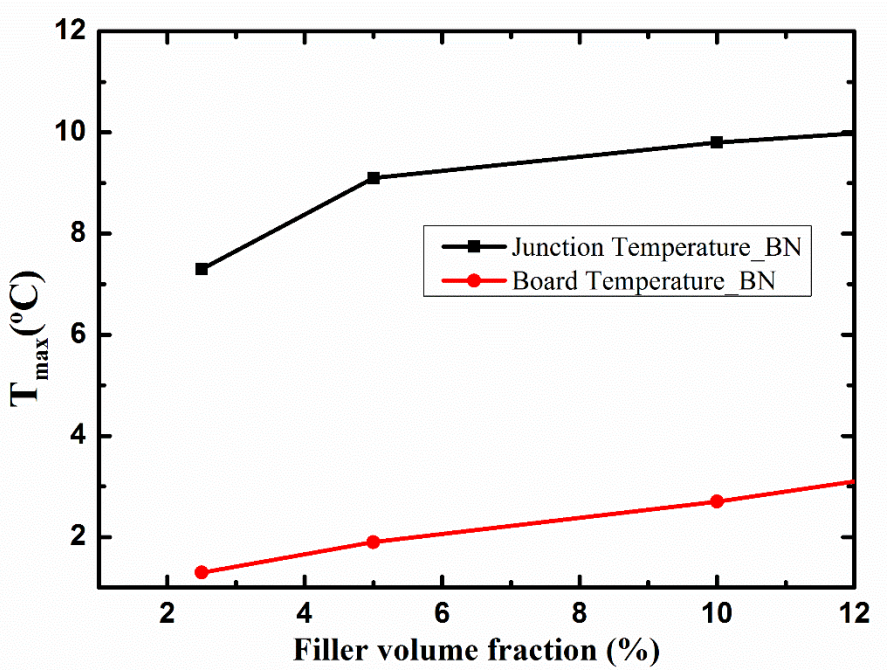


Fig. 6.7. Measured temperature reduction of (a) LED emitter and (b) PCB board, for single LED emitter [14].

Our thermal radiation coating was also employed to LED PCB layer to scrutinize its cooling performance in the real case. Schematic of thermal radiation coating on PCB with single SMD LED emitter is displayed in Fig. 6.5. Fig. 6.7 shows the measured emitter and coating surface temperature reduction under different filler volume concentration. Different from the trend in the case of Al board, junction temperature reduction in Fig. 6.7 will monotonously rise. The results also consist with that in [9]. This is because, higher filler concentration boosts emissivity, simulating the corresponding radiation heat transfer of the coating composites into the environment. What's more, for coating composite with BN volume concentration of 30%, a maximum junction temperature reduction of 11 $^{o}$C can be achieved. Temperature reduction of board surface is also shown in Fig. 6.7. As expected, BN filled silicone has the best cooling efficiency and the board temperature is lowest. The practical implication is, it's safe for the manufacturers to reduce the PCB area thanks to our thermal radiation coating. Since the cost of

PCB layer occupies quite a large portion of LED products, the overall cost is expected to be cut down.

### 6.4.3 Thermal radiation coating on PCB of light bar

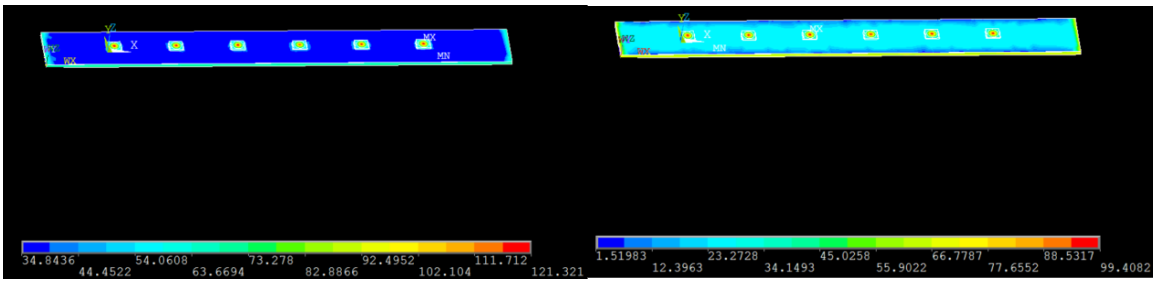


(a) (b)

Fig. 6.8. Simulated temperature distribution of light bar with thermal radiation coating, the emissivity of which is (a) 0.01 and (b) 0.95.

With the above verified simulation method, more complicated cases, such as light bar in backlight unit of TV display coated with thermal radiation coating, can be modeled. The detailed temperature distribution of light bar without and with coating is given in Fig. 6.8 (a) and (b), respectively. Note that, it can be observed that thermal radiation coating acts as not only cooling material, but also a mean to keep the temperature distribution more uniform. The mechanism is, radiative thermal power from hotspots can be emitted to other cooler areas without intermediate media, so the temperature of the whole electronic device is able to be redistributed by adjusting the emissivity of materials. This means, it will significantly reduce the risk of hotspots and thermal breakdown.

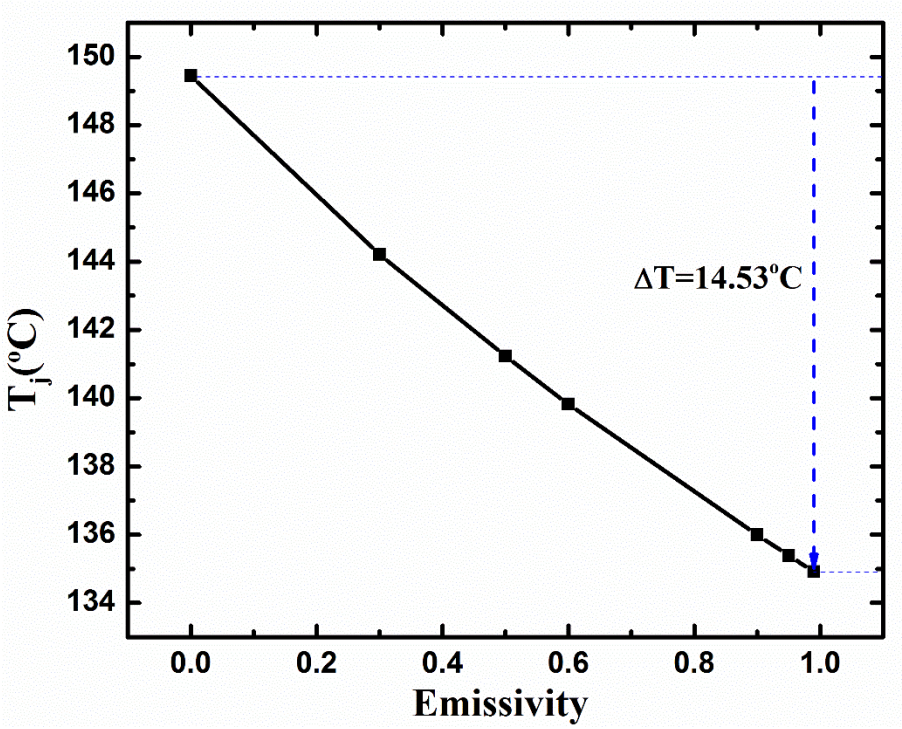


Fig. 6.9. The maximum junction temperature varied with emissivity of thermal radiation coating.

Fig. 6.9 shows the maximum junction temperature of light bar as a function of coating emissivity. There can be a maximum temperature reduction of 14.53 °C. The defined threshold of junction temperature is 150 °C according to the industry requirement. This nearly 10% of temperature reduction reflected the effectiveness of our thermal radiation composites and the great errors brought into the previous simulation work without considering thermal radiation effect. As mentioned in [1], especially when surface area of electronic device is large enough, thermal radiation load should be included in our simulation.

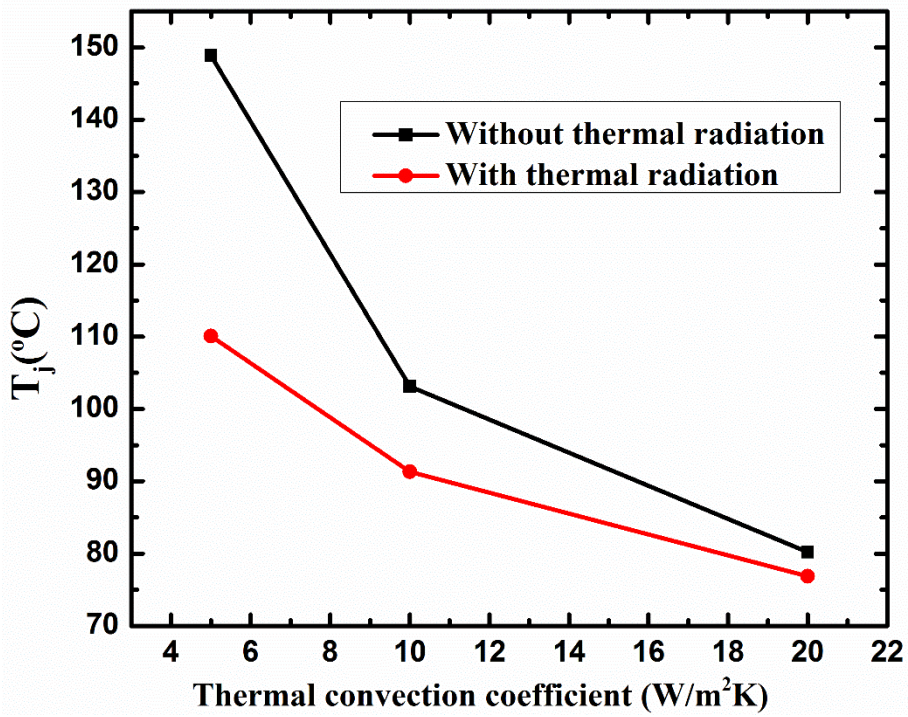


Fig. 6.10. The maximum junction temperature under different thermal convection coefficients with and without consideration of thermal radiation.

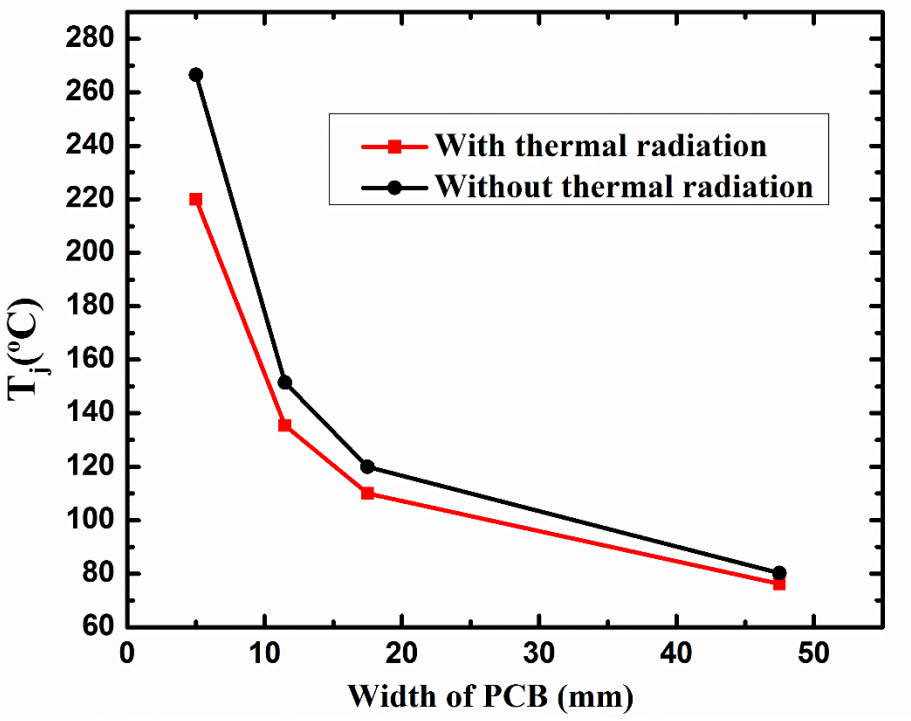

Fig. 6.11. The maximum junction temperature varied under different widths of PCB layer with and without consideration of thermal radiation.

Fig. 6.10 shows the impact of thermal convection coefficient on the effect of radiation coating. Let's define the factor to denote its effectiveness $R = \frac{T_{\max\_without} - T_{\max\_with}}{T_{\max\_without}}$. $T_{\max\_without}$ and $T_{\max\_with}$ is the maximum temperature without and with thermal radiating coating, respectively. After calculation, for natural thermal convection coefficient of 5, 10, 20 W/m$^2$K, $R$ is 26%, 11.5%, 4.2%. Consequently, the effect of radiation coating will be enhanced for the case of small thermal convection. It can be explained that, smaller heat transfer by convection means coating surface temperature is higher. According to Stefan–Boltzmann law, the black-body radiant emittance is proportional to the fourth power of its thermodynamic temperature. Meanwhile, the effect of thermal convection is reduced. Thus, the weight of radiated power is higher.

According to Fig. 6.11, the maximum temperature decreases with PCB area. Similarly, $R$ is calculated as 17.5%, 10.6%, 8.3%, 5.1%, for PCB width of 5, 11.5, 17.5, 47.5mm. It's complied with the assumption that larger area of coating will enhance thermal radiation [1].

To analytically analyze the impact factors of $R$, the decreased effective thermal resistance of PCB after applying thermal radiation coating on to PCB layer is calculated as follows [5]:

$$\Delta R_{eff} = \frac{\Delta T}{hA\Delta T + \varepsilon_1 \sigma A(T_s^4 - T_a^4)} - (R_i + \frac{L}{kA} + \frac{\Delta T}{hA\Delta T + \varepsilon_2 \sigma A(T_s^4 - T_a^4)}) \quad (6\text{-}1)$$

In which, $h$ is the constant of free convection, $A$ is the area of PCB layer, $\Delta T$ is the different between the ambient temperature and the surface temperature of PCB, $\varepsilon_1$ is the emissivity of PCB insulation layer, $\varepsilon_2$ is the emissivity of thermal radiation coating, $\sigma$ is the Stephan-Boltzmann

constant, and $T_s$ and $T_a$ are the surface temperature of PCB layer and ambient temperature, respectively.

It can be seen that thermal resistance reduction will be inversely proportional to the PCB area $A$ or width as well as thermal convection coefficient $h$. This is complied with the simulation results obtained in Fig. 6.10 and Fig. 6.11. For other factors such as thickness $L$ and interfacial thermal resistance $R_i$, their impact on $\Delta R_{eff}$ or $R$ can also be estimated. Both the FEM simulation and analytical solution are efficient tools to predict the effectiveness of thermal radiation cooling in our thermal design of electronic devices.

## 6.5 Conclusions

The paper aims to raise attention of the effect of thermal radiation cooling on hotspot elimination as well as develop simulation and analytical methods to help determine when radiation cooling should be considered. By applying thermal radiation coating in the real applications, such as single LED emitter and light bar of backlight in TV set, the hotspot temperature can be reduced by 11 $^{o}$C and 14.5 $^{o}$C, respectively. This is nearly temperature drop of 10% and good evidence that radiation cooling plays a significant role in the overall cooling design. Further, thermal radiation can redistribution temperature of the whole electronic device and make temperature distribution more uniform, thus reduce the risk of hotspot. The last but not the least, the impact factors of the effectiveness of radiation coating are studies both numerically and analytically. The simulation methods can be applied to more complicated electronic devices and practical guidance can be provided to predict the situations that thermal radiation should not be ignored.

**Reference**

[1] K. D. Vogeleer, *et al.* "Theoretical Analysis of Radiative Cooling for Mobile and Embedded Systems," *arXiv preprint arXiv:1410.0628*, 2014.

[2] M. SHIMIZU and H. YUGAMI, “Thermal Radiation Control by Surface Gratings as an Advanced Cooling System for Electronic Devices,”*J. Therm. Sci. Tech.*, vol. 6, no. 2, pp. 297-306, 2011.

[3] S. Wijewardane and D. Y. Goswami, “Thermal property of transparent silver nanowire films,”*Semicond. Sci. Tech.*, vol. 29, pp. 1-6, 2014.

[4] L. Lu, X. Fan, J. Zhang, X. Hu, G. Li, and Z. Zhang, “Evolution of structure and infrared radiation properties for ferrite-based amorphous coating,” *Appl. Surf. Sci.*, vol. 316, no. 4, pp. 82-87, 2014.

[5] Y. L. Hsin, C. K. Chang, M. H. Wang, H. C. Yeh and T. Y. Su, “Self-assembly of Carbon Particles as a Heat Sink Coating to Promote Radiative Cooling,” *J. Chinese Chem. Soc.*, vol. 60, pp. 1309-1316, 2013.

[6] D. Zhu, K. Li, F. Luo and W. Zhou, “Preparation and infrared emissivity of ZnO Al (AZO) thin films,” *Appl. Surf. Sci.*, vol. 255, pp. 6145-6148, 2009.

[7] M. Janicki and A. Napieralski, “Modeling electronic circuit radiation cooling using analytical thermal model,” *J. Microelec.*, pp. 781-785, Jan. 2000.

[8] D. Kim, J. Lee, J. Kim, C. H. Choi and W. Chung, “Enhancement of heat dissipation of LED module with cupric-oxide composite coating on aluminum-alloy heat sink,” *Energy Conver. Manag.*, vol. 106, pp. 958-963, 2015.

[9] Y. H. Kim, Y. W. Kim and S. M. Park, “A study on the radiation heat transfer effect of CNT coating for the single chip COB LED,” *J. Info. Display*, vol. 16, no. 1, pp. 23-30, 2015.

[10] X. Han, X. Cui, K. Ma and G. Deng, “Carbon nano capsule coating for high power LED thermal management,” *Mater. Res. Innov.*, vol. 19, pp. 1112-1116, 2015.

[11] T. J. Hsiao, T. Eyassu, K. Henderson, T. Kim and C. T. Lin, “Monolayer graphene dispersion and radiative cooling for high power LED,” *Nanotech.*, vol. 24, pp. 1-10, 2013.

[12] B. Yan, “Thermal Analysis of High Power White Light-emitting Diodes”, Ph.D. Dissertation, Mater. Sci. Eng., Univ. Calif. Irvine, Irvine, CA, 2012.

[13] Y. Shao, “Study of Polymer-filler Composites Based High Performance Diffuse Optical Reflectors for Optoelectronic Device Applications”, Ph.D. Dissertation, Mater. Sci. Eng., Univ. Calif. Irvine, Irvine, CA, 2016.

[14] Y.C. Shih and F.G. Shi, “novel silicone-based composites with high thermal radiation cooling for White LED applications” (to be submitted).

# CHAPTER 7:

# THERMAL MANAGEMENT STRATEGY FOR LED FILAMENT BULB UTILIZING COMBINED THERMAL RADIATION AND CONVECTION COOLING

## 7. 1. Abstract

Due to its long lifetime, low cost and high energy efficiency, LED filament bulb has been the potential replacement of conventional light sources. However, the bottleneck in LED-filament development is thermal management of the whole bulb without traditional heat sink and consequential degradation of light output performance. Passive cooling combining thermal conductive phosphor-silicon composite with thermal radiation coating wrapped around the filaments is adopted to boost both thermal conduction and radiation into the environment. Notice that the temperature distribution within phosphor layer is non-uniform, thermal radiation coating can make phosphor temperature more uniform as well as reduce the risk of thermal quenching and hotspot. Here, the effect of our self-developed thermal radiation coatings with different emissivity are compared and investigated. What's more, open slots or holes on the bulb can be considered to enhance the thermal convection of the filament. According to our simulation results, filament thickness, thermal convection coefficient and emissivity of radiative coating are among significant impact factors to lower the filament temperature. There can be more than 20 $^{o}$C of temperature reduction with thicker encapsulant and highly emissive coating. With this optimized passive cooling design, thermal issue of LED filament bulb can be mitigated largely and cost-performance ratio is at a relatively low level.

## 7.2 Introduction

LED filament has gain its popularity recently as a replacement of conventional light sources, due to the advantage of retro-style, energy saving and low cost. Since its introduction, the challenging thermal issue and the consequential low light output has been considered as the key bottleneck to its development. The potential cooling strategies include passive cooling and active cooling. Compared with passive cooling methods, active cooling ones are more costly, space-consuming and heavier. To maintain the omnidirectional and limited-space feature of LED filament, traditional active cooling means such as heat sink, fan, fluid flow cannot be applied, which further worsen the situation for thermal design [1]. Researchers and engineers have devoted much efforts to cool down the filament. A commonly used way is to fill the inert gas (He, Ne or their mixture) to boost thermal radiation and conduction into the environment. However, it is still not effect enough to keep the junction temperature under threshold [2-3]. Other cooling methods include optimized filament layout design, adding metal heat sink, enlarged substrate area, etc [4-6]. Nonetheless, none of these has be approved to effectively resolve the thermal problems of LED filament.

In this work, a novel cooling strategy of LED filament is proposed by adding thermal radiation coating at the back of substrate and surface of phosphor layer due to its semitransparent feature. Here, Sapphire substrate is selected because the board needs to be transparent, thermal conductive and electric isolated. Besides, open slots on the LED lamp enable additional natural convection cooling, especially in the case of outdoor and other ventilated applications. Thanks to our thermal radiation coating, not only junction temperature can be dropped quite below the maximum temperature threshold, but also the uniformity of total temperature distribution can be enhanced. Thus, the input power can be further raised and light output is stimulated. And the

process cost of gas injection and sealing is saved. Significant implications of optimizing the effect of thermal radiation coating in the LED filament are also included.

## 7.3 Numerical and Experimental Methods

### 7.3.1 Simulation

Two configurations are proposed to address the thermal issue of LED filament by applying our thermal radiation coatings. The first approach was to wrap the whole LED filament up with phosphor layer and the overlying radiation coating. As can be seen from Figure 7.1, 28 dies (1016 LED chips) are mounted directly onto the transparent or semi-transparent substrate. This Chip-on-Board (COB) structure enables less thermal dissipation from the primary heat source – LED chips to substrate, however, it's not efficient enough without external heat sink. It's not feasible to add heat sink because of the omnidirectional and compact feature of LED filament. Then phosphor layer was applied to the substrate with LED dies to form a retro-style filament-like shape. After that, different thermal radiation materials can be coated onto outer surface of phosphor layer. The width $W$ and length of substrate is 1.5 mm and 38 mm, respectively. The thickness of thermal radiation coating is set as 0.05 mm and that of clear die attach adhesive (CDAA) is 0.004 mm. The potential substrate materials can be glass, sapphire, GaN on Si, semi-transparent ceramic, etc. Semi-transparent ceramic is the desirable substrate because the board needs to be transparent, thermal conductive and electric isolated. Our-developed thermal radiation coating is polymer-filler composite composed of silicone as well as fillers such as $TiO_2$ and ZnO, emissivity of which has been given in Table 7.1. The baseline data means there's no coating on the test platform. The detailed description for emissivity measurement can be referred in [7]. Thermal conductivity of components in our simulation are listed in Table 7.2.

The second means to employ thermal radiation material is coating it at the back of substrate and upper surface of phosphor layer [8-9]. This is a more compact design, geometry and materials of which are similar with that in the first approach.

For both configurations, each die is added with 0.03 W electrical power and the outer surface of the whole filament should have a natural convection coefficient because open slots or holes were generated on the bulb to enhance thermal convection. Finite Element Method (FEM) is deployed to simulate the temperature distribution of LED filament.

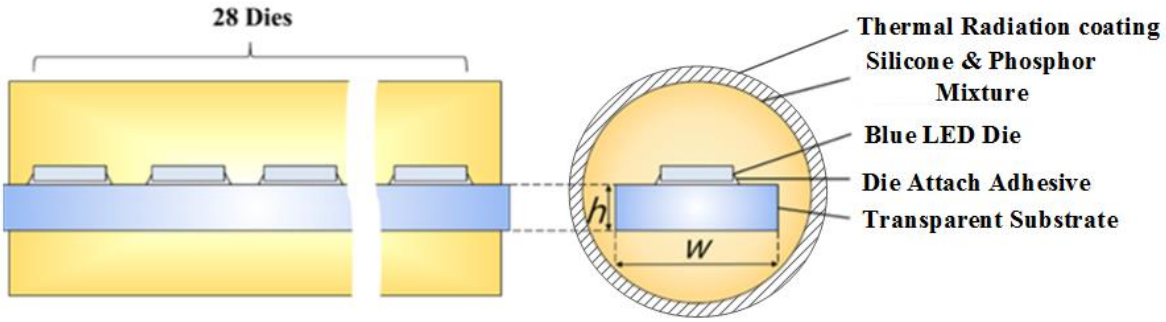


Fig. 7.1. Simulation model of the LED filament wrapped up with phosphor layer and radiation coating.

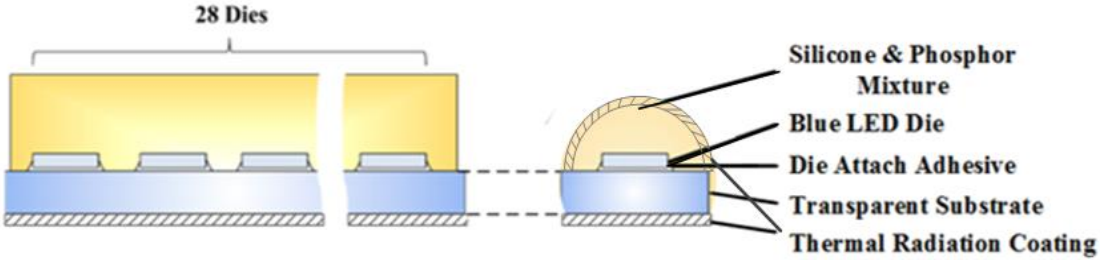


Fig. 7.2. Simulation model of the LED filament coated with thermal radiation material at the back of substrate and surface of phosphor layer.

TABLE 7.1. MEASURED EMISSIVITY OF DIFFERENT COATING MATERIALS [7]

| Specimen | Baseline | Silicone | 10% ZnO | 10% $TiO_2$ |
|---|---|---|---|---|
| **Measured** | 0.22 ±0.02 | 0.78 ± 0.02 | 0.92 ± 0.03 | 0.9 ±0.02 |
| **Reference** | 0.1-0.3 | 0.65-0.8 | 0.85-0.93 | 0.85-0.9 |

TABLE 7.2. THERMAL CONDUCTIVITY OF COMPOENTS

| Component | Material | Thermal conductivity (W/m-K) |
|---|---|---|
| **Chip** | GaN/AlGaN | 130 |
| **Substrate** | Sapphire | 27 |
| **DAA** | Silicone | 0.18 |
| **Lead** | Copper alloy | 259.6 |
| **Phosphor** | YAG:Ce | 11.3 |
| **Encapsulant** | Silicone | 0.2 |
| **PCB** | Ceramic | 27 |

### 7.3.2 Validation of simulation methods

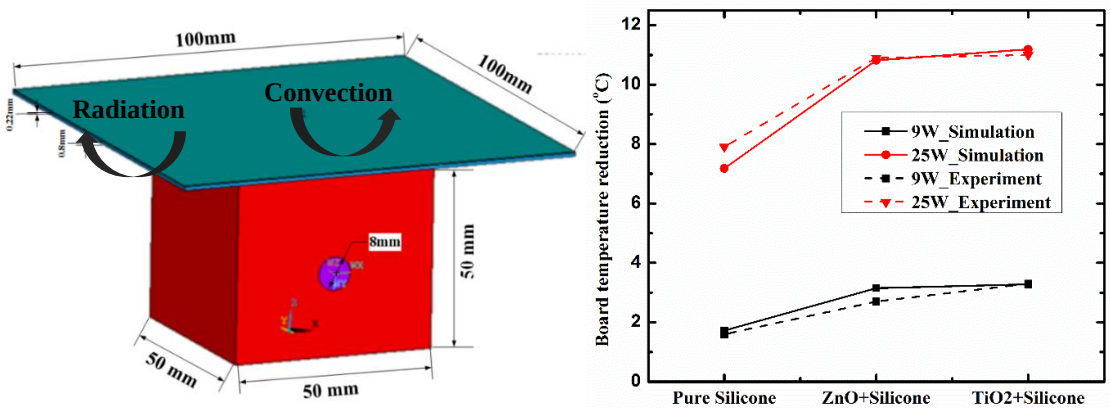


(a) (b)

Fig. 7.3. Simulation and experimental (a) model and (b) results comparison for the test platform coated with thermal radiation materials.

In order to verify our simulation method combining thermal radiation and convection effects, a test platform coated with thermal radiation materials was established and the corresponding FEM model was build. First, various coating materials were prepared. Silicone resin is mixed with various fillers by a Shinky high shear mixer at 2500 r/min for 5 minutes. Typical fillers with high emissivity are BN, $Al_2O_3$, ZnO with concentration from 2.5% to 30%. The next step is to degas the mixture in the vacuum chamber under the pressure of $10^{-2}$ Pa for 30 minutes. After that, the polymer-filler composite was coated onto polished Al plates and cured. After the specimen preparation, the test platform was established. Detailed experiment set-up has been demonstrated in [7, 10]. According to figure 7.3 (b), the simulation and experimental results agree quite well with each other. This is evidence that our simulation is reasonable to provide predictions for LED filament coated with thermal radiation coating.

## 7.4 Results

### 7.4.1 Thermal radiation coating on cylindrical LED filament

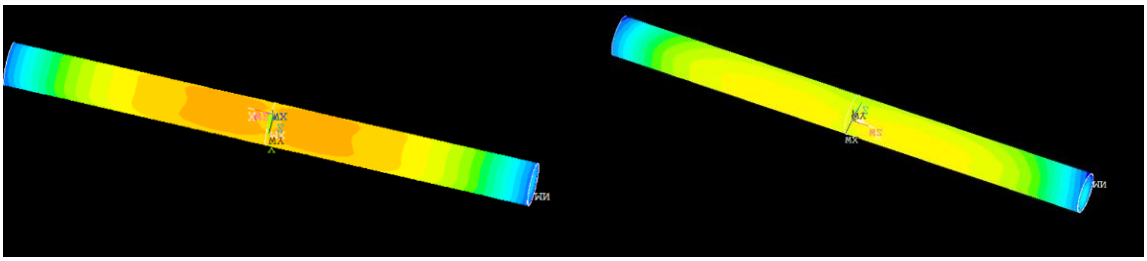

(a) (b)

Fig. 7.4. Temperature distribution of LED filament without (a) and with (b) thermal radiation coating on outer surface of phosphor layer.

Fig. 7.4 displays the overall temperature distribution of LED filament before and after applying thermal radiation coating. It can make phosphor temperature more uniform, especially that in the middle of filament. This will reduce the risk of thermal quenching and hotspot within phosphor layer.

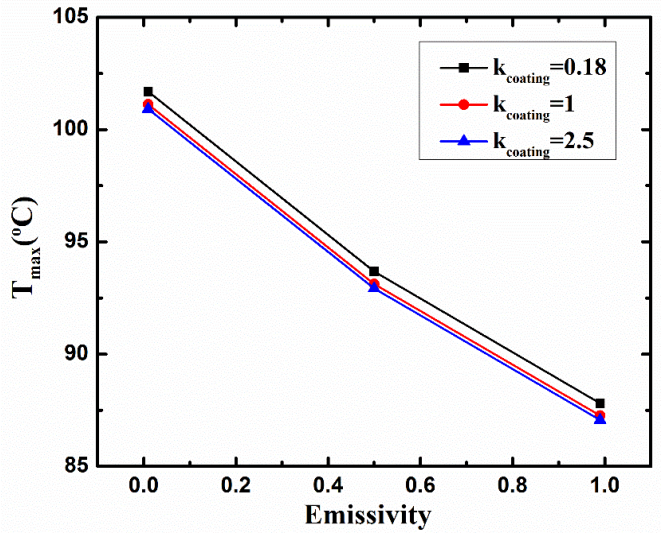


Fig. 7.5. The maximum temperature changes with thermal conductivity and emissivity of coating (thermal convection coefficient $h$=25 W/m$^2$-K).

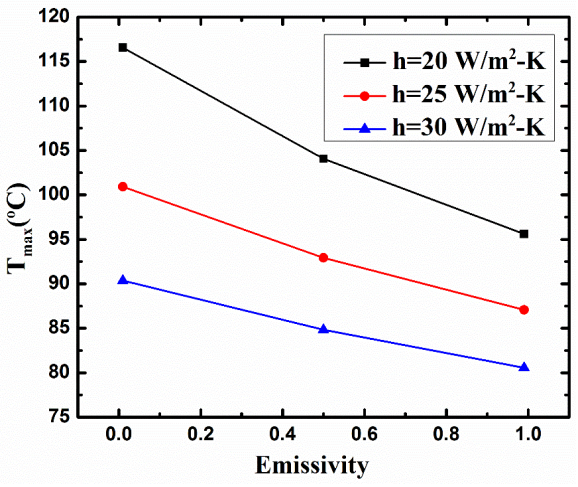


Fig. 7.6. The maximum temperature drops with thermal convection coefficient.

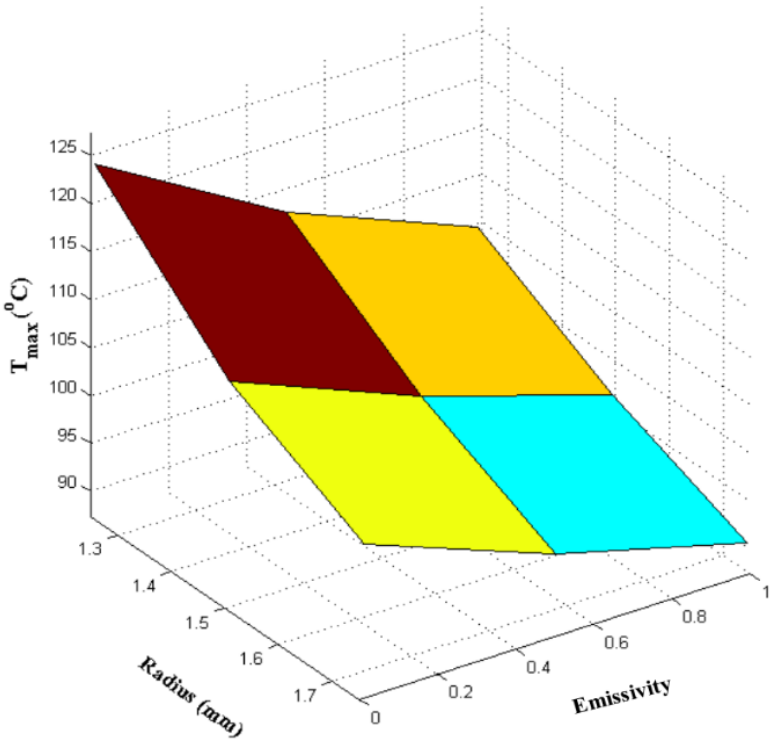


Fig. 7.7. The maximum temperature varies with emissivity of thermal radiation coating and radius of filament, the adopted thermal convection to 25 W/m$^2$-K.

Figs. 7.5-7.7 systematically discussed the impact of different parameters on cooling performance of radiative coating. Thermal conductivity of coating has a negligible effect on the peak temperature of LED filament, compared to emissivity of thermal radiation coating, thermal convection coefficient and radius of filament. There can be more than 10% of temperature reduction for materials with emissivity from 0.01 to 0.99. Thermal convection acts as a more important role in boosting the performance of thermal radiation. For non-radiative coating under less-thermal-convective air flow (or smaller open slots), the junction temperature of LED can be more than 30% higher than that with high-radiative coating and larger open slots. To enlarge radius of filament can enhance both thermal radiation and convection by increasing the outer surface of filament. Thus, our design of LED filament is thicker with transparent thermal radiation coating on its surface and open slots or holes on the light bulb.

It's also interesting to found that, after reducing the thickness of substrate, the junction temperature will be increased and illumination efficiency should be reduced. This results from smaller specific heat for thinner substrate. But according to our optical simulation with Monte-Carlo ray-tracing method, with thinner substrate, the light output will be increased. Thus, there is an optimized substrate thickness in terms of junction temperature.

### 7.4.2 Thermal radiation coating on semi-cylindrical LED filament

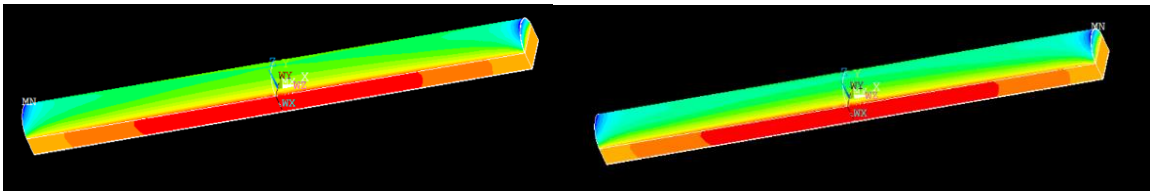

(a) (b)

Fig. 7.8. Temperature distribution without (a) and with (b) thermal radiation coating, by applying thermal radiation coating at the back of substrate and on the outer surface of phosphor layer.

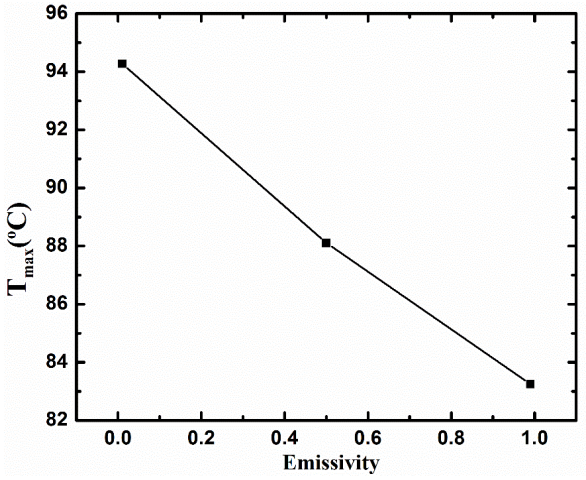


Fig. 7.9. The maximum temperature as a function of emissivity of thermal radiation coating.

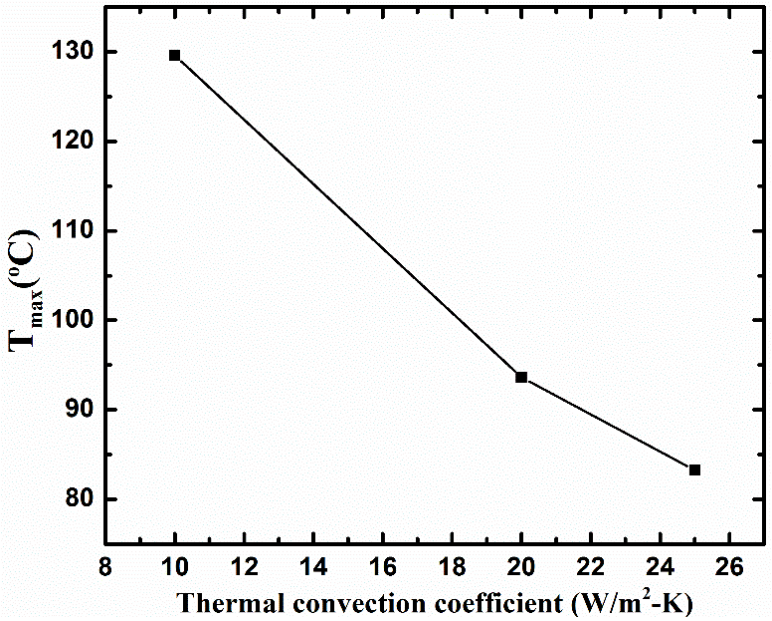


Fig. 7.10. The maximum temperature changes with natural convection coefficient.

Temperature distribution of the second configuration can be seen in Fig. 7.8. To keep the same volume of substrate, the width is changed to two times of the original one and the thickness is the half. It's found that the junction temperature will be reduced. Therefore, it's suggested that flattened substrate to be adopted to better heat dissipation. For figs. 7.9 and 7.10, the junction temperature is significantly decreased due to higher emissivity of coating and thermal convection coefficient, as expected.

After comparison, the maximum temperature is lower for the second approach than the first one with the same emissivity and thermal convection condition. And the design in second approach is more compact although it will bring about blue-light leakage from the side surface of substrate.

## 7.5 Conclusions

The paper aims to effectively resolve thermal issue of LED filament by combining thermal radiation and convection means. To achieve compact form factor and high coat-

performance ratio of electrical devices and packages, such as LED filament, neither large metal heat sink nor costly active cooling should be considered. In this work, the cost-effective and efficient thermal radiation coating was applied and discussed to lower down the peak temperature of LED filament. Additionally, open slots and holes were added to the light bulb to further enhance thermal convection. After verified with experimental data, our simulation results show a significant temperature reduction for both thermal designs. Other indications to better cooling performance for our cooling strategies were also provided. This is another evidence that thermal radiation coating developed in our lab can be promising thermal management strategy in the real applications.

**Reference**

[1] C. Xu, *et al.* "Thermal dissipation enhancement of LED filament," *17th intl. Conf. Elec. Pack. Tech.*, pp. 1212-1215, 2016.

[2] D. Starosek, A. Khomyakov, K. Afonin, Y. Ryapolova and V. Tuev, "Dependence on gas of the thermal regime and the luminous flux of LED filament lamp," *Prosp. Fund. Sci. Dev. (PFSD)*, pp. 06008-1-06008-2, 2016.

[3] W. Feng, B. Feng, F. Zhao, B. Shieh and R. Lee, "Simulation and optimization on thermal performance of LED filament light bulb," *12th China Intl. Forum Solid State Light.*, pp. 88-92, Nov. 2-4, 2015.

[4] H. Su, T. C. Cheng, H. Z. Liu and Y. M. Li, "LED light lamps using stack effect for improving heat dissipation," U.S. Patent 2014/0375201 A1, Dec. 25, 2014.

[5] S. Ge, H. Liu, Z. Ma and X. Ge, "LED filament," C.N. Patent 205424484U, Aug. 3, 2016.

[6] G. Jiang, H. Yang and C. Zhao, “Novel LED filament packaging structure,” C.N. Patent 204118125U, Jan. 21, 2015.

[7] B. Yan, “Thermal Analysis of High Power White Light-emitting Diodes,” Ph.D. Dissertation, Mater. Sci. Eng., Univ. Calif. Irvine, Irvine, CA, 2012.

[8] W. Ma, Q. Liao, P. Kong, Y. Kong, X. Yuan and M. Kang, “LED filament and LED filament bulb with thermal radiation material,” C.N. Patent 105927950 A, Sep. 7, 2016.

[9] P. wang, X. Zhang, Z. Cheng, Z. li, K. Wang and P. Zhang, “Semi-transparent ceramic bracket for LED filament and its processing technology,” C.N. Patent 104230348 A, Dec. 14, 2014.

[10] Y. Shao, “Study of Polymer-filler Composites Based High Performance Diffuse Optical Reflectors for Optoelectronic Device Applications,” Ph.D. Dissertation, Mater. Sci. Eng., Univ. Calif. Irvine, Irvine, CA, 2016.

# CHAPTER 8:

# A REAL-TIME MACHINE LEARNING APPROACH TO IMPROVE THERMAL DURABILITY AND STABILITY OF LI-ION BATTERY SYSTEM

## 8.1. Abstract

This paper proposed a novel Finite Element (FE) aided machine learning approach to boost both thermal durability and stability of Li-ion battery system. First, our developed thermal radiation coating was applied to cool down the battery pack. FE analysis indicates that for 3*3 cell array, not only the maximum temperature drops by approximately 20%, but also the uniformity of temperature was enhanced. Three corresponding machine learning (ML) methods were adopted to shorten the run time from more than 1 day to less than 0.5 min. The root-mean-square error (RMSE) of prediction can be 2.65. For thermal stability of Li-ion battery, it's pointed out that, leveraging ML technique to predict pattern of acceleration stage before onset of thermal runaway is the key to control and prevent battery explosion. Various parameters as the impact factors for acceleration pattern are discussed and scrutinized. It is suggested that more battery dataset for acceleration stage be public available to strengthen the prediction power of our ML methods.

## 8.2 Introduction

The issue of Li-ion battery explosion has posed potential threaten to public safety and given rise to widespread attentions [1]. Among all parameters that determine safety of Li-ion battery system, the importance of thermal duration and stability can never be overestimated.

In terms of thermal duration, various passive and active cooling strategies have been investigated to prevent battery from overheating and delay the onset of thermal runaway, such as

phase-change materials, highly thermal conductive heat spreader, reciprocating air flow [2-6]. However, for battery system in electronic devices with small form factor including scooter, smartphone and laptop, the feasible strategies should be compact, electrical insulated and able to be applied in a sealed environment. Here, novel thermal radiation coatings developed by our lab is adopted to effectively reduce the maximum temperature of Li-ion battery system. They are as thin as 0.1mm, with excellent electrical insulation and thermal radiation performance, which does not require inlet or outlet open slots for air and fluid flow [7-9].

Finite Element (FE) analysis is conducted as a common thermal simulation method. It can tackle electro-thermo-mechanical coupling as well as electrochemical-thermal problems in the level of both battery module and the whole electronic device. Nonetheless, it's still time consuming especially for device level simulations and requires numerous repetitive runs to go through multi-parameter problems. For instance, for transient electro-thermal simulation with millions of elements, it took 1 day to calculate one output data using server with 16 GB memory. It's also difficult to transverse all the parameters to find the optimum result due to limited time and computation resource. Therefore, machine learning approach based on FE analysis is proposed to accelerate prediction of cooling performance of thermal radiation material in Li-ion battery system. Machine learning algorithm has been studied for thermal management and controlling recently [10-12]. Hasan employed feed forward artificial neural network (ANN) exploiting FE analysis results for a bus ceiling lamp base [9]. ANN is then combined with genetic algorithm to find the optimized warpage value. Support vector machine (SVM) was developed in [11] to predict thermal error in machine tools after classifying thermal errors based on operation conditions. The paper [12] predicted thermal demand from skin temperature dataset using SVM classifier with a linear kernel. Parameters are optimized with grid search technique.

In terms of thermal stability, researchers have observed three thermal regimes: normal joule heating that can be dissipated in battery pack with external cooling strategy; acceleration stage when solid electrolyte interphase (SEI) begins to be decomposed and self-heating between electrolyte and anode generates gas and more heat; thermal runaway when cathode and anode react rapidly [13-15]. Most of related work focused on the first and third regime: thermal performance of battery under normal operation condition [16-17] and thermal runaway [18-19]. However, the acceleration stage, which has a higher heat generation than the first stage and prior to irreversible thermal runaway, has been rarely studied. Our work aims to predict the failure of li-ion battery before the onset of thermal runaway and be able to control or cut off the battery system in advance. And instead of control voltage or current under specified maximum value as in battery management system (BMS), machine learning algorithm is adopted here to learn the pattern of various parameters during acceleration, such as the acceleration rate.

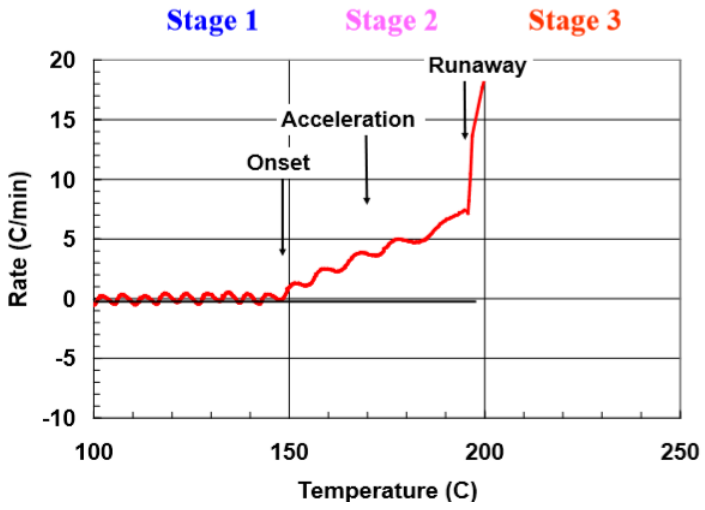


Fig. 8.1. Three thermal stages during forced thermal ramp test of Li-ion Gen 2 [20].

## 8.3 FE and ML Methods

### 8.3.1 Data preparation using FE Method

Three dimensional FE model is established with ANSYS to monitor the maximum temperature of battery system. The numerical method has been validated in our previous work [8]. Fig. 8.2 displays simulation model and temperature distribution of Li-ion battery system with (a) and without (b) thermal radiation coatings. 9 cylinders in the middle is 18650 cells with detailed structure shown in Fig. 8.3. Two layers attached to anode and cathode of cells are thermal radiation coatings. The outer surface of thermal radiation coatings is applied with natural thermal convection and other surfaces are adiabatic. Note that the maximum temperature is located in the middle of central cell, other thermal solutions such as metal heat sink attached to surface of other cells, air and fluid cooling cannot effectively dissipate heat power from center of battery pack into the outer environment. Our thermal radiation coating, however, is able to conduct heat from middle of each cell to its outer surface, then transfer to the environment through effective thermal radiation and convection. Coatings in Fig. 8.2 (a) are considered to be with emissivity close to 0 while that in Fig. 8.2 (b) with emissivity close to 1 for comparison. It can be seen that the peak temperature drops by 20% and temperature uniformity is enhanced.

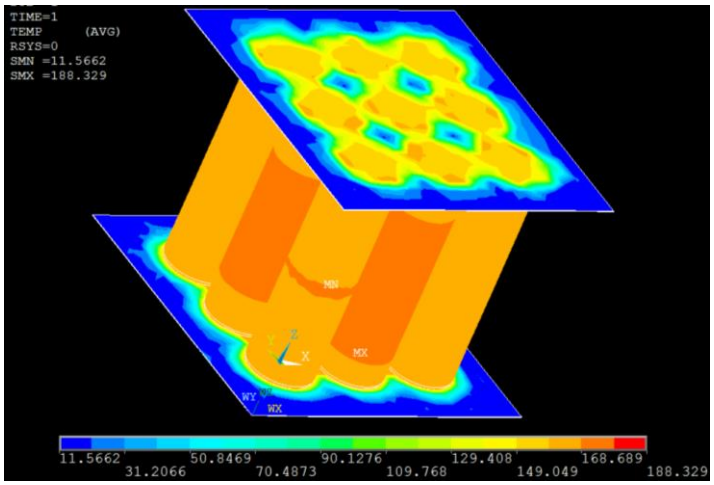


(a)

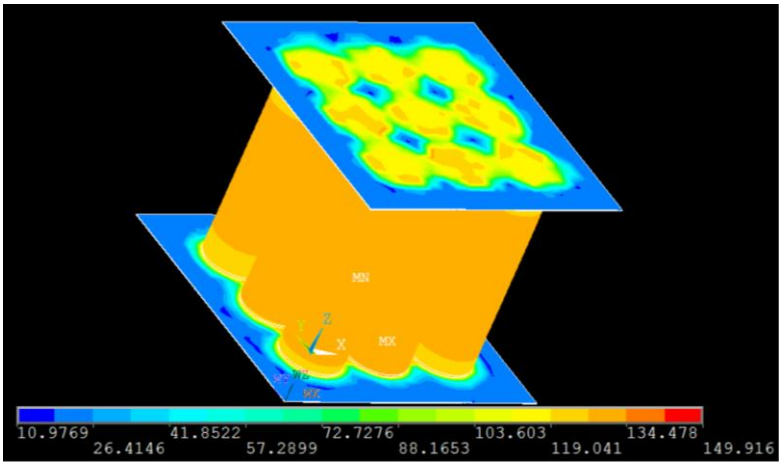


(b)

Fig. 8.2. Simulation model and temperature distribution of Li-ion battery system with (a) and without (b) thermal radiation coatings.

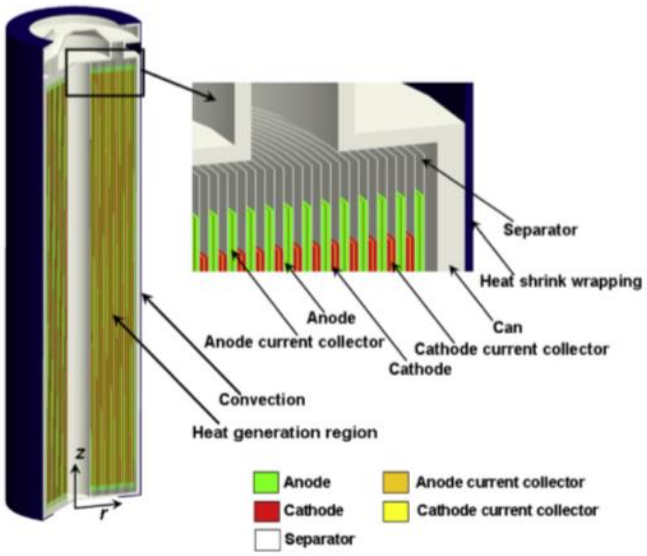


Fig. 8.3. Schematic of detailed structure of 18650 cell.

To include as much effective information as possible, temperature data are collected with FE calculations based on parameters listed in Table 8.1. The parameters are divided into three categories: properties of our thermal radiation coatings based on our measurements; input power

of cells calculated according to datasheet of 18650 cell and configuration of battery pack (other configurations and battery models can also be considered); environment parameters such as temperature and thermal convection coefficient *h* (other parameters can be pressure and humidity). In real applications, such as Electrical Vehicle and smartphone, the FE model for the whole system is much more complicated and requires more parameters to take into consideration. It will take about 30 min of CPU time for each calculation on i7-4510U processor with 8 GB memory.

TABLE 8.1. RANGE OF PARAMETERS FOR FE MODELS

| **Parameter** | **Input Power (W)** | **Gap between cells (mm)** | **Coating Area ($mm^2$)** | **$k_{coating}$ (W/m-K)** | **Thickness of Coating (mm)** | **# of cells** | **Environment Temperature ($^oC$)** | **Emissivity** | ***h*** **($W/m^2$-K)** |
|---|---|---|---|---|---|---|---|---|---|
| **Range** | 0.5-3.3 | 2.9-3.5 | 823.69-2550.25 | 0.2263-1 | 0.1-0.2 | 1-18 | 20-30 | 0.01-0.99 | 25-30 |

### 8.3.2 Machine learning method

To achieve real-time and semi-automatic thermal control of battery system, three machine learning methods are exploited to speed up the calculation. The target data is 47 peak temperature calculated by FE method in Section 8.3.1. The input data is 47 rows of 9 feature variables within the range listed in Table I. The ratio between learning sample size and number of features 47:9 is larger than the convention of a minimum 5:1 to prevent overfitting. For the feature of coating area, the values are two order of magnitude larger than other feature values. Thus we normalized it to the range (0, 1). We also calculated correlation map between features. The idea feature sets should have low inter-correlation and large correlation with output data. As shown in Fig. 8.4, input power

has highest correlation with the maximum temperature, which is reasonable empirically. Coating area has a relatively high correlation with cell gap. This consists with the assumption that coating area is slightly larger than area of battery pack.

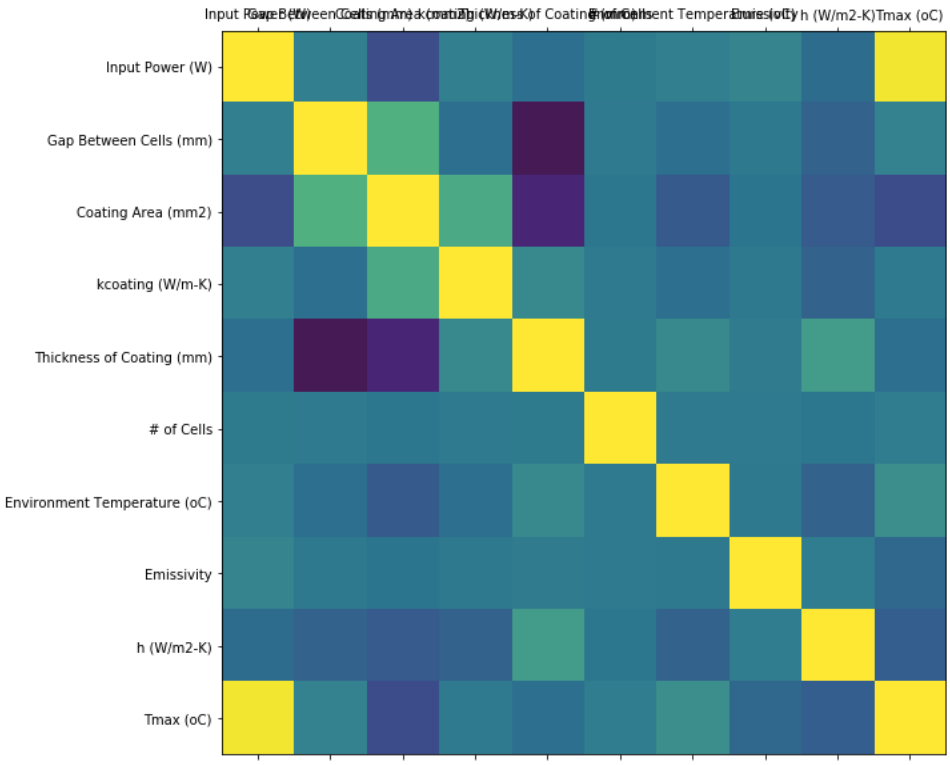


Fig. 8.4. Correlation map for training dataset.

Because the target data is continuous number, three state-of-the-art regression methods for multi-variables are discussed and compared: Linear Regression (LR), Random Forest Regression (RFR) and Support Vector Regression (SVR).

1) Linear regression (LR): LR is the simplest regression algorithm that mapping input dataset onto output data through linear relationship. To avoid overfitting, linear regression with regularization such as Lasso and Ridge regression are considered, too. The total dataset is split into training and validation set with a ratio 9:1. R2 score and root-mean-square error

(RMSE) are provide as evaluation terms. Optimal parameters were provided using grid search technique. 5-fold cross validation is used to tune parameters.

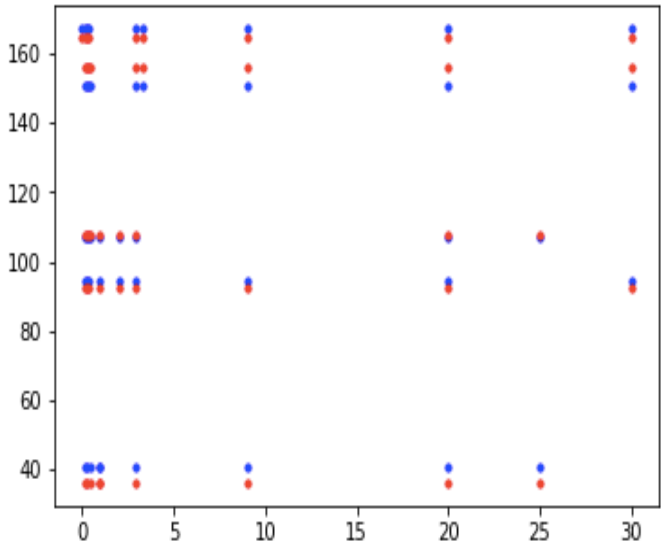


Fig. 8.5. Comparison between the truth (blue dot) and predicted value (red dot) of the peak temperature.

Fig. 8.5 implied how well our predictions fits the target temperatures. Simple LR has higher accuracy than Lasso or Ridge regression. The optimum R2 score is 0.97 and RMSE is 3.37.

2) Support Vector Regression (SVR): SVR uses a non-linear function to transform low-dimensional training samples into high dimensional kernel induced feature spaces. It is able to efficiently tackle problems with small sample size, nonlinearity and large dimensions. To fine tune SVR performance, parameters such as C (penalty for the error term), epsilon (the minimum distance from prediction to the actual values), kernel are searched. Kernels include linear, polynomial, Gaussian and sigmoid kernels. The performance is optimized when epsilon is 0.1, C is 1 and kernel is polynomial. The best R2 score is 0.98 and RMSE is 2.65.

3) Random Forest Regression (RFR): RFR uses a number of decision trees to fit sub-samples of the total dataset and voting to enhance accuracy and avoid overfitting. We tuned parameters of evaluation criterion and number of estimators. The best R2 score is 0.96 and RMSE is 3.79, when number of estimators is 500 and evaluation criterion is mean square error.

TABLE 8.2. COMPARISON AMONG THREE REGRESSION MODELS

| **Regressor** | **LR** | **SVR** | **RFR** |
|---|---|---|---|
| **R2 score** | 0.97 | 0.98 | 0.96 |
| **RMSE** | 3.37 | 2.65 | 3.79 |
| **Runtime for grid search (s)** | 0.2 | 42.6 | 24.0 |

The source of error can be limited amount of training data, thus limited information for regression model to learn. Another source is, the meshing of FEM model is not fine enough and there is discrepancy between calculated temperature and the true value. The third source of error lies in different prediction power of three regression models. Table 8.2 compares their accuracy as well as computational time. Linear regression has smaller RMSE and higher accuracy than random forest regression, which means that the input variables have a relatively simple relationship with the output values. Linear regression also has a much faster prediction speed than other two methods. However, support vector regression has a higher accuracy with prediction time compromised. It verifies the prediction power of SVR in the case with small sample size and high feature dimension as mentioned above.

## 8.4 Battery Safety Monitoring System

### 8.4.1 Parameters associated with acceleration stage

Here, some key factors within the acceleration stage that affect the possibility of Li-ion battery failure are discussed one by one. These parameters can be gathered and monitored online. The real-time control system combining both hardware and software components, including machine learning predictive model, battery management system (BMS) and various sensors, cooling material, will be proposed for the first time.

1) State of Charge (SOC)

According to Table 3 in [1], the Peak Heat Release Rate (PHRR) and maximum surface temperature of cell will increase monotonically with SOC, with the same type of cells applied with the same heat flux. Meanwhile, the first vent of battery will happen at an earlier time. Thus there is a greater chance that battery will be overheated and exploded with larger SOC, especially in the case of overcharging. Notice that SOC is proportional to mass loss rate, onset temperature and other parameters discussed in section 8.4.1, dimension reduction techniques such as Principle Component Analysis (PCA) and k-nearest neighbors algorithm (k-NN) can be employed to decouple the parameters and alleviate the multi-collinearity issue. If SOC change very slowly for a long period, the effect of aging should also be taken into consideration. Battery will have a lower exothermic rate after aging.

2) Pressure or mass loss rate

The initial venting of the cell gases indicates the occurring of acceleration stage. The gas releasing causes inner pressure of electronic devices rising, which can be detected by barometers. The gas composition includes $H_2$, CO, $CH_4$, $O_2$ and so on. To suppress its flammability, the percentage of $O_2$ should be under certain threshold. During accelerating stage, pressure rate will

rise at a larger speed and even drop sharply just before the onset of thermal runaway.

3) Environment temperature

The environment temperature for Li-ion battery ranges from -40 ℃ to 60 ℃. High ambient temperature or adiabatic condition may hinder inner heat from dissipating and increase the chance of thermal runaway. Critical environment temperature can be determined by Fig. 8.6 [22]. Our system is feasible to control the process of thermal runaway only when ambient temperature is under TNR as shown in Fig. 8.6.

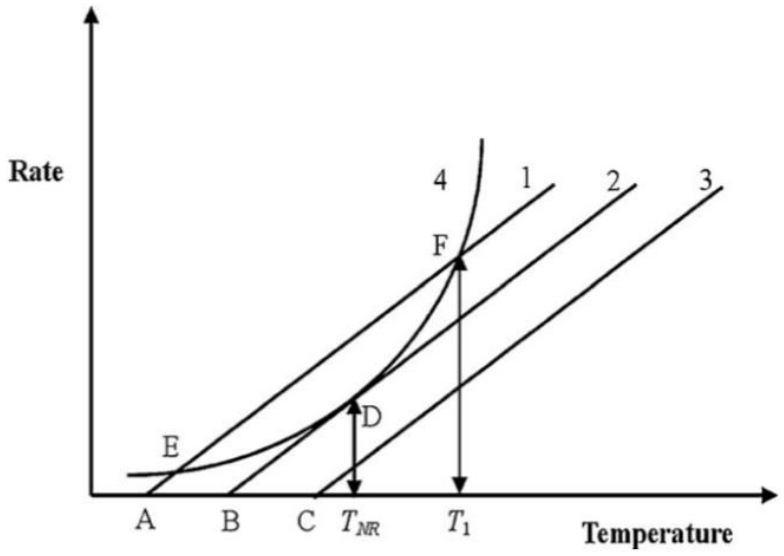


Fig. 8.6. Thermal diagraph of a reaction and heat loss from a vessel, at 3 ambient temperatures, A, B, and C. A can control the sample to temperature T1, B is at the critical temperature TNR and C cannot control the thermal runaway.

4) Voltage or current

As cell temperature increases, the external voltage decreases with a larger slope and suddenly drop to zero. This is due to internal short circuit of cell.

5) Surface temperature

The high internal temperature of cell will melt or ignite flammable components such as

electrolyte, leading to the cascading thermal runaway reactions. The battery capacity will drop by half with 10 ℃ of temperature increase. However, it's difficult to measure directly. Practically, it can be calculated by thermal resistance network method and measured surface temperature. Surface temperature rises sharply with aging time, then tends to be steady until the end of cycling.

6) Onset temperature

The onset of thermal runaway was defined by AllCell to occur when the cell self-heating rate reached 0.03 ℃/min.

7) Melting temperature of electrolyte, electrode, cathode

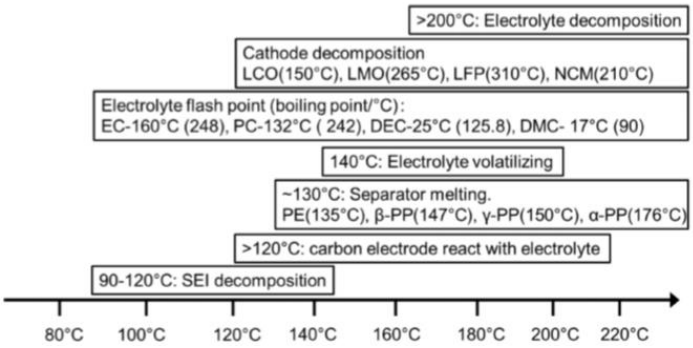


Fig. 8.7. Summary of side reactions that happen inside lithium-ion cell at different temperatures [21].

8) Depth of Discharge (DOD)

A high depth of discharge will potentially damage the cell. Cell temperature is monotonously increased with DOD under natural convection condition.

9) Current C rate

A high current rate, which is charging or discharging rate equal to battery capacity divided by one hour, has a positive correlation with reversible heat generation and shortens lifetime of battery.

### 8.4.2 Design of Li-ion battery safety monitoring system

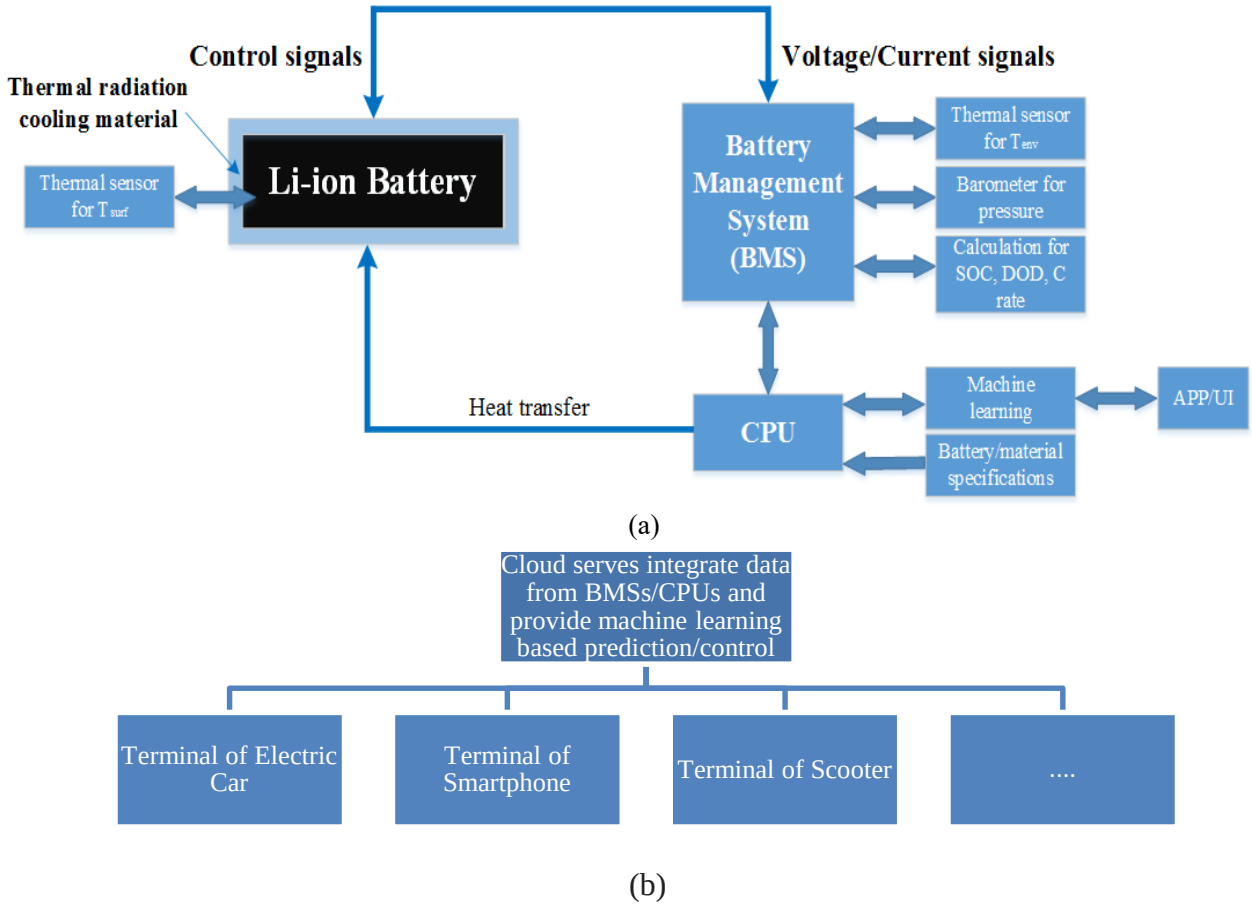


Fig. 8.8. The design of Li-ion battery safety monitoring system (a) and Cloud computing structure with large scale of terminals.

As shown in Fig 8.8 (a), all the parameters discussed in section 8.4.1 can be detected by BMS and sensors. The pattern of accelerating stage, which is indicated by inner temperature and heat generation rate curves, can be capture by the voltage/current and pressure data of BMS. All the parameters and electrical signals are input into CPU, within which machine learning algorithms can be applied to learn and predict the chance of battery failure or explosion. According to the prediction results, CPU can command BMS to control Li-ion battery instantly, make suggestions to users through APP/UI, adjust computing loads (thus heat transfer to battery). The responding and calculation time of BMS and CPU is much faster than duration of accelerating stage, thus there

is enough time for BMS to control the battery in time.

Each terminal in Fig. 8.8 (b) is one unit with similar structure as Fig. 8.8 (a). All the electrical devices with Li-ion battery system can upload training data to the centralized cloud computing source and be controlled.

Battery failures can be gradual or abrupt events. Although those battery or transportation safety standards such as UL, IEC standards systematically state electrical, thermal, mechanical, environmental reliability testing, only gradual or repetitive battery degradation can be monitored. According to reports from In-Depth Investigations (IDI), the cause of battery explosion can be counterfeit battery purchased online, battery crashed frequently, recalled battery, which are rare, stochastic, and transient. Machine learning algorithm can be adopted to predict the chance of battery explosion, provided enough onsite data of battery accidents and historical usage dataset. Unfortunately, as known to the author, there is no publically available large-scale data sets of battery usage histories and failure accidents that cover the parameters mentioned in section A. It is highly suggested that open source data repository be established to facilitate the research of machine learning based battery safety monitoring system and improve its accuracy through larger size of data.

## 8.5 Conclusions

The paper aims to utilize machine learning to dramatically speed up prediction of thermal performance of Li-ion battery system, compared to the traditional Finite Element method. First, our developed thermal radiation coating was applied to Li-ion battery system and its cooling performance was analyzed by FE. After that, three different ML algorithms were adopted and compared to predict thermal performance of the same system. The prediction time can be largely

reduced from 1 day to less than 0.5 min. Next, it was found that estimating the pattern of acceleration stage before the onset of explosion is the key to deal with fire hazard issues, not the normal temperature rising behavior or thermal runaway process that have been well studied previously. Thus, ML was employed to learn the pattern of acceleration stage and we were able to control or cut off battery before explosion happens.

**Reference**

[1] J. G. Quintiere, S. B. Crowley, R. N. Walters, R. E. Lyon, and D. Blake. (2016, Febr.). Fire Hazards of Lithium Batteries. National Technical Information Services (NTIS). Virginia. [Online]. Available: https://www.fire.tc.faa.gov/pdf/TC-TN15-17.pdf

[2] R. Mahamud and C. Park, "Reciprocating air flow for Li-ion battery thermal management to improve temperature uniformity", *J. Power Sources*, 196, pp. 5685-5696, 2011.

[3] L. H. Saw, Y. Ye and A. A. Tay, "Feasibility study of Boron Nitride coating on Lithium-ion battery casing", *Appl. Therm. Engi.*, 73, pp. 154-161, 2014.

[4] T. C. Cun and G. "Battery housing and vehicles", C.N. Patent 104025335 B, Oct. 12, 2016.

[5] R. C. Bhardwaj, "Graphene heat dissipators in portable electronic devices", U.S. Patent 2013/0136966 A1, May 30, 2013.

[6] M. Sugiura, Y. Kato, K. Sakakibara, "Battery pack with improved heat radiation and sealing", U.S. Patent 6537694 B1, Mar. 25, 2003.

[7] Y. Shao, "Study of Polymer-filler Composites Based High Performance Diffuse Optical Reflectors for Optoelectronic Device Applications," Ph.D. Dissertation, Mater. Sci. Eng., Univ. Calif. Irvine, Irvine, CA, 2016.

[8] B. Yan, “Thermal Analysis of High Power White Light-emitting Diodes,” Ph.D. Dissertation, Mater. Sci. Eng., Univ. Calif. Irvine, Irvine, CA, 2012.

[9] L. J. Huang, Y. C. Shih, and F. G. Shi, “Effectiveness of Polymer Composite Induced Passive Radiation Cooling in Thermal Management of LED Emitters and Modules: Impact on Hot Spot Elimination”, *IEEE Trans. on Compo. Packag. Manuf. Tech.*, 2017 (to be published)

[10] H. Kurtaran, B. Ozcelik, and T. Erzurumlu, “Warpage optimization of a bus ceiling lamp base using neural network model and genetic algorithm”, *J. Mater. Proces. Tech.*, 169, pp. 314-319, 2005.

[11] R. Ramesh, M. A. Mannan, and A. N. Poo, “Support vector machines model for classification of thermal error in machine tools”, *Int. J. Adv. Manuf. Technol.*, 20, pp. 114-120, 2002.

[12] C. Z. Dao, H. Zhang, E, Arens, and Z. W. Lian, “Machine learning approaches to predict thermal demands using skin temperatures Steady-state conditions”, *Build. Envir.*, 114, pp. 1-10, 2017.

[13] D. Doughty and E. P. Roth, “A General Discussion of Li Ion Battery Safety”, The Electrochem. Socie. Interf., 2012.

[14] Y. Y. Fu, S. Lu, K. Y. Li, C. C. Liu, X. D. Cheng, and H. P. Zhang, “An experimental study on burning behaviors of 18650 lithium ion batteries using a cone calorimeter”, *J. Power Sources*, 273, pp. 216-222, 2015.

[15] C. Y. Jhu, Y. W. Wang, C. M. Shu, J. C. Chang, and H. C. Wu, “Thermal explosion hazards on 18650 lithium ion batteries with a VSP2 adiabatic calorimeter”, *J. Hazardous Mater.*, 192, pp. 99-107, 2011.

[16] H. Tian, H., Wang, W., Shu, G., Liang, X. *et al.*, "Effect of Operating Parameters on Thermal Behaviors of Lithium-Ion Battery Pack," *SAE Technical Paper* 2016-01-1211, 2016, doi:10.4271/2016-01-1211.

[17] S. Goutam, J. M. Timmerans, N. Omar, P. V. Bossche, and J. V. Mierlo, "Comparative Study of Surface Temperature Behavior of li-ion battery", *Energies*, 8, pp. 8175-8192, 2015.

[18] Q. S. Wang, P, Ping, X. J. Zhao, G. Q. Chu, J. H. Sun, and C. H. Chen,"Thermal runaway caused fire and explosion of lithium ion battery", *J. Power Sources*, 208, pp. 210-224, 2012.

[19] A. W. Golubkov, D. Fuchs, *et al.*, "Thermal-runaway experiments on consumer Li-ion batteries with metal-oxide and olivin-type cathodes", *RSC Adv.*, 4, pp. 3633-3642, 2014.

[20] "D. H. Doughty, "Li-ion Battery Abuse Tolerance Testing—An Overview," Proc. AABC, Honolulu, HI, June 2005."

[21] J. Zhang, L. Su, Z. Li, Y. Sun and N. Wu, "The Evolution of Lithium-Ion Cell Thermal Safety with Aging Examined in a Battery Testing Calorimeter," Batteries, 2, 2016.

[22] Q. S. Wang, J. H. Sun, G. Q. Chu, "Fire safety science," Proc. 8th intl. Symp. Assoc. Fire Safety Science, pp. 375-382, 2005.

# CHAPTER 9:

# SUMMARY AND CONCLUSIONS

Optoelectronic devices such as LEDs and its applications have witnessed its continuous growth over the past decade and the consumer market focuses on extremely thin, light while high-performance electronic products. Novel packaging and assembly materials are among potential choices to overcome the challenges brought into thermal design of these devices.

The first chapter briefly covers the background introduction, basic concepts and methods involved in this dissertation. Continuously thinner and complex electronic devices are trending recently to meet the customers' demand. Thermal resistance network, FVM and FEM are among the most popular methods to detect thermal performance of diverse LED packages. Due to limited space and cost of these electronic devices, novel packaging materials as well as thermal radiation coating as passive cooling means are also introduced. Finally, machine learning algorithms are presented to shorten prediction time of FEM and a systematic design to reduce the risk of Li-ion battery explosion based on machine learning is proposed.

In chapter 2, thermal behavior of mid-power LED package while thinning it is discussed. FEM simulation is adopted to calculate temperature distribution of LED package and FVM experimental method is used to verify the numerical results. It is pointed out that, contrary to common understanding, junction temperature can be increased when thinning LED emitters. For chip coating white LED, maximum phosphor temperature tends to decrease with encapsulant thickness; while phosphor temperature of in-cup phosphor LED has the opposite behavior at first. Some suggestions can be provided for LED thickness design: (1) for monochromatic LED,

thickness of encapsulant has slight impact on junction and PCB temperature, thus it is safe to change the encapsulant thickness; (2) there is a peak phosphor temperature when encapsulant thickness is changed for in-cup phosphor LED, which should be treated carefully; (3) thermal conductive encapsulant and EMC leadframe can compensate temperature increase within LED; (4) phosphor concentration can also change thermal performance of phosphor layer with different encapsulant thicknesses.

In chapter 3, the research work in chapter 2 is expanded to both single-chip and multichip COB packaged LEDs. 3-D FEM model is established to study the effect of encapsulant thickness and verified by the experimental work. According to the numerical results, there is a lowest value of the maximum temperature while increasing encapsulant thickness from 0.2-0.9mm for single-chip COB LED. For the multichip case, however, the maximum temperature will keep rising with larger encapsulant thicknes. Other critical parameters such as different DAAs, radius of encapsulant layer, CCT are also investigated to help systematically understand the effect of encapsulnat thickness. To increase the overall input power, more chips and larger input power for each chip can result in different variation of the maximum temperature with encapsulant thickness.

In chapter 4, thermal modeling for light bars was developed and calculated to raise input power of EMC based LED backlights by employing novel package materials. The results showed that by utilizing DAA or encapsulant materials with higher thermal conductivities, the input power to each emitter can be increased and less light bars are needed in the LED backlight unit application. As shown in the result, the maximum input power is 1.5 W for an EMC-based SMD LED with the common DAA ($\kappa$ = 0.2 W/K-m). With the thermally conductive DAA ($\kappa$ = 1 W/K-m), at most 2 out of 7 light bars can be saved while maintaining the requirement of the same brightness. Further enhancement in thermal management could be achieved by changing DAA and

encapsulant materials simultaneously. This work presents a practical means to improve the cost-performance ratio and power efficiency of backlight units.

In chapter 5, an all-numerical opto-thermal coupled method is achieved to make both thermal and optical simulation of monochromatic LED package more efficient as well as accuracy. It's found that, considering optical results in thermal simulation, can reduce the chance of mis-predicting thermal behavior of LED package. This all-numerical means also save the long experiment time, while maintaining satisfied accuracy. So, it's more efficient than other simulation-experimental combined opto-thermal coupling method. The results indicates that junction temperature of LED package will be non-monotonously changed with different filler concentration. Either Optical or thermal calculation cannot predict the right trend that junction temperature changes.

Chapter 6 aims to raise attention of the effect of thermal radiation cooling on hotspot elimination as well as develop simulation and analytical methods to help determine when radiation cooling should be considered. By applying thermal radiation coating in the real applications, such as single LED emitter and light bar of backlight in TV set, the hotspot temperature can be reduced by 11 $^{o}$C and 14.5 $^{o}$C, respectively. This is nearly temperature drop of 10% and good evidence that radiation cooling plays a significant role in the overall cooling design. Further, thermal radiation can redistribution temperature of the whole electronic device and make temperature distribution more uniform, thus reduce the risk of hotspot. The last but not the least, the impact factors of the effectiveness of radiation coating are studies both numerically and analytically. The simulation methods can be applied to more complicated electronic devices and practical guidance can be provided to predict the situations that thermal radiation should not be ignored.

Chapter 7 expands the work in Chapter 6 to the case of LED filament. It effectively resolves thermal issue of LED filament by combining thermal radiation and convection means. To achieve compact form factor and high coat-performance ratio of electrical devices and packages, such as LED filament, neither large metal heat sink nor costly active cooling should be considered. In this work, the cost-effective and efficient thermal radiation coating was applied and discussed to lower down the peak temperature of LED filament. Additionally, open slots and holes were added to the light bulb to further enhance thermal convection. After verified with experimental data, our simulation results show a significant temperature reduction for both thermal designs. Other indications to better cooling performance for our cooling strategies were also provided. This is another evidence that thermal radiation coating developed in our lab can be promising thermal management strategy in the real applications.

Chapter 8 utilized machine learning to dramatically speed up prediction of thermal performance of Li-ion battery system, compared to the traditional Finite Element method. First, our developed thermal radiation coating was applied to Li-ion battery system and its cooling performance was analyzed by FE. After that, three different ML algorithms were adopted and compared to predict thermal performance of the same system. The prediction time can be largely reduced from 1 day to less than 0.5 min. Next, it was found that estimating the pattern of acceleration stage before the onset of explosion is the key to deal with fire hazard issues, not the normal temperature rising behavior or thermal runaway process that have been well studied previously. Thus, ML was employed to learn the pattern of acceleration stage and we were able to control or cut off battery before explosion happens